2016

Plasticity of the Nuclear Pore Complex Revealed With Proteomics

Zhanna Hakhverdyan

PLASTICITY OF THE NUCLEAR PORE COMPLEX

REVEALED WITH PROTEOMICS

A Thesis Presented to the Faculty of

The Rockefeller University

in Partial Fulfillment of the Requirements for

the degree of Doctor of Philosophy

by

Zhanna Hakhverdyan

June 2016

PLASTICITY OF THE NUCLEAR PORE COMPLEX REVEALED WITH PROTEOMICS

Zhanna Hakhverdyan, Ph.D.

The Rockefeller University 2016

Cellular functions are performed by the concerted action of macromolecular assemblies. These protein machines rarely have permanent, invariable structures. Instead, the subunits forming the macromolecular assemblies exchange between free and bound states, changing the composition, conformation and function of the assembly. Characterizing the function of macromolecular assemblies, therefore, requires the study of their dynamics.

I have developed a strategy for *in viv*o assessment of macromolecular plasticity and have successfully applied it to the yeast nuclear pore complex (NPC), one of the largest and most elaborate protein machines in the cell. NPC is a massive protein assembly situated in the nuclear envelope and mediating macromolecular transport between the nucleus and cytoplasm. To study the NPC plasticity I have combined multiple methodologies: affinity capture, metabolic labeling and mass spectrometry. Moreover, to identify the required affinity capture conditions I have developed a high-throughput screen, which has

successfully worked with numerous protein complexes, in addition to the NPC, to reveal novel interactions and arrangements of proteins within a complex.

My study on NPC plasticity has produced the first comprehensive description of NPC subunit dynamics, although for the most dynamic subunits I can only approximately estimate the exchange rate. I have also mapped the subunit dynamics on the architecture of the NPC. The central core of the NPC was revealed to be very stable, while the peripherally associated subunits exchanged with varying rates. Moreover, the rate of exchange appeared well correlated with the strength of the interaction that the NPC subunit forms with the scaffold. Notably, NPC subunits directly involved in the transport function of the NPC were among the most dynamic ones, implying that modulating the association dynamics of those subunits might alter the nuclear transport function.

The dynamics of NPC modules, as well as the plasticity changes in NPC subunit mutants have suggested that the core of the complex is extremely stable because of the additive effect of numerous weak interactions formed between NPC subunits and also the surrounding nuclear envelope membrane. The individual weak interactions may be a mechanism to prevent off target NPC assembly.

Lastly, I propose a study to directly test the existence of a potential NPC repair mechanism, which is a topic of heated debate and has direct implication for aging in all eukaryotes.

Նվիրվում է ծնողներիս՝ Հախվերդյան Լևոն և Զրվանդյան Արմենուհի

ACKNOWLEDGEMENTS

Firstly, I would like to thank my thesis adviser, professor Rout, for mentorship and support, for creating a nurturing and fun environment in the lab where a budding scientist can spend seven years of her life in a blink of an eye. I am also grateful to him for being supportive and understanding, for giving me countless opportunities to present at conferences and collaborate with wonderful people, for imparting his yeast biology wisdom on me and for forcing me to be an independent thinker.

I would like to thank the members of my thesis committee, Fred Cross and Brian Chait, who always pushed me to think harder without taking “No” for an answer, also for all the help and comments. I would like to thank my external examiner Patrick Lusk for all the valuable critique of my thesis work and his time.

I would like to thank all the past and present members of the Rout lab, who have been a tremendous resource of both scientific advice and emotional support. In particular, I would like to acknowledge: Javi, my mentor, consultant and colleague, who has been a source of ideas and inspiration that were a great driving force for my thesis project; John, for instilling in me his pain-in-the-neck meticulousness towards data documentation and for being a mentor and a friend; Natalia, for all the feedback and time she has dedicated both inside and outside of the lab and Ryo, for his harsh but fair critique and for our countless coffee discussions that will surely be one of my fondest memories of Rockefeller.

I would like to thank the Chait lab members, for all the useful discussions and technical help I have gotten over the years. I am especially grateful and indebted to Kelly; I would not be half way done with experiments without her help. I am also grateful to Dom for copyediting and critiquing my fellowship and work applications and being a good friend.

I would like to thank all of my collaborators: David Fenyo and Sarah Keegan for all the bioinformatics help I have gotten over the years; my female role models, Mary Munson and Svetlana Dokudovskaya; and Patrick Lusk and David Kaback, for introducing me to new and exciting biological problems and enriching my learning experience.

I would like to acknowledge my capable undergraduate students, Astrid and Ariana. Besides putting in hard work and pushing my projects forward they also taught me how to be a mentor and a better communicator.

I would like to acknowledge the graduate program and the Dean's office staff at Rockefeller for their help in preparing the thesis and also making the administration of the program so seamless and smooth that graduate students have nothing but their research to worry about.

Last but not least I would like to thank my parents and family for always supporting my decision to pursue science and being there for me in all my troubles and life pursuits.

TABLE OF CONTENTS

DEDICATION……..**iii**

ACKNOWLEDGEMENTS……**iv**

TABLE OF CONTENTS……**vi**

LIST OF FIGURES……**vii**

LIST OF TABLES……....**x**

CHAPTER 1: INTRODUCTION……..……**1**

CHAPTER 2: AFFINITY CAPTURE SCREEN……..……**15**

CHAPTER 3: KEEPING TRACK OF NPCS AND NUPS……**31**

CHAPTER 4: NPC DYNAMICS……..……**53**

CHAPTER 5: NPC DYNAMICS PERTURBATION……..**74**

CHAPTER 6: DUSCUSSION AND FUTURE DIRECTIONS……..**87**

CHAPTER7: MATERIALS AND METHODS……..……**102**

APPENDIX……..……..**116**

BIBLIOGRAPHY……..……**129**

LIST OF FIGURES

Figure 1-1: Diagrammatic representation of turnover and exchange……..**1**

Figure 1-2: Cryoelectron microscopy map of the yeast NPC (adapted from (Yang, Rout et al. 1998))…….**4**

Figure 1-3: Localization of major substructures and their component nups in the NPC (from (Alber, Dokudovskaya et al. 2007))……**6**

Figure 1-4: Schematic representation of the iFRAP assay and example data (adapted from (Rabut, Doye et al. 2004))…….**8**

Figure 1-5: Schematic of rat metabolic labeling experimental setup and inner ring nup data (adapted from (Toyama, Savas et al. 2013))…….**10**

Figure 1-6: Schematic illustration of NPC composition during different types of mitosis (from (Fernandez-Martinez and Rout 2009))……**12**

Figure 2-1: The diagram of the affinity capture screen workflow (adapted from (Hakhverdyan, Domanski et al. 2015))……**17**

Figure 2-2: Clustering analysis of SDS-PAGE and MS data of Nup1-SpA affinity capture (adapted from (Hakhverdyan, Domanski et al. 2015))……...**20**

Figure 2-3: Affinity capture analysis of Nup1-SpA, Nup53-SpA and Pom152-SpA (adapted from (Hakhverdyan, Domanski et al. 2015))……..**23**

Figure 2-4: SDS-PAGE and MS analysis of diverse protein complexes (adapted from (Hakhverdyan, Domanski et al. 2015))……..**25**

Figure 2-5: Analysis of the optimized Rtn1 affinity capture (adapted from (Hakhverdyan, Domanski et al. 2015))……**27**

Figure 2-6: Analysis of the abundance of proteins in high citrate affinity capture……..**28**

Figure 3-1: The overall dynamics of the NPC……..……**31**

Figure 3-2: Diagram of metabolic labeling and quantification workflow……**33**

Figure 3-3: Selective tagging of NPCs……...…**34**

Figure 3-4: Diagram of nup turnover experiment……....**35**

Figure 3-5: Diagram of the nup exchange experiment……**36**

Figure 3-6: Measuring old label usage in protein synthesis in the first 3 h after the switch……**40**

Figure 3-7: The expression of wild type and conditional alleles of Nup84 with and without cltc……..……**42**

Figure 3-8: The use of cltc for conditional nup expression……**44**

Figure 3-9: Picking an optimal scaffold component for affinity tagging and purification……**45**

Figure 3-10: The schematic of an I-DIRT experiment……**47**

Figure 3-11: GFP-Nup84 I-DIRT with and without GA cross linker……...**48**

Figure 3-12: Turnover data and fit for two NPC components……**49**

Figure 3-13: Exchange data and fit for two NPC components……..…**50**

Figure 4-1: Hypothetical comparison of turnover and exchange for nups with different exchange rates……..…**54**

Figure 4-2: The analysis of heavy protein decay half-lives in exchange and turnover experiments……..……**58**

Figure 4-3: The analysis of protein degradation in the turnover experiment.....**61**

Figure 4-4: A hypothetical diagram of the Nup84 complex (outer ring) exchange between NPCs.....**67**

Figure 4-5: Heat map of the relative mobility of nups.....**72**

Figure 5-1: Analysis of the Nup145N-C fusion mutant.....**78**

Figure 5-2: The dynamics of Nup84 complex constituents.....**79**

Figure 5-3: Immunoelectron localization of asymmetrically biased nups (from (Rout, Aitchison et al. 2000)).....**80**

Figure 5-4: Analysis of the Nup145NΔFG truncation mutant.....**84**

Figure 6-1: Schematic representation of NPC assembly (adapted from (Rothballer and Kutay 2013)).....**88**

Figure 6-2: An experiment to test a potential NPC repair mechanism.....**100**

Figure 7-1: Schematic of diploid Nup145N-C fusion strain construction.....**104**

LIST OF TABLES

Table 3-1: Heavy lysine labeling efficiency of various strains tested in this study……...…..**39**

Table 4-1: Table with Nup exchange half-lives (includes reference data from (Rabut, Doye et al. 2004))…….……**59**

Table 4-2: Nup degradation half-lives in two turnover experiments and from a proteome-wide turnover study (includes reference data from (Christiano, Nagaraj et al. 2014))…….……**64**

Table 7-1: List of strains……...……..**106**

Table 7-2: List of plasmids……..**107**

Table 7-3: List of primers……..……**107**

CHAPTER 1: INTRODUCTION

Cellular processes are largely carried out by macromolecular assemblies, as opposed to individual molecules (Alberts 1998, Gavin, Aloy et al. 2006). To understand the functions of those assemblies we need to understand their composition in space and time. Some macromolecular assemblies are incredibly dynamic; for example the entire cycle of clathrin-coated vesicle assembly and disassembly, involving ~100 proteins, is complete within ~45-80 sec (reviewed in (Kirchhausen, Owen et al. 2014)). Other macromolecular assemblies, such as Cajal bodies, do not undergo dramatic assembly and disassembly cycles (outside mitosis), but nevertheless continuously exchange subunits with the nucleoplasm (Dundr, Hebert et al. 2004). Yet a third group, such as the ribosome, is largely stable once assembled (Chen, Sperling et al. 2012). The processes affecting

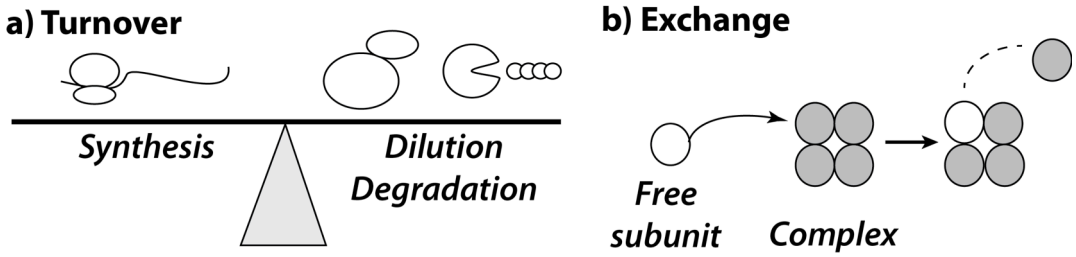

Figure 1-1: Diagrammatic representation of turnover and exchange. a. Turnover is the balance between protein synthesis and loss: synthesis is on one side of the scale, while loss due to degradation and dilution by cell division is on the other side. **b.** Exchange is the replacement of a complex bound subunit by a free subunit. In this schematic a protein complex is represented by a homotetramer; a free subunit displaces a complex-bound subunit, which becomes free and can repeat the cycle.

macromolecular dynamics can be broadly divided into turnover and exchange (**Fig. 1-1**).

Protein turnover is the balance between synthesis and loss (reviewed in (Garlick and Millward 1972)) (**Fig. 1-1a**). There are two processes contributing to the loss of proteins: 1. bulk vacuolar or targeted proteasomal degradation; 2. dilution by cell division. While dilution by cell division depends on the growth rate, the degradation rates are intrinsic to the protein and can span several orders of magnitude, from minutes to several tens of hours (Boisvert, Ahmad et al. 2012, Christiano, Nagaraj et al. 2014). Protein degradation is largely carried out by the proteasome and is a point of regulation for multiple cellular processes, e.g. cell cycle, transcription factor regulation, quality control assurance etc. (reviewed in (Ciechanover 2005, Sorokin, Kim et al. 2010)).

Exchange is the process by which complex-bound subunits are replaced with free subunits (**Fig. 1-1b**). Assembly and disassembly of macromolecular complexes can be thought of as extreme cases of exchange, when the equilibrium is strongly shifted towards the association or dissociation respectively. The shift in the equilibrium between association and dissociation of bound subunits can be modulated by posttranslational modifications in response to the needs of the cell. This, in turn, can produce macromolecular assemblies with different composition, conformation and function (De Souza, Osmani et al. 2004, Williamson 2008, Niño, Guet et al. 2016). Moreover, other cellular processes, e.g. degradation, can have different effects on free and complex-

bound subunits (Boisvert, Ahmad et al. 2012). This heterogeneity makes the study of macromolecular complex dynamics challenging.

One method of choice for studying *in vivo* protein dynamics is fluorescence microscopy, which has numerous advantages: direct localization, quantification and mobility measurement of a fluorescently tagged protein (reviewed in (Lippincott-Schwartz, Snapp et al. 2001)). However, it is largely limited to studying one or two proteins at a time. Thus characterizing the whole macromolecular assembly requires fluorescently tagging and analyzing individual subunits. Another technique, metabolic labeling coupled to mass spectrometry (MS), has emerged as a major approach for global proteome characterization, e.g. turnover, changes in expression, phosphorylation, etc. (reviewed in (Beynon 2005, Hoedt, Zhang et al. 2014)).

I have used the yeast nuclear pore complex (NPC) as a model system to develop a metabolic labeling approach coupled to affinity capture (AC) and MS for studying the dynamic organization of macromolecular assemblies in living cells. The yeast NPC is an excellent model system for the following reasons:

1. Its constituent proteins, functions and architecture are well characterized assisting in the analysis and interpretation of dynamics data;

2. The NPC has some very stable and some mobile components allowing the characterization of different exchange rates;

3. Yeast NPCs do not coordinately disassemble and reassemble during the cell division (as they do in e.g. metazoa), thus eliminating a major complication to NPC dynamics studies and making the problem more tractable.

Each point is discussed individually.

1. NPC architecture and function

Macromolecular traffic between the nucleus and cytoplasm is facilitated by a multisubunit protein assembly, the NPC. NPCs are doughnut-shaped proteinaceous machines embedded inside the nuclear envelope, which thus create channels through which macromolecules can be selectively transported (reviewed in (Wente and Rout 2010, Aitchison and Rout 2012)). The NPC is composed of ~450 polypeptides, which make up ~50 MDa in mass, thus making it one of the largest macromolecular assemblies in the cell (Alber, Dokudovskaya

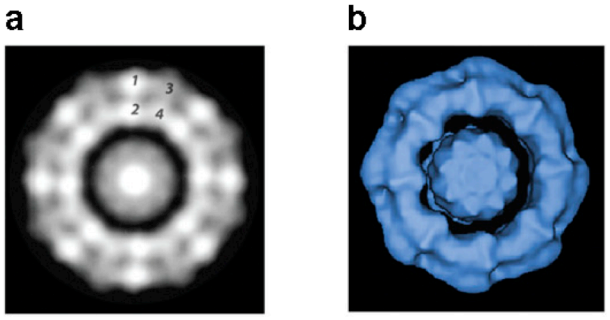

Figure 1-2: Cryoelectron microscopy map of the yeast NPC. Republished with permission of Elsevier Science & Technology Journals from (Yang, Rout et al. 1998); permission conveyed through Copyright Clearance Center, Inc. 8 spokes as well as the inner and outer rings can be directly visualized. **a.** En face slice of the mass density distribution. **b.** En face surface-rendered view.

et al. 2007, Alber, Dokudovskaya et al. 2007). There are ~30 different kinds of proteins, termed nucleoporins or nups, making up the complex (Rout, Aitchison et al. 2000). The NPC has an overall 8-fold radial symmetry through the axis of the pore, such that there are 8 repeating units called spokes making up the structure (**Fig. 1-2**). The NPC is too large and too flexible for the solution of its atomic structure to be amenable for any single conventional structure determination method. However, its molecular architecture has been solved with an integrative approach combining multiple sources of biochemical, biophysical and cell biological data (**Fig. 1-3**) (Alber, Dokudovskaya et al. 2007, Alber, Dokudovskaya et al. 2007). The structure revealed that nups are organized in coaxial rings.

The scaffold is made up of 4 coaxial rings: two inner rings flanked by two outer rings on either side. The scaffold is the core of the complex to which other, more peripherally localized proteins bind. Moreover, the inner and outer rings are made up of proteins structurally analogous to vesicle-coating complexes. The two rings coat the entire curved surface of the nuclear membrane surrounding the NPC. Since many of those proteins also possess membrane binding amphipathic ALPS motifs, it is thought that the core scaffold is responsible for both inducing the membrane curvature and stabilizing the otherwise energetically unfavorable highly curved pore membrane (Alber, Dokudovskaya et al. 2007, Alber, Dokudovskaya et al. 2007, Fernandez-Martinez and Rout 2009, Schwartz 2016).

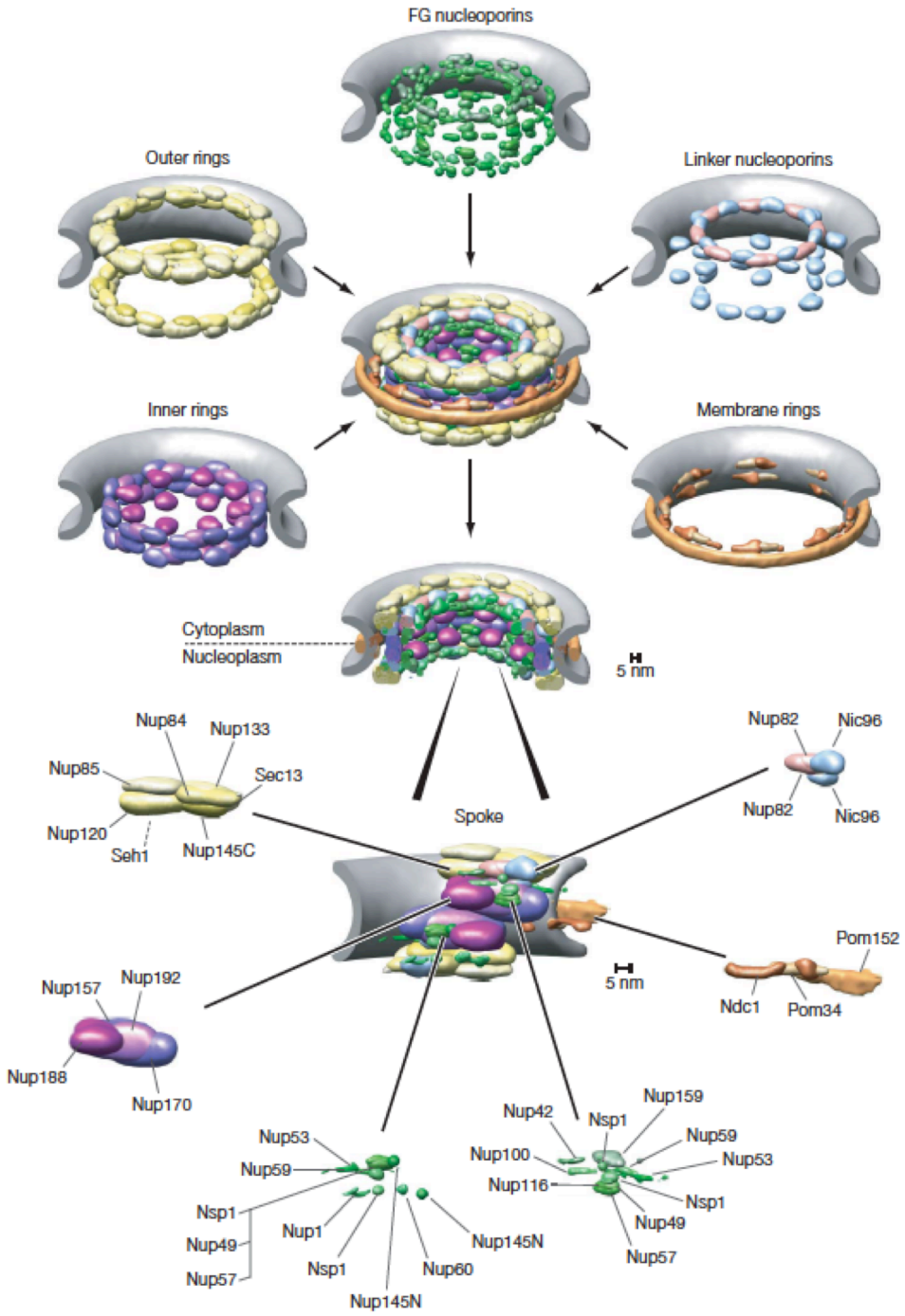

Figure 1-3: Localization of major substructures and their component nups in the NPC. Reprinted by permission from Nature Publishing Group from (Alber, Dokudovskaya et al. 2007); permission conveyed through Copyright Clearance Center, Inc. Nups are represented by their localization volumes in the calculated map. The volumes are determined by the probability of occupying a certain region in space given all the data constraints.

The transmembrane protein ring binds to the scaffold and additionally anchors the NPC within the nuclear envelope. It is less likely that the transmembrane ring plays a critical role in stabilizing the pore as it is poorly conserved among eukaryotes, appears to be entirely missing in trypanosomes and is dispensablefor growth in a fungus *Aspergillus nidulans* (Liu, De Souza et al. 2009, Obado, Brillantes et al. 2016, Schwartz 2016).

Finally, the central channel is filled with intrinsically disordered phenylalanine-glycine (FG) repeat containing proteins. These proteins create the selective diffusion barrier. Proteins > 40 Kda in size cannot traverse the NPC channel without specialized transport factors at biologically relevant rates. Transport factors recognize nuclear localization or export signals on the cargo proteins and ferry them across the NPC. Transport factors are thought to pass the NPC, because of FG-repeat binding sites on their surface, although the exact transport mechanism is still debated (reviewed in (Terry and Wente 2009, Wente and Rout 2010)). Two of the different models proposed for transport are: the virtual gating model and the selective phase (hydrogel) model (reviewed in (Patel, Belmont et al. 2007)). The first one postulates that the entropic cost of traversing a confined channel is offset by favorable enthalpy of transport factor FG-nup interactions, such that the overall passage is energetically favorable (Rout, Aitchison et al. 2000); while the second one proposes that FG-repeats form a saturated meshwork of hydrophobic interactions, thus creating a selective hydrophobic phase in the channel, which can only be traversed because of

transport factor – FG interactions specifically breaking the hydrophobic gel-forming interactions (Ribbeck and Görlich 2001, Ribbeck and Görlich 2002).

2. NPC dynamics

The NPC is often referred to as the stationary phase of transport while the transport factors carrying the cargo are considered the mobile phase. However, some nups can exchange between free and NPC-bound states within seconds (Dilworth, Suprapto et al. 2001, Griffis, Craige et al. 2004, Rabut, Lénárt et al. 2004).

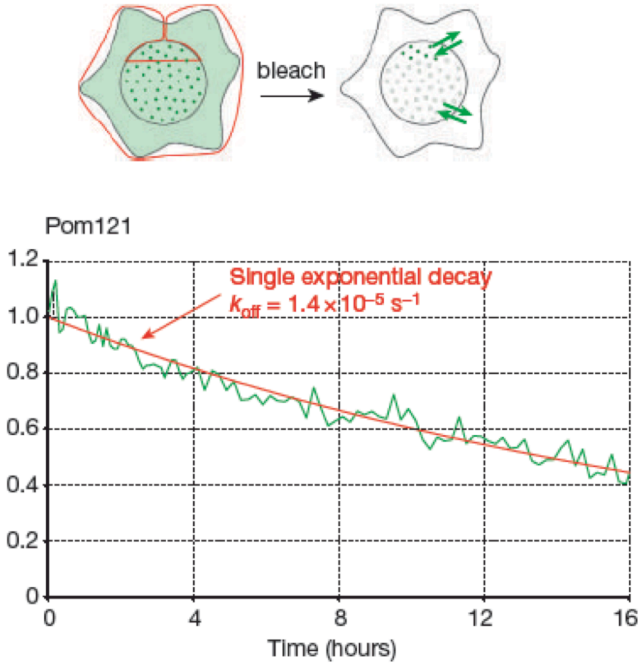

Figure 1-4: Schematic representation of the iFRAP assay and example data. Reprinted by permission from Nature Publishing Group from (Rabut, Doye et al. 2004); permission conveyed through Copyright Clearance Center, Inc. An example data and model fit from Rabut *et al.* study are shown for Pom121, a transmembrane nup.

An iFRAP (inverse recovery after fluorescence photobleaching) approach has been used in mammalian cells to characterize the mobility of 19 nups (**Fig. 1-4**). In an iFRAP assay the entire cell is bleached except a small sliver of the nuclear envelope. The loss of fluorescence from the unbleached region is monitored over time to infer the rate of GFP-tagged nup dissociation from NPCs. One of the main findings of this study was that nup residence times span several orders of magnitude, from a few seconds to tens of hours (Rabut, Doye et al. 2004).

Fluorescence microscopy is well suited for the mammalian NPC dynamics study, because NPCs are immobilized in the nuclear envelope by lamins (Daigle 2001, Shumaker 2003). However in fungi there are no lamins and NPCs freely move in the plane of the nuclear envelope at a rate of ~1 μm/sec (Steinberg, Schuster et al. 2012), making FRAP analysis for individual nup dynamics infeasible.

One of the main advantages of the iFRAP method is the sensitivity in the fast dynamics range of seconds to minutes. Some potential caveats of this iFRAP method are: exogenous expression of nups, fusion of a fluorescent tag onto nups and the use of a translation poison to stop protein synthesis and cell division. Overexpression of nups can alter their dynamics (Daigle 2001). Similarly, fusion of a large 3xGFP (triple green fluorescent protein) tag can also interfere with the protein function. For example, this study attempted to tag all 30 nups, but only 19 of the tagged nups successfully localized to the NPC (Rabut, Doye et al. 2004).

Lastly, the cells were treated with cycloheximide for hours, which may also introduce artifacts (Christiano, Nagaraj et al. 2014).

Longevity of nups has been assessed with a metabolic labeling study of whole rats (**Fig. 1-5**) (Savas, Toyama et al. 2012, Toyama, Savas et al. 2013).

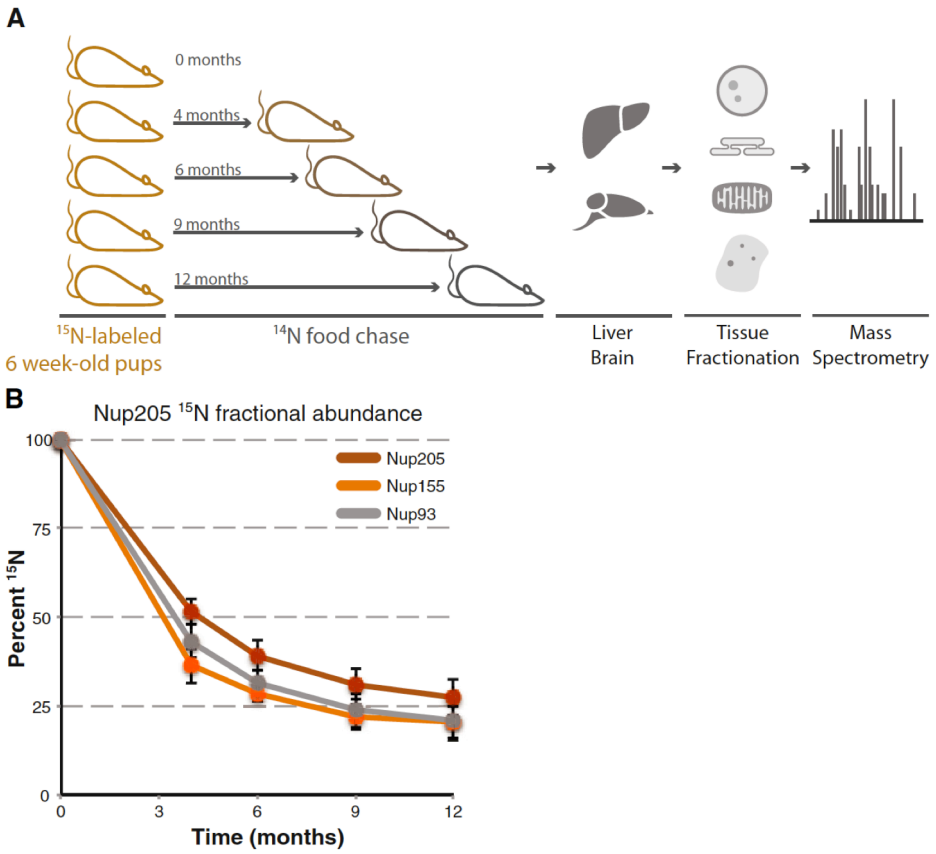

Figure 1-5: Schematic of rat metabolic labeling experimental setup and inner ring nup data. Republished with permission of Elsevier Science & Technology Journals from (Toyama, Savas et al. 2013); permission conveyed through Copyright Clearance Center, Inc. **a.** Pregnant mothers and pups were fed a ^{15}N labeled diet until 6 weeks post-natal, after which the pups were switched to a ^{14}N diet and sacrificed after indicated time. Different organs were harvested, fractionated and analyzed by MS. **b.** Decay of the ^{15}N fraction for the inner ring nups from brain tissue.

The main finding of this study (as it relates to NPC dynamics) was that in post-mitotic cells, such as neurons, the NPC scaffold nups are exceptionally stable. A potential caveat of this study is the inability to differentiate synthesis of new NPCs from the replacement of old NPC components by new ones (i.e. turnover and exchange). Still, this study provided tremendous insight into protein turnover and NPC biology in different mammalian tissues.

3. NPCs during mitosis

The spindle organizer is a specialized organelle, which attaches to kinetochores of replicated chromosomes and segregates them between the daughter cells during mitosis. The nuclear envelope presents a barrier between the spindle organizer and chromosomes. Different eukaryotes have come up with different solutions to this problem. In some eukaryotes, such as baker's yeast, the spindle pole body is embedded in the nuclear envelope, such that its nuclear face has direct access to chromosomes. The nuclear envelope of such organisms remains intact throughout the cell cycle (closed mitosis). In other eukaryotes, such as the metazoa, the nuclear envelope is completely dissolved to allow access of the cytoplasmic spindle machinery to the nuclear contents (open mitosis). Those two extremes are not the only available options and variations of partially open mitosis have been observed. The structural integrity of the NPC closely mirrors the integrity of the nuclear envelope during mitosis (**Fig. 1-6**). For example in yeast, NPCs are intact during the entire cell cycle, while the

mammalian counterparts are disassembled and reassembled with each cell cycle (reviewed in (De Souza and Osmani 2007, Kutay and Hetzer 2008, Fernandez-Martinez and Rout 2009, Imamoto and Funakoshi 2012)). As a consequence of complete reshuffling of NPC subunits during mitosis, the dynamics of fully assembled NPCs cannot be studied in actively dividing mammalian cells.

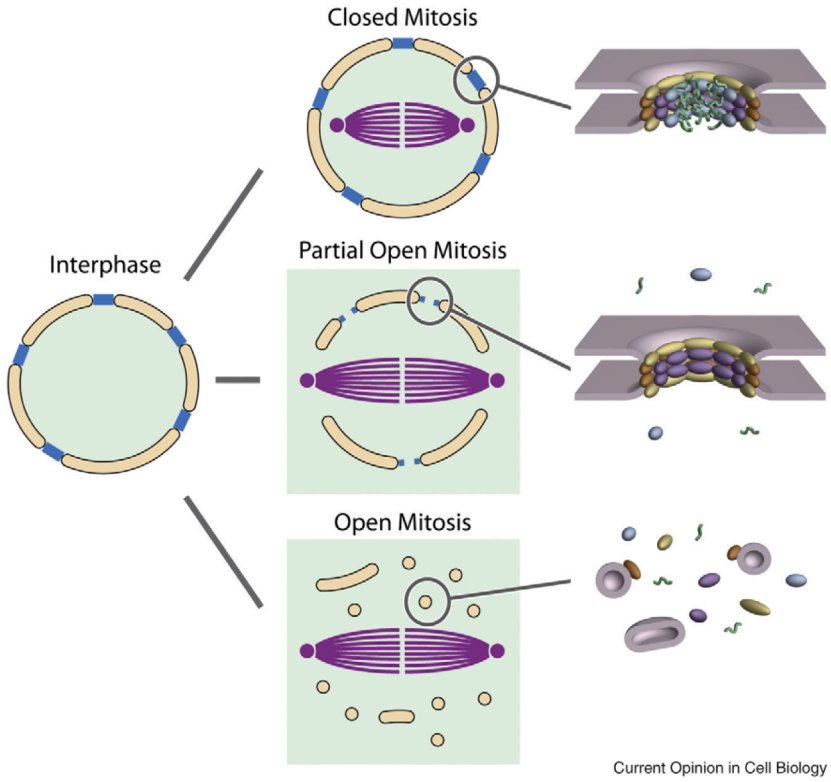

Figure 1-6: Schematic illustration of NPC composition during different types of mitosis. Republished with permission of Elsevier Science & Technology Journals from (Fernandez-Martinez and Rout 2009); permission conveyed through Copyright Clearance Center, Inc. The composition of NPC during mitosis mirrors the state of the nuclear envelope. The NPC is intact during closed mitosis and disassembles during open mitosis.

In contrast, since I use baker's yeast as a model organism I am able to characterize the dynamics of fully assembled NPCs in actively dividing cells. Moreover, since yeast is a genetically amenable model organism I can test potential determinants of NPC dynamics with genetic perturbations.

Overview of the approach

My overall approach consists of 3 methods, which will be discussed in Chapters 2 and 3:

1. A method for a single-step affinity isolation of NPCs from cells;
2. A method to track NPCs over time;
3. A method to track NPC constituents over time;

In a single experiment I measure the dynamics of all NPC subunits while the cells are actively dividing, and only a single nup is tagged and subject to exogenous expression while the rest are wild type. Thus, I avoid non-physiological influences of non-dividing cells and tagged proteins while being able to distinguish between assembling NPCs and exchange into existing NPCs.

Summary of the chapter

Macromolecular dynamics is an incredibly complex process, consisting of multiple pathways acting in parallel. I have designed a method combining approaches from yeast cell biology, genetic engineering, biochemistry and proteomics to characterize the dynamics of the NPC. The latter is a large

macromolecular assembly, with characterized constituents and architecture. The dynamics of some nups have also been characterized, so that I can benchmark my results. Finally, by using yeast as a model organism I have eliminated the contribution of NPC disassembly-reassembly on overall NPC dynamics and created a method compatible with genetic perturbation probing of NPC dynamics.

CHAPTER 2: AFFINITY CAPTURE SCREEN

Chapter introduction

The goal of this study is the analysis of dynamic composition of the NPC. However, the NPC needs to be isolated before its compositional change can be analyzed. For example, the whole cell contains both dissociated and bound subunits of the NPC; separation of the NPC allows the study of bound subunits alone. This imposes certain requirements on the isolation procedure:

1. The whole NPC needs to be isolated;

2. The procedure has to be fast, such as to prevent appreciable dissociation of bound subunits;

3. The isolation needs to be efficient, given the low abundance of NPCs (100-150 copies per yeast cell) (Rout and Blobel 1993, Winey, Yarar et al. 1997).

Affinity capture is the most widely used method for protein complex isolation and interactomic characterization (Rigaut, Shevchenko et al. 1999, Breitkreutz, Stark et al. 2007). One of the central challenges of affinity capture approaches is the identification of suitable reagent mixtures, which will maximize the yield and stability of protein complexes while minimizing the number of co-purifying contaminants (Ugwu and Apte 2004, Cristea, Williams et al. 2005, Oeffinger 2012). Identification of such mixtures requires testing and optimization of multiple parameters affecting protein-protein interactions, such as ionic

strength, salt type, detergent type, buffer type, pH etc. (Seddon, Curnow et al. 2004, Ugwu and Apte 2004, Boström, Tavares et al. 2005, Zhang and Cremer 2006, Sahin, Grillo et al. 2010). Since those parameters need to be tested in combination, the number of potential mixtures to test grows rapidly with each parameter addition. The problem of optimal affinity capture reagent search is similar to protein crystallization problem, where the reagent search is largely empirical. In crystallography this problem was solved by development of massively parallel, high-throughput screens (Stevens 2000, Wooh, Kidd et al. 2003). Inspired by the crystallography approach our lab has developed a high-throughput affinity capture screen in collaboration with Jensen lab (mammalian affinity capture screens), Aitchison lab (robotic automation), Fenyo lab (bioinformatic analysis of 96-well screens) and Chait lab (mass spectrometric analysis), as well as the high energy physics instrument shop at the Rockefeller University (dispensing manifold manufacturing and optimization) and a biotech company Orochem Technologies (filter design and manufacturing) (Hakhverdyan, Domanski et al. 2015).

Description of the screen and its development

The affinity capture screen starts with distribution of cryomilled cell material into a 96-well plate with a dispensing manifold (**Fig. 2-1i**).

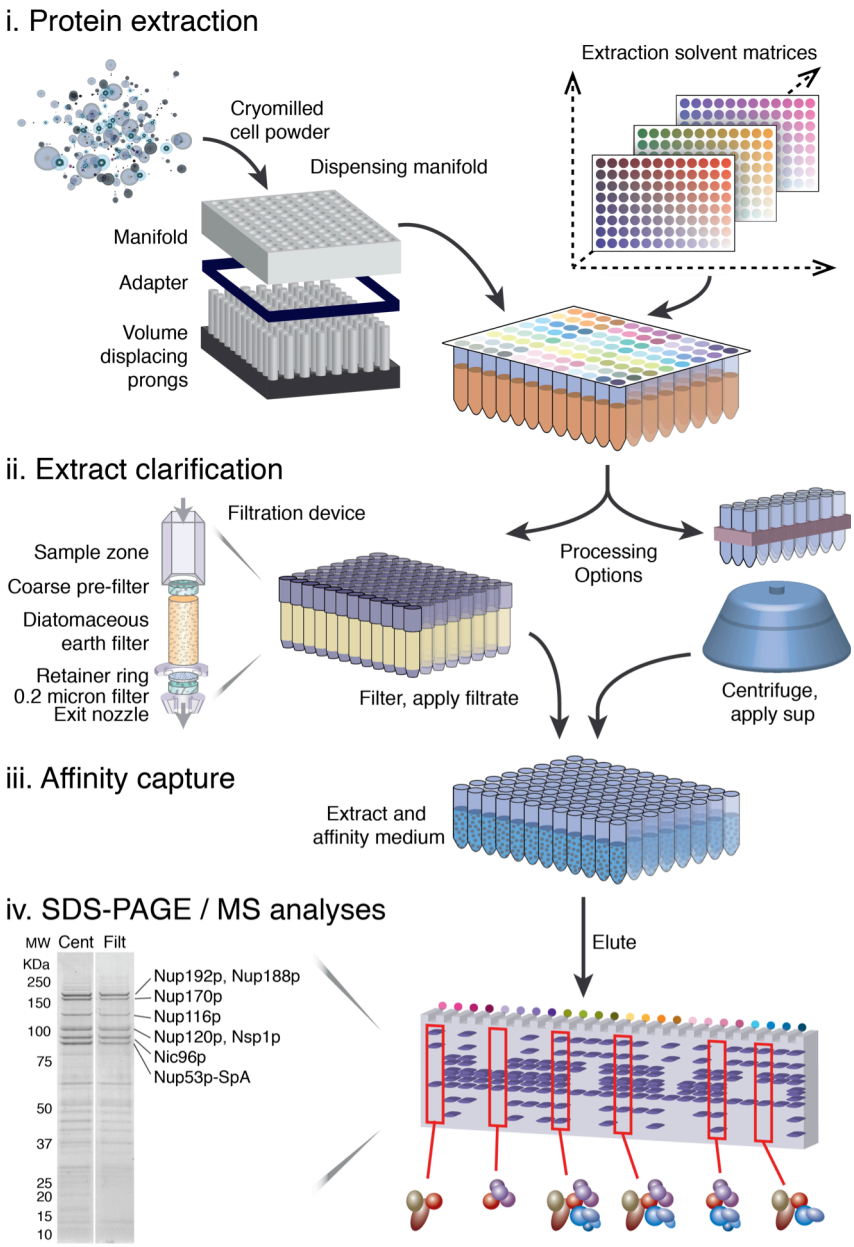

Figure 2-1: The diagram of the affinity capture screen workflow (Hakhverdyan, Domanski et al. 2015). i. Cryogenically disrupted cell material is mixed with a library of test solvents in a 96-well plate. **ii.** The resulting crude lysate is clarified via filtration or centrifugation. **iii.** The clarified extract is applied to affinity medium. **iv.** Eluted proteins are resolved on a gel and analyzed by MS. The gel on the left compares the quality of two extract preparations: high-speed centrifugation (Cent) and filtration with the novel device (Filt). In both cases Nup53-SpA was successfully affinity captured.

Disrupting cells at cryogenic temperature provides superior protein extraction yield and minimizes the potential for proteolysis and complex destabilization (Oeffinger, Wei et al. 2007). But it also makes it challenging to aliquot small amounts of frozen cell material into each well of a 96-well plate without thawing. For this reason we have designed a specialized manifold which allows distribution of a calibrated amount of powder per well (with Loren Hough, John LaCava and Vadim Sherman).

Next, a pre-mixed array of test solvents is added to the powder and rapidly mixed to fully re-suspend the cell material. This completes the protein extraction step (**Fig. 2-1i**). However, the generated crude lysate cannot be used for affinity capture without clarification. Extract clarification presented the next challenge in the screen development: commercially available 96-well plates do not tolerate high centrifugal forces necessary for clarification and filters are prone to clogging. To overcome this hurdle we designed a 96-well filtration device (**Fig. 2-1ii**) (with John LaCava, Asha Oroskar and Anil Oroskar). The main feature of this device is a multi-layer filter. Each layer traps particles of decreasing size such that by the time the protein extract reaches the 0.2 μm filter it passes without clogging.

After clarification the protein extract is incubated with affinity medium containing magnetic beads conjugated with an antibody against the protein or tag of interest (**Fig. 2-1iii**). Next, the beads are washed and the affinity-isolated proteins eluted off the beads. Finally, the protein content of the elutions is analyzed by SDS-PAGE and mass spectrometry (**Fig. 2-1iv**).

Testing affinity capture reagents on the NPC

I have used the NPC as a test bed for developing the screen for the following reasons:

1. The NPC consists of both soluble and membrane proteins, which can present their own unique challenges (Helbig, Heck et al. 2010);

2. The NPC has a modular architecture, allowing the purification of sub-complexes of different size.

3. Protein composition of the NPC and its modules is largely known, allowing for quick interpretation and feedback on the data quality (Alber, Dokudovskaya et al. 2007, Alber, Dokudovskaya et al. 2007).

4. It represents the main target for my current project, analyzing the dynamics of the protein constituents of the NPC.

Two replicate screens were carried out for the tagged NPC constituent, Nup1-SpA. The affinity capture data was analyzed in two ways: one set by SDS-PAGE and Coomassie staining, the other directly by LC-MS/MS (liquid chromatography – tandem mass spectrometry) (with Kelly Molloy). The two datasets were correlated to compare the analytical power of the two methods in resolving affinity capture profile differences. SDS-PAGE data was clustered based on the intensity rank of bands exhibiting similar apparent molecular mass with a custom image analysis algorithm (designed by David Fenyo and Sarah Keegan and available at copurification.org) (**Fig. 2-2**).

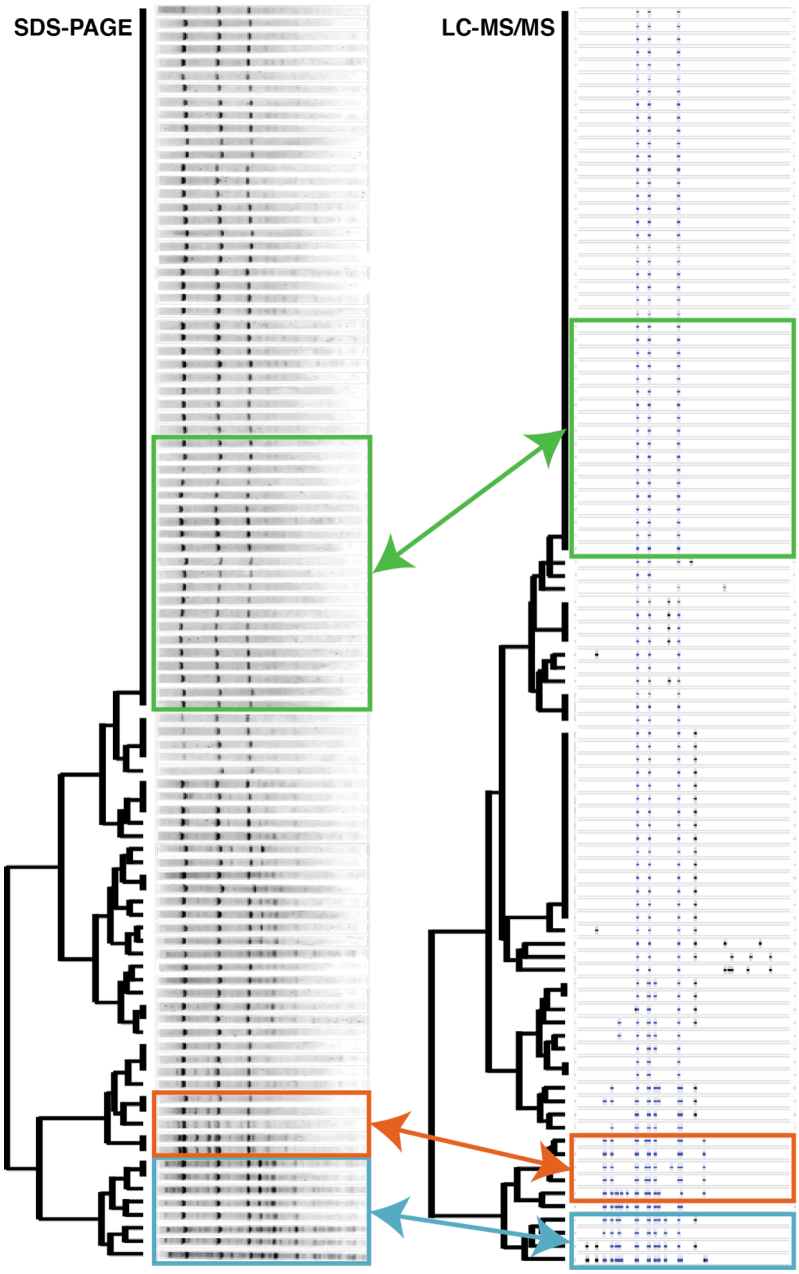

Figure 2-2: Clustering analysis of SDS-PAGE and MS data of Nup1-SpA affinity capture (Hakhverdyan, Domanski et al. 2015). The MS data is represented as a pseudo-gel for a visual comparison. Known Nup1 interacting proteins are blue bands, the rest are black. Each band represents a protein above a certain intensity threshold. The green, orange and blue boxes mark profiles with similar extraction solvent reagent composition in both analyses. Cophenetic correlation coefficient is 0.53, p-value $< 1 \times 10^{-7}$.

The MS data was clustered based on the presence of common proteins passing an intensity threshold filter (**Fig. 2-2**). The resulting dendrograms were compared with a cophenetic correlation and found to be statistically significantly similar (bioinformatic analysis performed by Devid Fenyo and Sarah Keegan).

Firstly, this indicated that SDS-PAGE and direct sample-to-MS approaches are comparable readouts of the affinity capture profiles. However, SDS-PAGE is a lot cheaper and simpler to implement. Hence, one can first identify all the different profiles by SDS-PAGE and then process the promising samples by MS. Of course, in this particular case there was a great deal of prior information on *bona fide* interactors of Nup1; hence, there is an ongoing effort with the Fenyo group to create an unsupervised, machine learning algorithm for discerning optimal affinity capture profiles from both gel and MS data.

Secondly, the clustering analysis revealed that most profiles contain a 3-protein complex (e.g. green box on **Fig. 2-2**): Nup1 and Karyopherin α:β. The minor differences among those profiles were largely due to contaminants (we assessed contaminants based on their frequency of occurrence in affinity capture experiments (Mellacheruvu, Wright et al. 2013)). This means that the majority of test solvents did not stabilize the interaction of Nup1 with its nup partners, which is consistent with its peripheral location (Chapter 1, **Fig. 1-3**) on the NPC and weak interaction with the NPC scaffold (Chapter 4 discusses this in more detail). However, in a few profiles (orange and blue boxes, **Fig. 2-2**) Nup1 co-purified with other nups. Those test solvents (containing high concentration of citrate and

acetate ions) were investigated and optimized further, with another round of the screen parameterizing the buffer components in smaller concentration increments. From those, two distinct optimized affinity capture solvents were identified: in the first high citrate concentration-based buffer, Nup1 co-purified with the inner ring and inner channel FGs; and in the second high acetate concentration-based buffer, all NPC subunits were observed (**Fig. 2-3**, Nup1-SpA, conditions ii and iii). It is worth noting that the latter analysis was based on cutting bands from the gel and identifying the most abundant species by MS. A high sensitivity LC-MS/MS analysis of the whole fraction of high citrate affinity capture can identify all NPC components, albeit at a lower intensity (not shown).

Interestingly, similar results were observed when other members of the NPC were subjected to affinity capture in the same 3 solvents identified for Nup1. The analysis of two of these proteins, Nup53 and Pom152, is shown in **Fig. 2-3**. We observe the same behavior going from left to right: i. small composite (a mixture of protein complexes, composed of subsets of proteins identified in the affinity capture), few interactors; ii. inner ring, central channel FGs (and cytoplasmic filaments), iii. nearly the whole NPC. This implies that for large macromolecular assemblies, such as the NPC, the affinity capture solvent optimization can be carried out for a handful of proteins and applied to the rest of the complex.

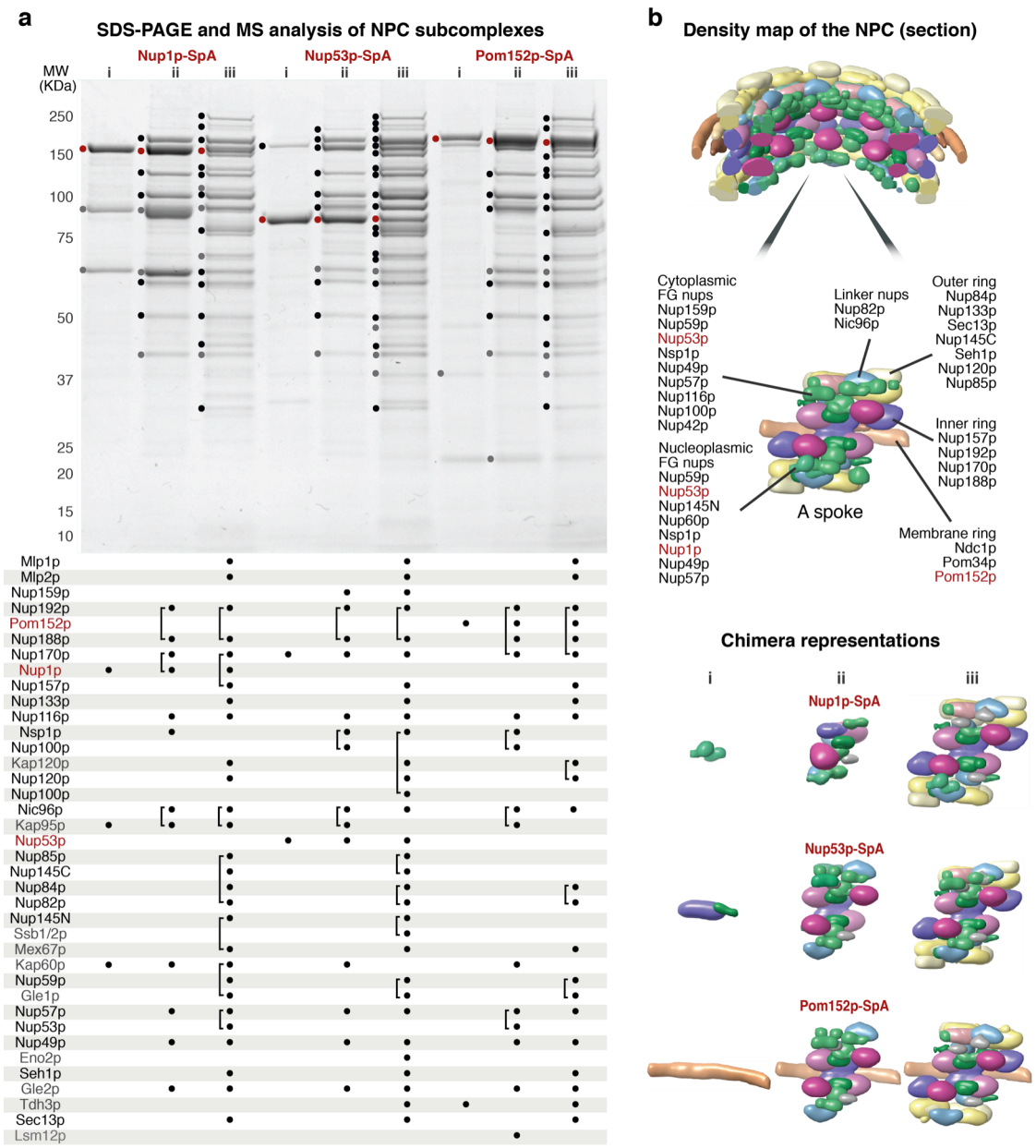

Figure 2-3: Affinity capture analysis of Nup1-SpA, Nup53-SpA and Pom152-SpA (Hakhverdyan, Domanski et al. 2015). 3 distinct affinity capture solvents were used. **a.** SDS-PAGE and MS analyses. The bands that have been analyzed are indicated by a dot. The most abundant protein species in each band is indicated underneath the gel. **b.** Chimera representations of the affinity captured profiles, demonstrating the purification of composites of increasing size (Pettersen, Goddard et al. 2004, Alber, Dokudovskaya et al. 2007, Alber, Dokudovskaya et al. 2007).

Applying the screen on diverse protein complexes and model organisms

To assess the general applicability of the screen we tested proteins with different subcellular localizations, affinity tags and from different model systems (with John LaCava, Michal Domanski and Kelly Molloy). In all cases novel co-purification profiles or interactions were observed in addition to well-characterized interactions (**Fig. 2-4**). Some interactions recapitulated genetic interaction data or were in the same cellular pathway. To validate these interactions reverse affinity capture was performed on some putative interactions (**Fig. 2-4a**, from cytoskeleton (Arp2) and endoplasmic reticulum (Rtn1)). Affinity capture profiles of Arp2 interactors overlapped in protein composition with each other and Arp2 profile. Affinity capture profiles of Rtn1 interactors were nearly identical to each other and Rtn1. Both results confirmed the findings of our screen and additionally demonstrated its utility in identifying novel interactions even for well-studied protein complexes.

Notably, our screen identified new interaction partners for Rtn1. Rtn1 is an endoplasmic reticulum (ER) integral membrane protein, which simultaneously embodies multiple challenges facing affinity capture studies: it is spread between multiple localizations, performs different functions, likely forms dynamic or transient interactions and as a transmembrane protein is particularly difficult to purify (De Craene, Coleman et al. 2006, Dawson, Lazarus et al. 2009, Helbig, Heck et al. 2010, Babu, Vlasblom et al. 2012). For an orthogonal test of newly identified Rtn1 interactions I performed an I-DIRT (isotopic differentiation of

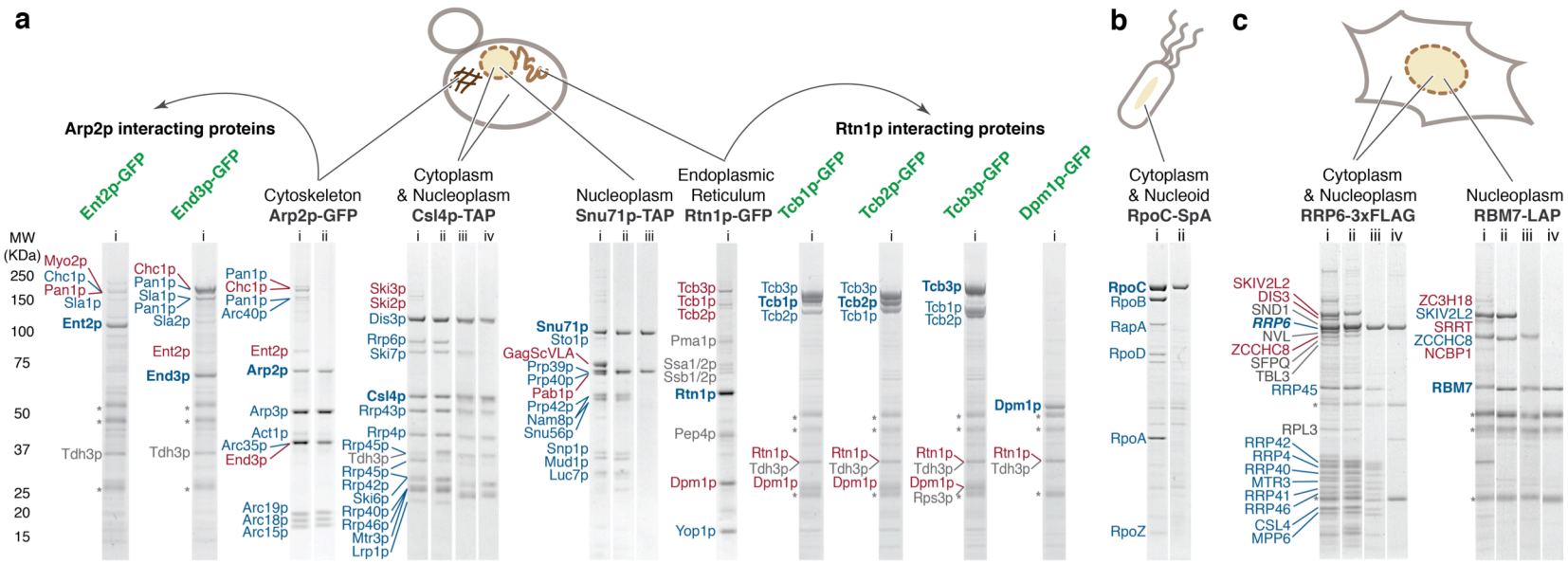

Figure 2-4: SDS-PAGE and MS analysis of diverse protein complexes: a. yeast, b. bacteria, c. human cells (Hakhverdyan, Domanski et al. 2015). Representative profiles are shown. Schematic diagrams of cells indicate the cellular compartment containing the affinity-captured protein. Reverse affinity capture profiles of putative interactions are indicated by an arrow, originating from the profile where they were first observed. Proteins identified by MS are marked next to each profile. Proteins labeled in blue are previously characterized physical interactions; those in red are novel interactions or proteins recalcitrant to co-purification; gray marks contaminants based on frequency of occurrence and metabolic labeling analysis (**Fig. 2-5**); bands marked by an * denote the heavy and light chains of the antibody used for purification.

interactions as random or targeted) analysis with the optimized affinity capture condition (Tackett, DeGrasse et al. 2005) (**Fig. 2-5a**). I-DIRT is a metabolic labeling method, which allows distinguishing interactions formed *in vivo* from interactions likely formed after lysis. Indeed, the interactors identified in our SDS-PAGE analysis were classified as likely in vivo interactors (**Fig. 2-5a**, gray distribution). Also, the proteins we characterized as likely contaminants based on their frequency of occurrence in affinity capture experiments (Mellacheruvu, Wright et al. 2013) were classified as likely post-lysis interactions. Moreover, the ontological classification of proteins in the specific interactors group as largely consisting of ER membrane and lipid metabolism proteins is consistent with the subcellular localization of Rtn1.

Lastly, I compared the optimized affinity capture profile identified for Rtn1 with a profile produced by a standard TAP (tandem affinity purification) approach, which has been used for a high-throughput affinity capture study for membrane proteins (**Fig. 2-5b**) (Babu, Vlasblom et al. 2012). I failed to observe tricalbins (Tcb1/2/3) or Dpm1 as distinct bands by SDS-PAGE on the standard TAP profile. Moreover, the analysis of standard TAP profile by LC-MS/MS revealed that more than half of proteins co-purifying with Rtn1 constitute abundant cytosolic proteins involved in sugar metabolism and protein translation. While in the optimized affinity capture profile those common contaminants constitute a small fraction. Thus, the optimized affinity capture condition co-purified more likely specific

proteins (ER/ lipid metabolism) and less contaminants (sugar metabolism/ translation) than the standard TAP procedure.

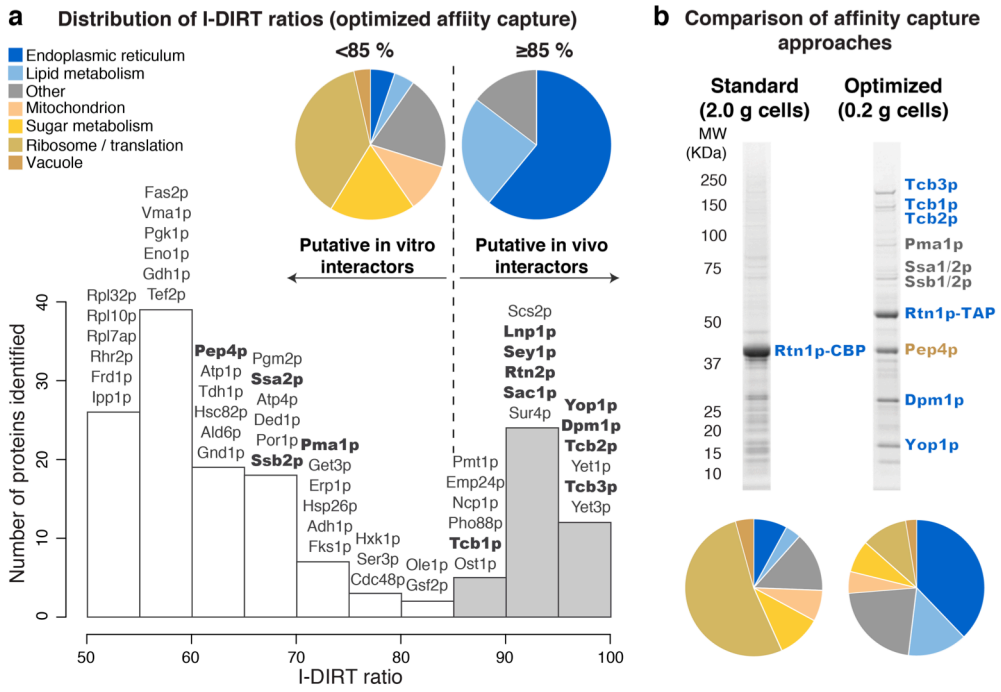

Figure 2-5: Analysis of the optimized Rtn1 affinity capture (Hakhverdyan, Domanski et al. 2015). a. I-DIRT ratio distribution of proteins identified in the optimized Rtn1 affinity capture profile. Distribution corresponding to likely *in vivo* interactions is shaded gray. Representative proteins are shown above each bin. Proteins in bold face are either known interactors of Rtn1 or were identified in our screen by SDS-PAGE and MS analysis. The proteins in white and gray distributions were individually grouped according to cellular pathways. The resulting frequency pie charts are displayed above the corresponding distribution. **b.** Comparison of SDS-PAGE profiles produced by standard TAP (tandem affinity purification) procedure and our screen. A replicate sample was analyzed by LC-MS/MS. The resulting protein data sets were grouped according to cellular pathways as in **a**. The resulting distributions are displayed below each lane.

Characterizing the high citrate affinity capture profile

For the remainder of the NPC dynamics analyses I have used the high citrate concentration-based condition for affinity capture. Although high acetate provides a superior yield and coverage of nups, it is not compatible with the glutaraldehyde (GA) crosslinking step necessary for my approach (this is discussed in more detail in Chapter 3), because ammonium reacts with GA

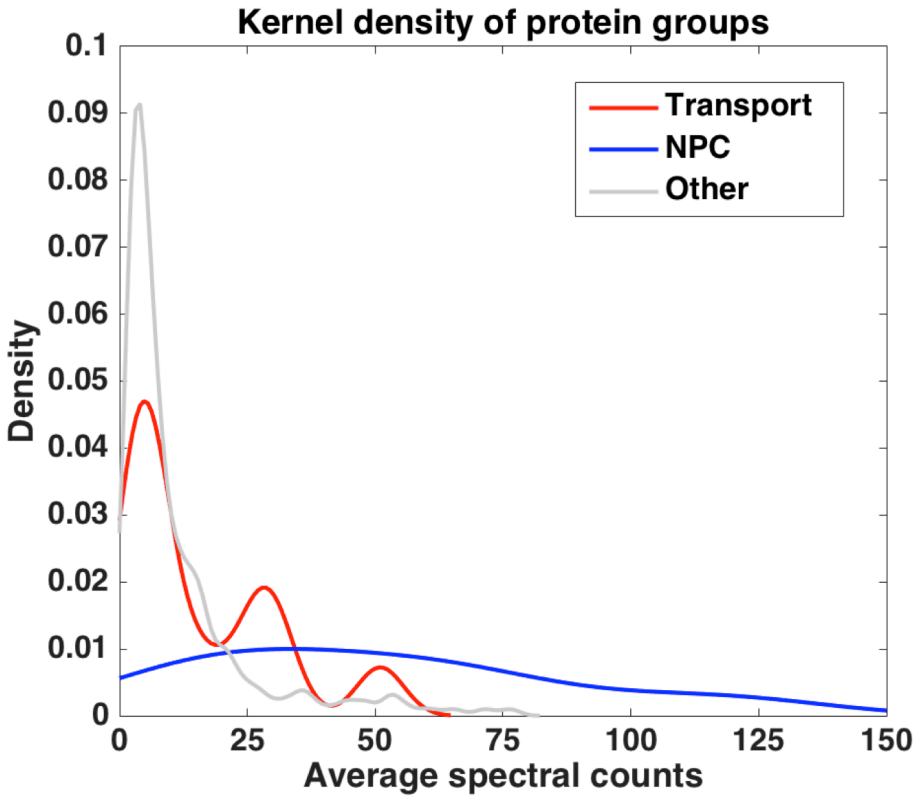

Figure 2-6: Analysis of the abundance of proteins in high citrate affinity capture. The spectral counts for protein hits in 5 GFP-Nup84 affinity capture experiments were averaged. The protein hits were grouped in 3 categories: NPC, transport factor and everything else (non-specific). Next, a kernel density plot was produced for each group. Spectral counts are used as proxy for abundance.

(Migneault, Dartiguenave et al. 2004, Subbotin and Chait 2014). To gain better insight into the protein composition of the affinity-purified sample, I characterized the abundance of co-purified protein species (**Fig. 2-6**).

I used gene descriptions from the *Saccharomyces* Genome Database (SGD, http://www.yeastgenome.org) for the protein hits in the sample to group them in 3 categories: NPC component, transport factor and everything else (labeled non-specific on the graph). For each category, I analyzed the distribution of the abundance of protein species based on spectral counts. Indeed, the vast majority of non-specific proteins were observed with <10 spectral counts. Curiously, the majority of transport factors were also observed with <10 spectral counts, perhaps indicating a heterogeneous population caught in transit. The blue distribution of the NPC components was shifted noticeably to the right indicating much more abundance. Based on those observations, NPC components and some transport factors are the most abundant species and the sample and a simple spectral count filter can eliminate a large proportion of non-specific interactions. Thus, the high citrate concentration based affinity capture condition satisfies all the requirements for my assay:

1. Allows the identification and quantification of all NPC components in a single step;
2. Is compatible with cross linking;
3. Is largely composed of my proteins of interest (NPC components and transport factors).

Chapter summary

Together with colleagues in several collaborating laboratories I have developed a high-throughput affinity capture screen. This screen allows timely and cost-effective identification of optimal affinity capture conditions. We have successfully applied the screen to numerous protein complexes. Additionally, our approach was used for characterization of the yeast exocyst and Trypanosome NPC (Heider, Gu et al. 2015, Obado, Brillantes et al. 2016).

The high-throughout affinity capture screen also allowed the identification of optimal purification condition for the whole NPC capture, which I have used throughout the NPC dynamics study.

In the next chapter I will discuss the experimental design of nup dynamics measurement.

CHAPTER 3: KEEPING TRACK OF NPCS AND NUPS

Chapter introduction

Multiple processes, presented diagrammatically in **Fig. 3-1**, affect the NPC dynamics. Turnover is the replacement of old protein by new protein in the total population (NPC and free pool) and includes nup synthesis and degradation, while exchange is the substitution of an NPC-incorporated nup by one in the free pool. Since the cells are constantly growing, synthesis has to keep up with both growth and proteins lost due to degradation – this is represented by synthesis

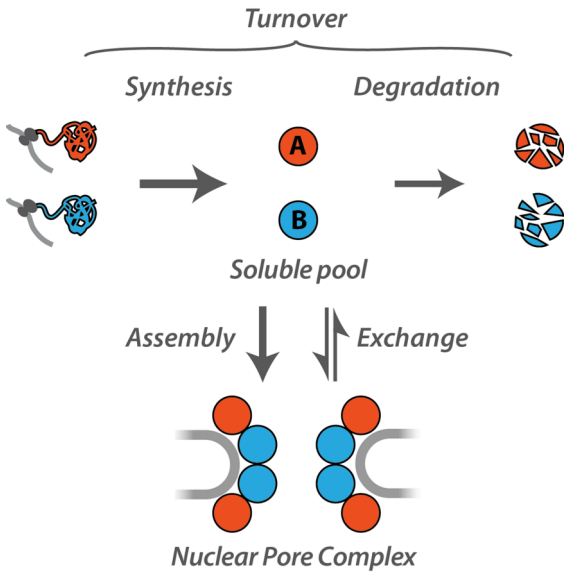

Figure 3-1: The overall dynamics of the NPC. For simplicity, in this and subsequent diagrams, the NPC represented with two kinds of proteins – A and B. After ribosomal synthesis A and B can assemble into new complexes, exchange into existing complexes or be degraded. The grand total of these processes is the turnover.

being greater than degradation (**Fig. 3-1**), and results in new nups that dilute old nups over time even in the absence of appreciable degradation.

Fundamentally, in order to assess turnover and exchange of nups I need to be able to track nups and NPCs over time. To do this I need to differentiate between:

1. old and new nups;
2. old and new NPCs.

1. Differentiating old and new nups

To differentiate between old and new nups I employed metabolic labeling with isotopically heavy and light lysine, as diagrammed in **Fig. 3-2** (Doherty, Hammond et al. 2009, Cambridge, Gnad et al. 2011, Christiano, Nagaraj et al. 2014). Initially, all proteins are labeled with heavy lysine (**Fig. 3-2a**). Once the cells are switched to light lysine containing medium all the newly synthesized proteins incorporate the light label, thus allowing me to differentiate between the old, heavy-labeled and new, light-labeled protein by mass spectrometry (**Fig. 3-2b**). Quantitative mass spectrometry also provides the relative amounts of light and heavy protein, allowing the assessment of the remaining old protein fraction at each time point. Initial approximation assumes both turnover and exchange to be first order reactions (Rabut, Doye et al. 2004, Beynon 2005, Cambridge, Gnad et al. 2011). Thus, both processes can be described by fitting an exponential model to the time course data (**Fig. 3-2c**).

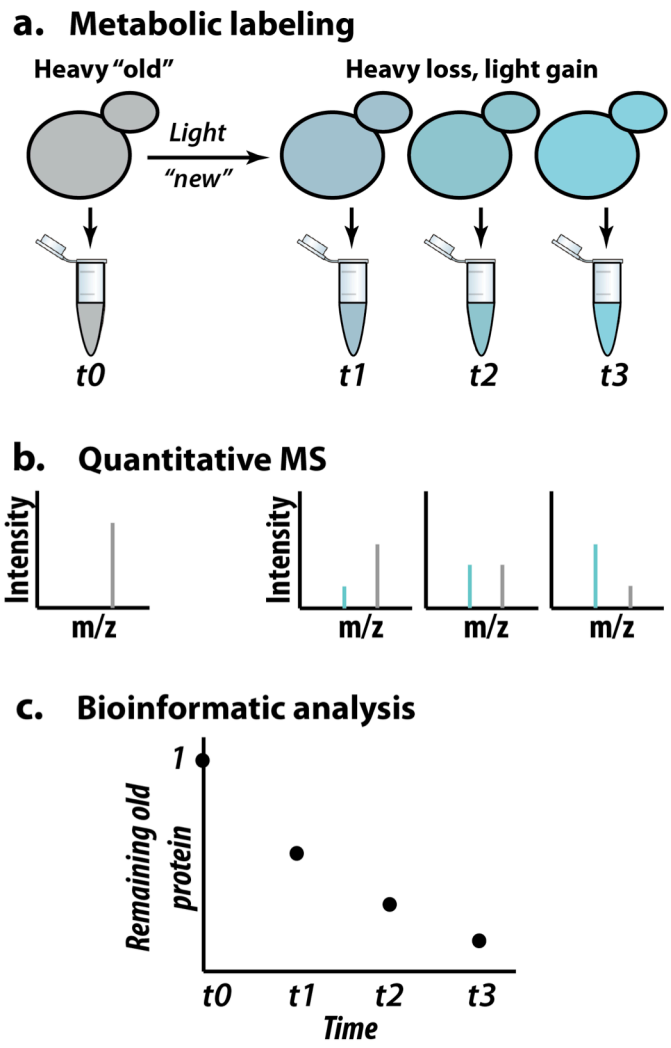

Figure 3-2: Diagram of metabolic labeling and quantification workflow. a. Metabolic labeling. The cells are initially heavy labeled, after which they are switched to a light labeled medium. Samples of cells are collected over time. **b.** Quantitative MS. The time course samples are analyzed by MS to quantify the relative amount of the old and new (heavy and light) protein. **c.** The fraction of the remaining old protein (heavy/ (heavy + light)) is plotted for each time point and an exponential model fit provides the decay constant and half-life of the old protein loss.

2. Differentiating old and new NPCs

The method I have developed to characterize both turnover and exchange individually is achieved by uncoupling NPC assembly and exchange by selective affinity tagging. This is represented in **Fig. 3-3**. The general principle is that in order to track NPCs over time I need to differentiate between old and new NPCs. Whilst this is not important for the turnover assessment, since the analysis is performed on the total population of NPCs, it is essential for the exchange characterization, where I specifically analyze old NPCs.

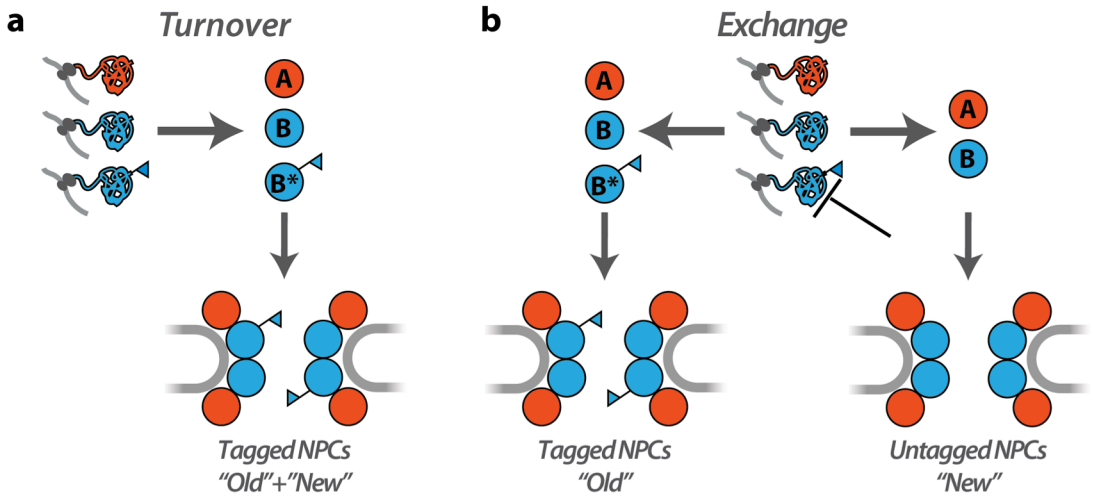

Figure 3-3: Selective tagging of NPCs. Two variants of the subunit B are expressed: a wild-type copy and an affinity tagged copy B*. While B is expressed constitutively, the expression of B* is conditional. **a.** In the turnover experiment B* is always expressed, thus all NPCs will contain B*. **b.** In the exchange experiment the cells are initially expressing B*, resulting in the incorporation of B* into NPCs (panel **b** left arrow). Later the expression of B* is repressed, after which all newly assembled NPCs will lack B* (panel **b** right arrow). In this way old and new NPCs can be distinguished by the presence or absence of B*.

Turnover experimental setup

The diagram representing the setup of the experiment to measure the turnover rate of nups in the NPC is shown in **Fig. 3-4**. Since the cells are growing exponentially the turnover is always described by a steep exponential decay curve, even for proteins that do not degrade appreciably (because of growth dilution) (Pratt, Petty et al. 2002, Doherty, Hammond et al. 2009, Boisvert, Ahmad et al. 2012, Christiano, Nagaraj et al. 2014).

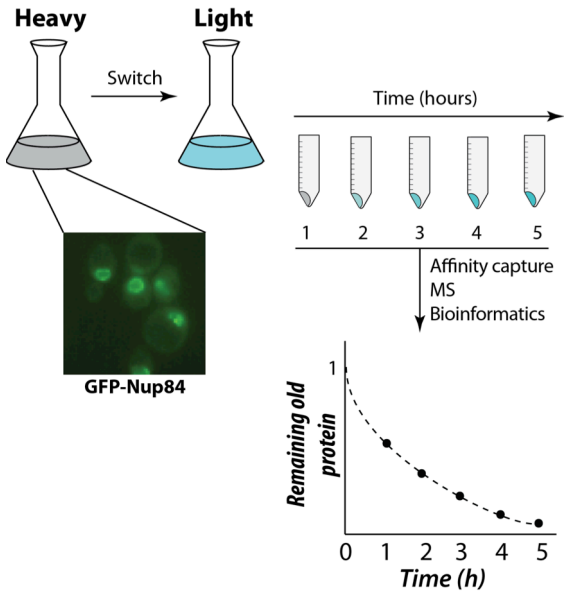

Figure 3-4: Diagram of nup turnover experiment. Firstly, the cells are completely heavy labeled. Next, the cells are switched to a light medium. The cells are grown for 5 h. Each hour a sample is harvested and flash-frozen. The frozen samples are disrupted and NPCs affinity captured through a GFP tag. The purified samples are analyzed by quantitative MS and the remaining old protein is plotted against time for each nup. An exponential curve is fit to the data to determine the decay rate and half-life.

Exchange experimental setup

The diagram representing the setup of the exchange experiment is shown in **Fig. 3-5**.

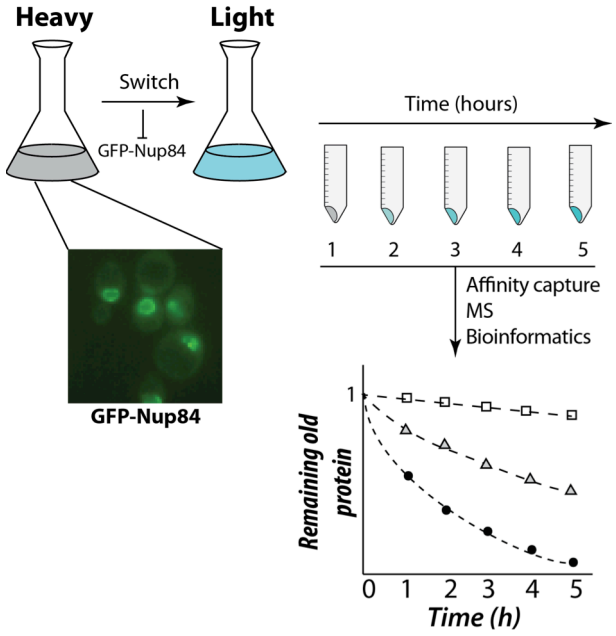

Figure 3-5: Diagram of the nup exchange experiment. Firstly, the cells are completely heavy labeled. Next, the cells are switched to light medium. Simultaneously, the expression of the GFP-tagged nup is repressed. The cells are grown for 5 h. Each hour a sample is harvested and flash-frozen. The frozen samples are disrupted and NPCs affinity captured through the GFP tag, which is still present in the "old" NPCs. The purified protein samples are analyzed by quantitative MS and the remaining old protein is plotted against time for each nup. An exponential curve is fit to the data to determine the decay rate and half-life.

I expect that three types of scenarios, describing slow, intermediate and fast exchange, may be observed:

1. The heavy protein decay constant obtained in the exchange experiment is the same as the one for the turnover experiment (black circles on the diagram). This would imply that the protein has a high rate of exchange.

2. The decay constant is very small (clear squares on the diagram). This means the protein does not exchange appreciably.

3. The decay constant is somewhere in between the two previous scenarios (grey triangles on the diagram). This would imply an intermediate exchange rate.

Premises of the experimental design

The analysis and interpretation of the data from the exchange and turnover experiments relies on several premises outlined below:

1. Heavy lysine labeling is complete;
2. Lysine label switch is quick and complete;
3. Repression of the tagged protein is quick and tight;
4. The affinity tagged protein does not exchange *in vivo*;
5. There is no *in vitro* exchange of nups during affinity capture;
6. The decay of old heavy labeled nups is a first order reaction.

I have individually tested and validated these premises as outlined in the following:

1. Heavy lysine labeling is complete

Incomplete labeling with heavy lysine can cause errors in my data analysis, this is because I assume that at t_0 the heavy label fraction = 1 (cells are completely labeled). It has been demonstrated that yeast cells can be labeled to near completion with isotopically heavy amino acids (Pratt, Petty et al. 2002, Fröhlich, Christiano et al. 2013). Most yeast metabolic labeling experiments have been performed with strains auxotrophic for the amino acids used in the labeling experiment (Jiang and English 2002, Pratt, Petty et al. 2002, Zhu, Pan et al. 2002, Gruhler, Olsen et al. 2005, Christiano, Nagaraj et al. 2014). In some cases prototrophic yeast strains have been used with successful heavy lysine incorporation (Fröhlich, Christiano et al. 2013). In my experiments I have used a lysine auxotrophic strain DF5 and achieved ~97% heavy lysine labeling efficiency (**Table 3-1**, AIR02, AIR03, ZH38 strains). However, when using a lysine prototrophic strain (YOL19 background), I found the labeling inefficient, at ~30% (**Table 3-1**, ZH31, ZH32 strains), indicating that despite the presence of lysine in the growth medium, cells continue to synthesize their own lysine. Perhaps, depending on the yeast background, lysine biosynthesis is repressed to different degrees (or takes longer to be affected) by lysine in the growth medium. However, deletion of the LYS2 gene rendered cells auxotrophic for lysine and produced ~99% labeling efficiency (**Table 3-1**, ZH42 strain); and it is this and similar strains that I have used throughout this study.

Table 3-1: Heavy lysine labeling efficiency of various strains tested in this study. For genotypes of strains see Chapter 7, **Table 7-1**. An aliquot of cells was lysed and the contents resolved on a gel. A small region of the gel corresponding to abundant proteins (37-50 KDa) was excised and analyzed by MS. Labeled fraction is calculated as the average heavy/ (heavy + light) intensity ratio for all observed peptides.

Strain	Background	Lysine auxotroph	Labeled fraction	Standard error
AIR02	DF5	Yes	0.970	0.025
AIR03	DF5	Yes	0.969	0.021
ZH38	DF5	Yes	0.961	0.034
ZH31	YOL19	No	0.312	0.008
ZH32	YOL19	No	0.288	0.006
ZH42	YOL19	Yes	0.991	0.004

2. Lysine label switch is quick and complete (after 1 h)

One concern with metabolic label switching experiments is that there may be a large pool of the "old" amino acid that will still be available for new protein synthesis, thus skewing the old protein decay measurements. To assess this, I employed a dual labeling strategy with arginine (R) and lysine (K) (**Fig. 3-6**) (Cambridge, Gnad et al. 2011). Consider completely heavy K labeled cells (K_H). Next, the cells are switched to light K (K_L) and heavy R (R_H):

$K_H \rightarrow K_L + R_H$.

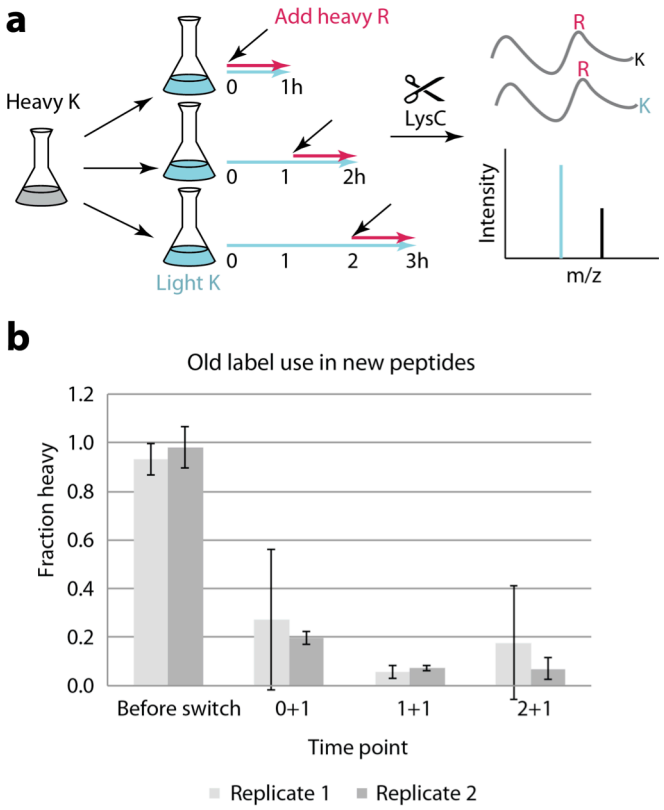

Figure 3-6: Measuring old label usage in protein synthesis in the first 3 h after the switch. a. Diagrammatic representation of the experimental setup. Firstly, cells are completely heavy lysine labeled. Then the cells are switched to light lysine and split into 3 cultures. The first culture gets a spike of heavy arginine immediately, the second – 1h after growth in light lysine, the third – 2h after growth in light lysine. The cells are grown for an additional hour after the spike to allow heavy arginine incorporation. Abundant lysate proteins from the three samples are subjected to quantitative MS and the heavy lysine fraction is quantified for peptides also containing heavy arginine, the "new" peptides. **b.** Heavy label fraction data described in (**a**) for two biological replicates. The data from a control sample collected before the light switch is shown for comparison. Each bar is an average of multiple proteins and the error bar is SEM. 4-6 proteins were analyzed for each sample in replicate 1. Whereas, the second replicate is an aggregate of ~50 proteins/sample and thus is more reliable.

In principle, two types of dipeptides can be synthesized K_HR_H or K_LR_H. The ratio of $K_HR_H/(K_HR_H + K_LR_H)$ will inform on the relative amount of old lysine label use in new protein synthesis (since all the heavy R containing proteins are new). The delay in between the light K switch and heavy R addition allows time for the old lysine pool to be used up. Note that light R is also present throughout the analysis, but the MS data can be filtered bioinformatically to only measure the peptides containing heavy R.

During the first hour after the switch I observed ~20% label recycling after which it dropped to a negligible level (~5%) (**Fig. 3-6b**). These data are in agreement with findings of a recent proteome-wide turnover study in yeast, which revealed that only ~2% of the surveyed proteins had a degradation half-life <1.25 h and 86% had a degradation half-life of ≥5 h (Christiano, Nagaraj et al. 2014). With little degradation the old lysine label largely remains bound in proteins and is unavailable for protein synthesis.

To avoid issues with residual lysine pool and label recycling I decided to not measure time points between 0 - 1 h in the analysis. Instead I started the time course at 1 h.

3. Repression of the tagged protein is quick and tight

If the affinity tagged protein (GFP-Nup84) takes a long time to be repressed or if the repression is incomplete then it will assemble into new NPCs artificially inflating the exchange rates of all nups. I use a tetracycline responsive riboswitch to rapidly repress the affinity tagged nup. When inserted in the 5' UTR

of the gene of interest the tetracycline binding aptamer acts as a synthetic riboswitch, repressing the translation of the cognate mRNA upon tetracycline binding. The high affinity binding between the aptamer and tetracycline and its derivatives, such as chlortetracycline (cltc), is thought to stabilize the mRNA structure and inhibit ribosomal engagement (Berens, Thain et al. 2001, Hanson, Berthelot et al. 2003, Xiao, Edwards et al. 2008). **Figure 3-7** is a diagrammatic representation of the wild type and conditional Nup84 expression with and without cltc.

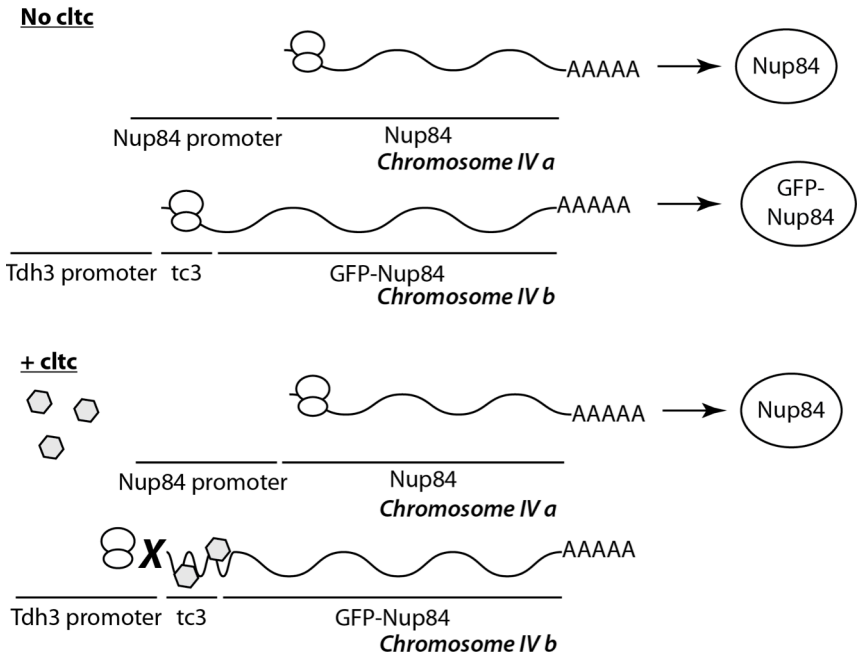

Figure 3-7: The expression of wild type and conditional alleles of Nup84 with and without cltc. The conditional allele is in the endogenous locus, although the gene promoter and 5'-UTR are replaced; tc3 encodes 3 tetracycline binding aptamers. Upon cltc addition, the binding of cltc to the aptamer inhibits ribosomal engagement and no more tagged protein is synthesized.

I chose to conduct the tests with cltc for its superior stability and binding to the aptamer (Muller 2006, Okerman, Van Hende et al. 2007). Cltc had negligible effect on the growth of wilt type cells and the cells where one copy of Nup84 has been repressed grew somewhat slower (not shown). When tested on the strain with conditional Nup84 expression, as expected, cltc had rapid, repressing effect (**Fig. 3-8a**). To assess how rapid and strong the repression was I employed a pulsed metabolic labeling approach (**Fig. 3-8b**). For the first three hours there was immediate and tight repression of the controlled protein expression (as evident by little new label incorporation), while at later time points very minor expression was observed. In the control experiment without cltc, rapid new label incorporation was observed.

Note that this experiment sets the duration limit for the labeling time course for two reasons: (i) there is no point in labeling for more than 5 h for the turnover experiment, because the light label fraction is at ~93%, making the heavy label fraction ~7%, which is at the limit of reliable MS detection (Beynon 2005); (ii) in the exchange experiment going beyond 5 h is problematic because the repression becomes slightly leaky.

I have also tested cltc repression with other tagged nups with similar efficiency (not shown).

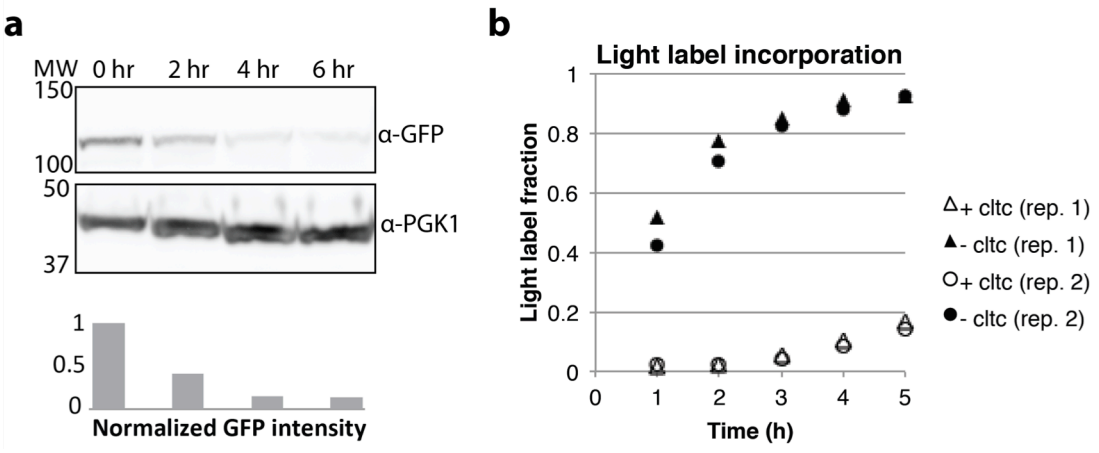

Figure 3-8: The use of cltc for conditional nup expression. a. Western analysis of a time course of the cltc responsive GFP-Nup84 strain in the presence of cltc for the indicated amount of hours. PGK1 was used as a loading control. The bottom chart shows the relative intensity of GFP-Nup84 (normalized to PGK1), which is consistent with quick repression and dilution by cell division. **b.** Light label incorporation with and without cltc. Cltc responsive GFP-Nup84 strain was first fully heavy labeled then pulsed with light label with or without cltc and the fraction of the incorporated light label was analyzed over time by quantitative MS. Two biological replicates are shown. Each point is an average of multiple peptides. Standard error of the mean (SEM, not shown) <10%.

4. The affinity tagged protein does not exchange *in vivo*

If the affinity tagged protein has a low stability in the NPC (high exchange rate), the exchange experiment will be compromised: even after the expression shut off the old GFP-tagged nup would exchange and reside in newly synthesized NPCs, thus artificially increasing the exchange rate of all nups.

Since it has been previously suggested that at least some core scaffold proteins may have low to negligible exchange rates (Rabut, Doye et al. 2004, D'Angelo, Raices et al. 2009, Toyama, Savas et al. 2013) I decided to tag a few representatives of each major sub-complex in the core scaffold: outer ring (Nup84, Nup120, Nup133), inner ring (Nup157, Nup170, Nup188 and Nup192),

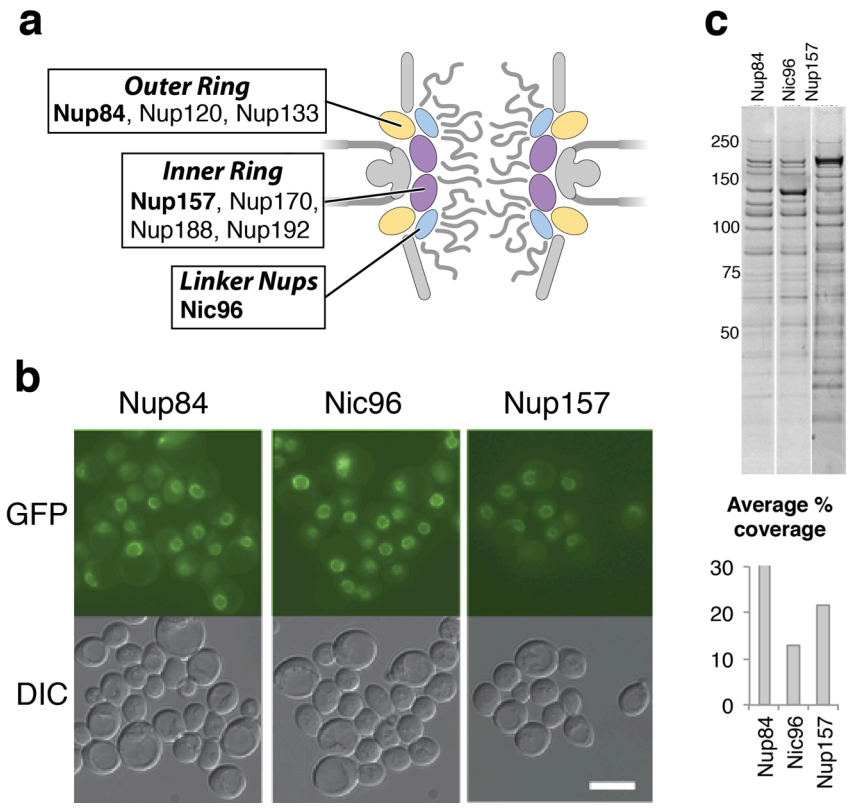

Figure 3-9: Picking an optimal scaffold component for affinity tagging and purification. a. Diagram of the NPC. The scaffold is colored and labeled. The proteins that have been tagged are indicated. **b.** Fluorescence microscopy confirmation of tagged nup localization. **c.** SDS-PAGE and MS analysis of NPC purification using the indicated tagged protein. The bar chart shows the average percent coverage (in the MS data) of co-purifying nups using the various tagged nups for whole NPC affinity isolation.

as well as their associated linker nup (Nic96) (**Fig. 3-9a**) (Alber, Dokudovskaya et al. 2007, Alber, Dokudovskaya et al. 2007). All proteins were successfully tagged and localized to the nuclear rim (3 representative strains shown **Fig. 3-9b**).

Next, I tested Nup84, Nic96 and all the inner ring proteins for NPC affinity capture. Nup84 AC worked well and co-purified the majority of nups (**Fig. 3-9c**; the NPC purification conditions and profiles have been discussed in Chapter 2). Most inner ring proteins failed to efficiently co-purify with other nups, even in a highly stabilizing condition (not shown), while Nup157 co-purified with numerous other nups albeit at a low relative stoichiometry (**Fig. 3-9c**). This behavior has been observed before for the inner ring proteins (Alber, Dokudovskaya et al. 2007). Nic96 produced a large excess of the handle protein and numerous co-purifying nups (**Fig. 3-9c**). In principle, all three proteins can be used in the assay; however Nup84 gave an excellent co-purifying nup yield (average peptide coverage ~30%), without a need for further optimization. Hence, I have performed all the tests with GFP-Nup84 tagged strains.

Running a pilot exchange experiment with GFP-Nup84 (not shown) revealed negligibly slow exchange rates for the majority of the scaffold, including Nup84, thus confirming that Nup84 is an optimal choice.

5. There is no *in vitro* exchange of nups during affinity capture

The exchange experiment will be inaccurate if nups exchanged between old and new NPCs in the lysate during the affinity capture. To test this I

performed an I-DIRT experiment (Tackett, DeGrasse et al. 2005). The experimental schematic is presented in **Fig. 3-10**. The results are presented in **Fig. 3-11**, red data points. There appears to be some minor *in vitro* exchange of constituents as evident by heavy label fraction values < 1, consistent with prior work (Oeffinger, Wei et al. 2007). To minimize this in vitro exchange, I have employed a published glutaraldehyde (GA) cross linking stabilization technique, **Fig. 3-11**, blue data points (Subbotin and Chait 2014). With cross linking the lysate mixing has been reduced to negligible levels (<5% - 10%).

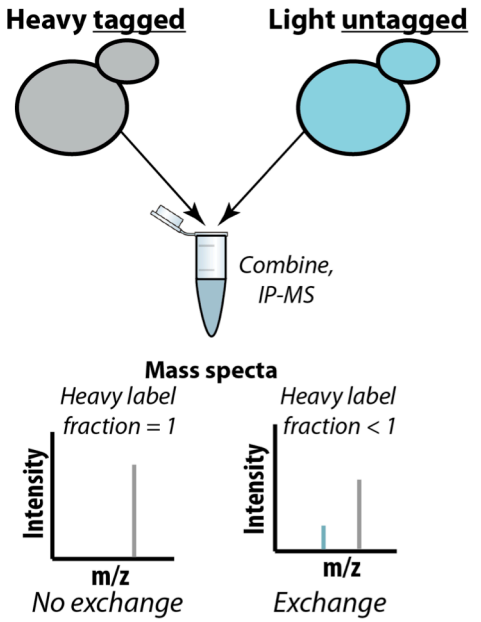

Figure 3-10: The schematic of an I-DIRT experiment. Firstly, the affinity tagged strain is grown in heavy medium and an untagged strain in light medium. The cells are mixed, lysed and subjected to affinity capture. The resulting sample is analyzed by quantitative MS. If there is no exchange between the tagged protein and a co-purifying protein then the protein will be completely heavy labeled (heavy label fraction = 1). If, however, the protein exchanges then the label will be mixed (heavy label fraction < 1).

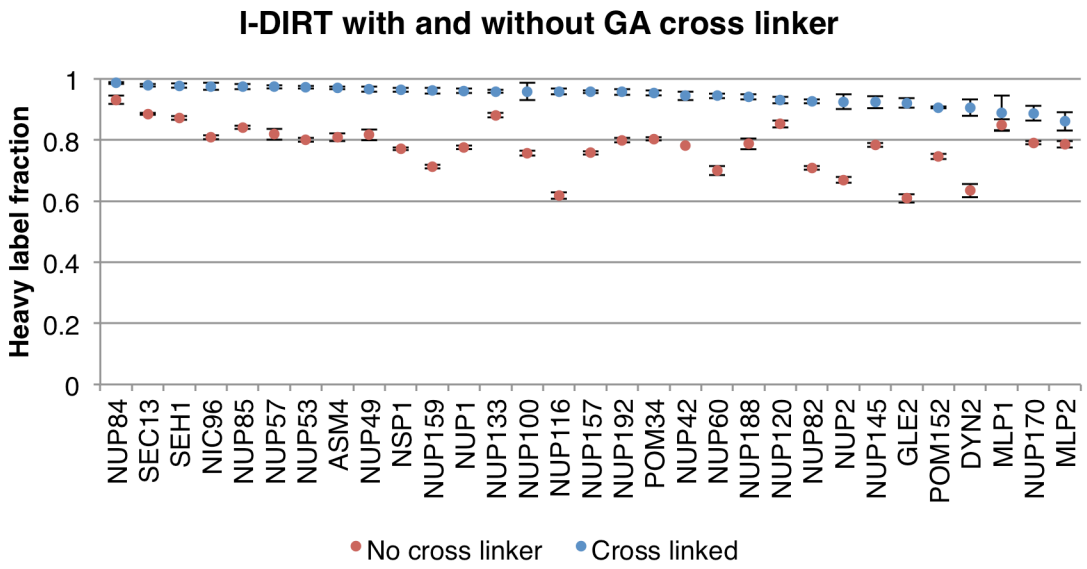

Figure 3-11: GFP-Nup84 I-DIRT with and without GA cross linker. Error bars are SEM of peptide measurements.

6. The decay of old heavy labeled nups is a first order reaction

A single exponential fit to the data can only be meaningful if the variable change obeys a first order reaction. That is, there is one major process influencing the remaining amount of the protein at any given time. Otherwise the data analysis would be more complicated. To assess if the turnover data for nups is a first order reaction I fitted a single exponential model for each nup time course data. The raw data from all the fits can be found in the Appendix (AIR02 strain). Two representative fits are displayed in **Figure 3-12**. The majority of nup data fits look like that of Nup57. The decay of the latter appears first order and intersects the hypothetical (0,1) starting point. In case of Nsp1 there is a delay of 1 h in the decay rate. After 1 h the decay of Nsp1 also becomes first order. It is

tempting to hypothesize that the delay is due to a large cytoplasmic pool, which takes longer to label with the light isotope. There is significant evidence in the literature that very large free pools of nups do not exist; estimates based on subcellular fractionation vary between ~5-20% for a free pool of nup compared with that bound to the NPC (Hurt 1988, Rout and Blobel 1993, Strambio-de-Castillia, Blobel et al. 1995, Rout, Aitchison et al. 2000). Curiously, a cytoplasmic pool of Nsp1 has been recently implicated in the inheritance of maternal NPCs by daughter cells (Colombi, Webster et al. 2013, Makio, Lapetina et al. 2013). However, preliminary Matlab simulations with Prof. Cross suggested that even a 100% pool would not produce such a delay in the decay time course. This implies that probably some nups take time to mature after synthesis. Indeed, early radioactive pulse-chase experiments with Nup62, mammalian Nsp1 homolog, indicate that after production Nup62 is incorporated with a half-life of 6 h (Davis and Blobel 1986).

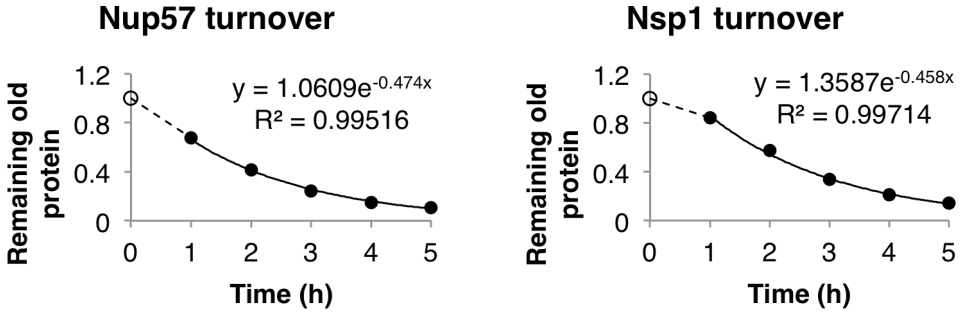

Figure 3-12: Turnover data and fit for two NPC components. Nup57 decay appears first order throughout the whole time course. For Nsp1 there is an hour delay before the reaction becomes first order. 0,1 time point is omitted from the fits.

Since nups do not have high degradation rates (Boisvert, Ahmad et al. 2012, Christiano, Nagaraj et al. 2014) the major influence on the heavy label decay is the dilution by growth. Indeed for most nups the turnover curve runs very closely with the dilution curve (reciprocal of growth). This will be discussed in more detail in Chapter 4.

I have also tested the first order reaction assumption for the exchange data. In this case the soluble pool of the tagged protein GFP-Nup84 can throw off the fit. If a large pool is present at the time of the expression shut off and label switch, it will continue assembling into new, light labeled NPCs thus artificially inflating the exchange rates of all the nups. This indeed appears to be the case during the first hour. **Figure 3-13** displays two representative fits. Nup57 fit has a steeper slope during the first hour and then it becomes shallow because the protein hardly exchanges out. Occam's razor suggests that during the first hour we see the contributions from the soluble GFP-Nup84 assembly into new NPCs. In case of Nsp1 this effect is much less pronounced presumably because the

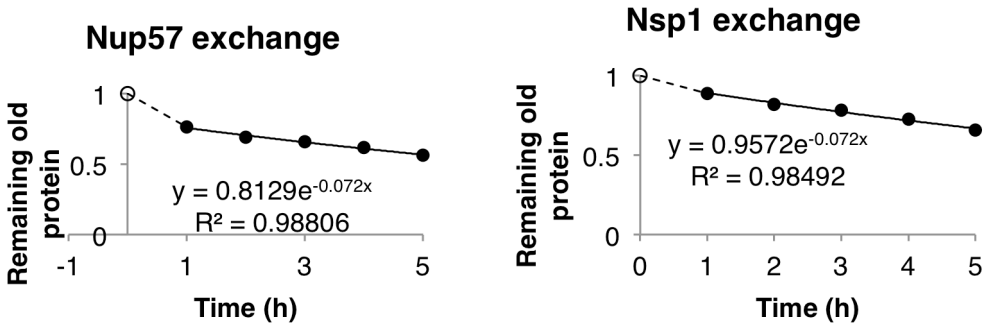

Figure 3-13: Exchange data and fit for two NPC components. 0,1 time point is omitted from the fit.

production of incorporation competent, mature Nsp1 takes as long as the depletion of the GFP-Nup84 pool.

Other considerations

In bakers yeast the density of NPCs in the nuclear envelope remains essentially unchanged throughout the cell cycle with a moderate peak in the S phase (Winey, Yarar et al. 1997, Khmelinskii, Keller et al. 2010). Because there are no apparent bursts of nup and NPC biogenesis I found it unnecessary to synchronize the cells by cell cycle stage. However, for all labeling experiments the cells were kept in the exponential phase. This provided for a nearly constant label incorporation and dilution rates, which is one of the assumptions of both turnover and exchange experiments.

Chapter summary

I have developed a metabolic labeling and selective tagging approach to analyze the turnover and exchange rates of NPC subunits. I have tested and validated the premises of my experimental design. Here is the summary of the inferences I will use in my data analysis:

1. directly before light label switch old (heavy) label fraction = 1;
2. after 1 h of growth all newly synthesized proteins are light labeled;
3. GFP-Nup84 repression is instantaneous and complete;
4. GFP-Nup84 does not exchange *in vivo*;

5. NPC subunits do not exchange during affinity purification;

6. after 1 h the heavy isotopic label decays with a first order reaction in both turnover and exchange experiments.

For the analysis of the turnover data I do not distinguish between free and bound nups. Since the major influence on the turnover is the dilution by growth any difference in the turnover rates of the free and bound nups will be marginal. For the analysis of the exchange data I assumed that once an old (heavy) subunit exchanges out of the old NPC it is infinitely diluted in the free light-labeled pool and does not go back on old NPCs (which also get diluted with time). I will discuss the validity of the later assumptions in the next chapter where I discuss the data and interpretation.

CHAPTER 4: NPC DYNAMICS

Chapter introduction

I will now discuss the results of the turnover and exchange experiments. To illustrate the process of data interpretation I would like to present two extreme case scenarios (**Fig. 4-1**). In the first scenario, a hypothetical "Nup A" never exchanges out once assembled into NPCs (**Fig. 4-1a**). In the turnover experiment, the heavy labeled fraction of Nup A is going to decay rapidly with time because of cell growth and new (light) labeled NPC assembly. However, in the exchange experiment the heavy protein fraction for Nup A will remain constant, since light labeled Nup A cannot exchange into existing old NPCs and the newly assembled light NPCs are not affinity captured. Thus the heavy label decay rates for Nup A will be very different in the turnover and exchange experiments. In the second scenario, a hypothetical "Nup B" exchanges instantaneously between the soluble pool and NPCs (**Fig. 4-1b**). Hence there is no separate assembly step for this protein. In the turnover experiment the heavy labeled fraction of Nup B will decay rapidly with time because of growth and NPC assembly. In the exchange experiment the heavy labeled fraction of Nup B will also decay rapidly, because Nup B freely exchanges between newly assembled light NPCs, soluble pool and old heavy labeled NPCs. Hence, the heavy labeled fraction of Nup B will decay with the same rate in either turnover or exchange experiments.

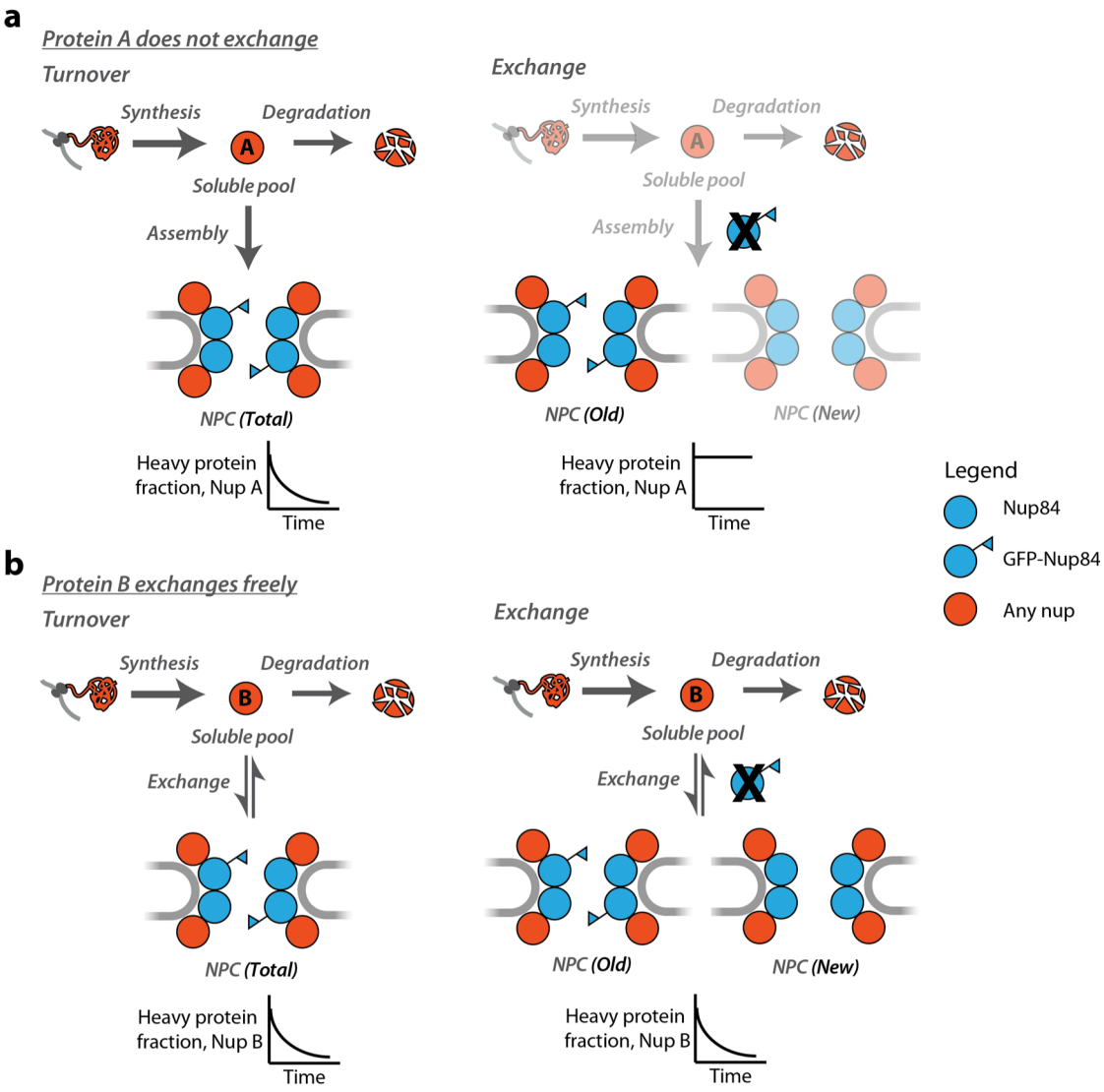

Figure 4-1: Hypothetical comparison of turnover and exchange for nups with different exchange rates. The old label is heavy and new label is light. In exchange experiments old NPCs refer to NPCs assembled before the label switch and GFP-Nup84 shut off and new NPCs – after. **a.** Comparison for a protein with 0 exchange rate. In the exchange experiment synthesis and degradation do not affect the heavy protein fraction of Nup A in old NPCs. New NPCs also do not have an effect, because they are not observed after the affinity capture. **b.** Comparison for a protein with fast exchange rate. Note that in the exchange experiment, new NPCs affect the rate of heavy label decay of Nup B in old NPCs, because Nup B freely exchanges with the soluble pool.

To a first approximation the decay rate of the heavy nup in the exchange experiment is the exchange rate of the nup between the soluble pool and NPCs assuming the following kinetic model:

$$NupL + NPC.NupH \overset{k}{\leftrightarrow} NPC.NupL + NupH \ (1),$$

where NupL is the light labeled soluble Nup, NPC.NupH is the old complex bound to heavy Nup, NPC.NupL is the old NPC bound to the light Nup and NupH is the heavy labeled soluble Nup. Both reactions have the same rate constant k (because it is the same reaction except for the label of proteins). From Equation (1) the change of the heavy Nup bound NPC with time can be expressed as:

$$\frac{dNPC.NupH}{dt} = k * [NupH] * [NPC.NupL] - k * [NPC.NupH] * [NupL] (2).$$

Making the following assumptions:

[NupL] = const, the concentration of the free light labeled nup is constant;

[NupH] ≈ 0, there is very little of the free heavy nup at any given time;

equation (2) reduces to:

$$\frac{dNPC.NupH}{dt} = -k * [NPC.NupH] \ (3).$$

Solving the differential equation with respect to time:

$NPC.NupH(t) = C * e^{-k*t}$ (4).

Setting the boundary condition NPC.NupH(0) = 1 (all bound nups are heavy labeled at time 0) we get:

$NPC.NupH(t) = e^{-k*t}$ (5).

I have used equation (5) for estimating the exchange rate of nups. However, the model works better for slow exchanging proteins, as for quickly exchanging proteins [NupH] ≈ 0 assumption is violated, which is why I cannot estimate the exchange rates of rapidly exchanging nups with this model. I am in the process of developing a kinetic model to address this issue, which incorporates the turnover rate of nups into the exchange experiment analysis.

Nonetheless, combining the two approaches, the kinetic model for slowly exchanging proteins and the direct comparison of decay rates in the turnover and exchange experiments for quickly exchanging proteins, provides information about all NPC subunits, regardless of exchange magnitude.

What are the exchange rates of nups?

If the reasoning presented in the introduction for discerning fast exchangers by comparing the heavy fraction decay between the exchange and turnover experiments is correct, then a key prediction is that transport factors, known fast exchangers of the NPC (Ribbeck and Görlich 2001, Smith, Slepchenko et al. 2002, Yang, Gelles et al. 2004, Yang and Musser 2006), should have identical heavy decay rates in both turnover and exchange experiments. The half-life of heavy protein decay in exchange vs turnover experiments is plotted in (**Fig. 4-2,** all the raw data is in the , AIR02 strain). We observe that for nups (blue circles) the heavy label decays over a much longer time ~2-15 h in the exchange experiment, than in the turnover experiment ~1.5-2

h. Whereas in the case of transport factors (red circles) the heavy label decay rates are indistinguishable in exchange and turnover experiments at 0.05 significance level. This means that my assay can sensitively distinguish fast-exchangers from stable residents of the NPC. Moreover, for those slow exchangers (**Fig. 4-2**, labeled “Slow” on the graph) the decay rate in the exchange experiment is a good estimate of exchange rates between the soluble pool and NPCs. While, for rapidly exchanging nups (**Fig. 4-2**, labeled “Fast” on the graph), the decay of the old protein in the exchange experiment is not a good estimate of soluble pool – NPC exchange rates. For those nups, assuming the light nup synthesis to be the rate-limiting step (few minutes) (Boehlke and Friesen 1975, Waldron and Lacroute 1975), the exchange rate is approximately estimated to be minutes to seconds, similar to that of transport factors. Finally for intermediate exchangers (**Fig. 4-2**, labeled “Intermediate” on the graph) the decay of the heavy label in the exchange experiment is an approximate representation of exchange rates. These results are highly reproducible: the Pearson correlation coefficient between the two biological replicates is 0.97, p-value = 1.82E-20.

The residence half-lives of nups in the two replicate exchange experiments are presented in **Table 4-1**.

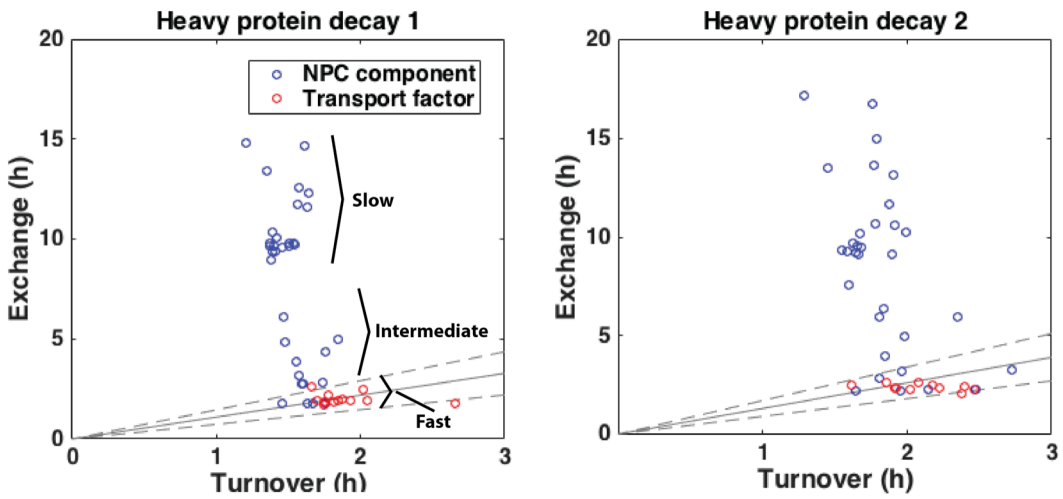

Figure 4-2: The analysis of heavy protein decay half-lives in exchange and turnover experiments. Half-life is calculated as ln(1/2)/k, where k is the fitted decay constant from the exponential model. Two biological replicates are shown. Nups and transport factors are plotted separately. The gray lines are average ± 2 standard deviations calculated for the reference distribution of abundant co-purifying proteins used in the statistical analysis.

Table 4-1: Table with Nup exchange half-lives. Average and standard deviation of exchange half-lives are presented for two biological replicates. Residence half-lives of mammalian nups are presented next to yeast homologs (Rabut, Lénárt et al. 2004).

Protein	Average T_{half} (h)	Standard dev. (h)	Classification	Rabut *et. al* 2004
NUP84	16.0	1.7	Slow	28 h
NUP145C	15.7	1.6	Slow	
NUP120	13.8	1.7	Slow	
NUP133	13.5	0.1	Slow	31 h
SEH1	12.8	0.6	Slow	28 h
NUP85	12.7	1.3	Slow	29 h
SEC13	11.7	0.1	Slow	39 h
NUP188	10.2	0.6	Slow	
NUP170	10.2	0.1	Slow	
NUP82	10.2	0.8	Slow	
POM152	10.0	0.6	Slow	3.0 min
NSP1	10.0	0.4	Slow	9.0 h
NIC96	9.7	0.0	Slow	49 h
NUP192	9.6	0.1	Slow	
NUP49	9.5	0.4	Slow	5.6 h
NUP159	9.5	0.5	Slow	30 h
NUP57	9.4	0.4	Slow	
NUP157	9.3	0.0	Slow	
POM34	9.1	0.2	Slow	
ASM4	8.5	1.3	Slow	3.7 h
NUP53	6.0	0.1	Intermediate	
NUP100	5.6	1.1	Intermediate	2.0 h
NUP145N	3.9	0.1	Intermediate	
NUP116	3.0	0.4	Intermediate	
MLP1	5.5	0.6	Intermediate	
MLP2	4.6	0.4	Intermediate	
GLE2	3.1	0.2	Intermediate	
GLE1	3.0	0.3	Intermediate	
NUP42	2.9	0.2	Intermediate	5.3 h
NUP2	2.1	0.3	Fast	14 s, 2.3 min
DYN2	2.1	0.4	Fast	
NUP1	2.0	0.3	Fast	18 s, 9.0 min
NUP60	2.0	0.3	Fast	
NDC1	2.0	0.2	Fast	

From the graph in **Fig. 4-2** and values in **Table 4-1** we can observe that more than half of nups (20 out of 35) have long residence times at the NPC: once they are assembled they are essentially not taken out any more. Some nups (10 out of 35) have intermediate residence times: once assembled into NPCs, those proteins are periodically replaced over a few hours. And finally, for a few nups (5 out of 35) the exchange is remarkably fast (estimated residence times minutes to seconds).

What are the degradation rates of nups and how do they compare to co-purifying non-NPC proteins?

To assess this I represented degradation with the following formula:

$K_{deg} = K_{loss} - K_{dil}$,

where K_{loss} is the heavy label fraction decay constant (exponential data fit in the turnover experiment) and K_{dil} is the reciprocal of cell division rate. Assuming 2 h doubling time:

$$\mathrm{Kdil} = \frac{\ln\left(\frac{1}{2}\right)}{2}$$

Meaning that as cells double, their contents doubles and the existing heavy label is diluted by ½ with the light label. Thus, for any given protein, assuming no degradation, the heavy label fraction would halve in that same period. The half-life is calculated as:

$$t = \frac{\ln(1/2)}{Kdeg}$$

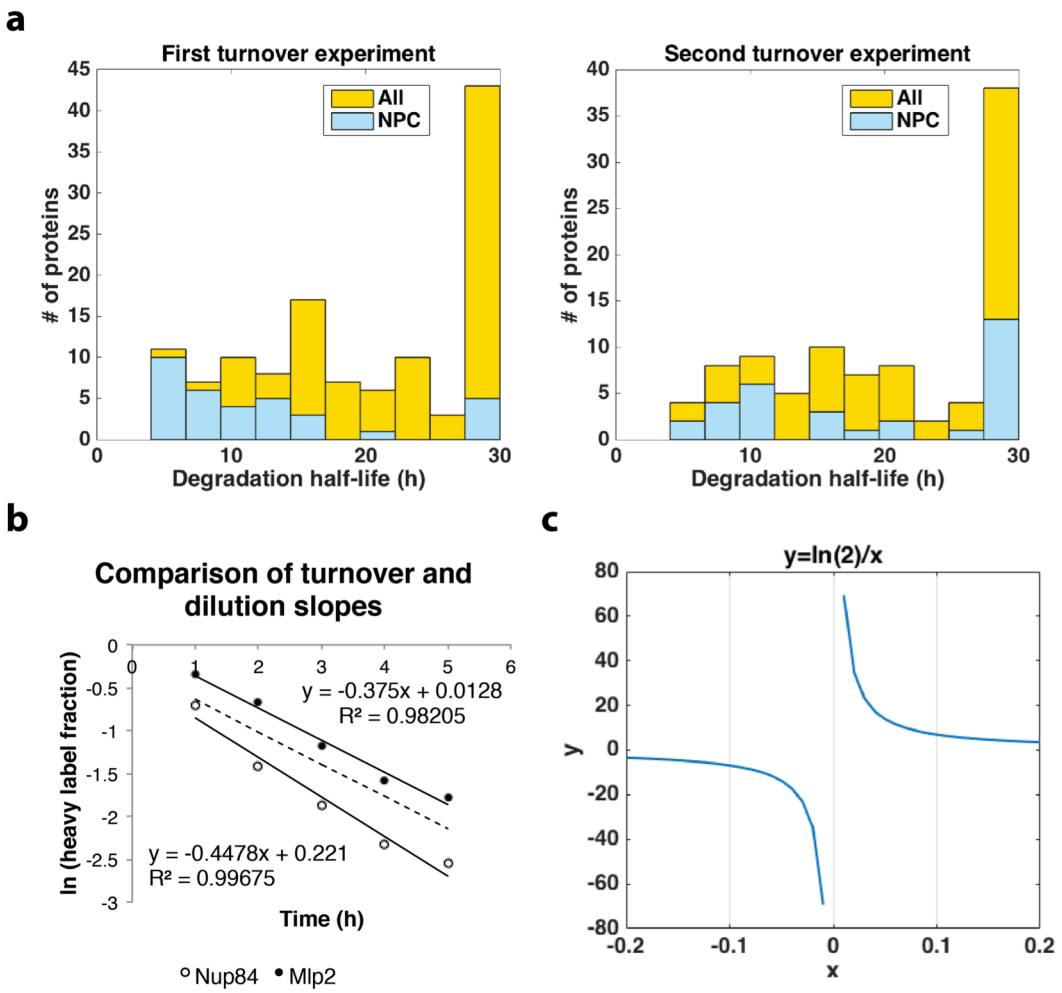

Figure 4-3: The analysis of protein degradation in the turnover experiment. a. Frequency distribution of degradation half-lives of proteins observed in the turnover experiments (two biological replicates). The data was first filtered for abundance (≥ 4 peptide identification per time point on average) then for fit quality (R squared > 0.85). NPC components are shown with all the co-purifying proteins. **b.** Plot of heavy decay fraction over time after log transformation for two representative nups. The slope of the lines corresponds to the turnover coefficients. Note that the values are negative because the heavy label fraction is < 1. The dashed line represents the dilution by cell division; the slope is the dilution coefficient. **c.** Plot of y=ln(2)/x function.

Note that the 2 h doubling time was assumed for illustration purposes. For my calculations I have estimated the division rate based on the average turnover rate of slowest 30 non-NPC co-purifying proteins.

Based on results of Christiano et al., 2014 we do not expect nucleoporins to have appreciable degradation rates, e.g. half-lives < 2 cell cycle. To compare the degradation rates of nups with other co-purifying proteins I have plotted the half-life distributions for the two replicates (**Fig. 4-3a**). Both distributions are enriched for long-lived proteins (half-life > 2 cell cycles), in which case the heavy label loss is largely dictated by cell growth dilution (Christiano, Nagaraj et al. 2014).

I did not observe any protein with half-life < 2h and the proteins identified in Christiano et al., 2014. as fast degrading proteins were absent from my datasets (Christiano, Nagaraj et al. 2014). It is likely that the reason for the bias towards long-lived proteins is that fast turnover proteins tend to have lower abundance (Boisvert, Ahmad et al. 2012) and the non-specific “passengers” in IP experiments tend to be abundant and stable proteins (Mellacheruvu, Wright et al. 2013).

I have tabulated the calculated Nup degradation half-lives in two biological replicates and present it with values from Christiano *et al*. in **Table 4-2**. Degradation data appears more variable than the exchange data. The reason for that is an extra transformation step (extra source of error). In order to get the

degradation constant K_{deg} I need to subtract the dilution coefficient from the turnover coefficient (**Fig. 4-3b**). Sometimes this results in a negative degradation constant, which does not have a biological meaning. **Fig. 4-3c** demonstrates how a small error in either the turnover data fit or growth rate estimation can result in a large error in the half-life calculation, because y=ln(2)/x function approaches the y-axis asymptote as x approaches 0. So the smaller is the degradation half-life, the more difficult it is to measure it accurately. Overall, the degradation values I measured agree with the estimates of Christiano *et al*. The GFP-tagged Nup84 appears to have a slightly shorter half-life than the other nups. One possible explanation for this observation is that overexpression of GFP-Nup84 from a strong exogenous promoter (TDH3) leads to a higher degradation rate. It has been observed that the excess unincorporated GFP tagged Nup107, the mammalian homolog of Nup84, is degraded more rapidly than the NPC bound Nup107 (D'Angelo, Raices et al. 2009). Moreover, downregulating the level of a single outer ring member protein by siRNA in mammalian cells has been shown to affect the level of other members of the outer ring complex (Walther, Alves et al. 2003).

Table 4-2: Nup degradation half-lives in two turnover experiments and from a proteome-wide turnover study (Christiano, Nagaraj et al. 2014). Values denoted by >30 h means decay too slow for accurately estimation.

Protein	Deg. half-life 1 (h)	Deg. half-life 2 (h)	Christiano *et al*. (h)
NUP84	4	4	11
NUP133	5	5	8
NUP49	6	8	12
NIC96	6	9	10
POM34	6	10	9
ASM4	6	8	10
POM152	6	10	9
NUP57	6	11	11
NUP157	6	7	10
NUP170	6	11	11
NUP192	7	11	8
NUP1	7	10	5
NUP53	7	21	8
NUP100	8	26	
NUP82	9	17	9
NUP188	9	>30	8
NUP159	10	>30	10
NSP1	10	>30	9
NUP145N	11	28	9
NUP145C	11	16	
NUP85	12	17	8
GLE1	12	21	8
NUP120	12	19	10
NUP116	13	>30	11
NUP42	14		9
SEC13	15	>30	13
NUP60	16	>30	8
SEH1	17	>30	10
DYN2	20	>30	8
GLE2	>30	>30	11
MLP1	>30	>30	8
MLP2	>30	>30	7
NDC1	>30		
NUP2	>30	>30	12

This implies that a change in stoichiometry of the NPC constituents, which may result from one subunit overproduction, is probably undesirable for the cell. Curiously, the immediate binding partner of Nup84, Nup133, had the second highest degradation rate in both experiments (**Table 4-2**). This suggests that the expression of Nup84 and some other nups may be co-regulated. But, most importantly, based on values in **Table 4-2** none of the protein has experienced a large degree of turn over by the 5 h time point. So I can still reliably measure the heavy labeled fraction.

Summary of degradation data observations

The majority of the proteins in my purification are long lived. The half-lives that I have measured for nups are similar to the published reference. Except for two proteins, Nup84 and Nup133, nup degradation half-lives are longer than the duration of my experiment. Even for Nup84, at 5 h time point the heavy label fraction has not turned over. Thus degradation does not have an appreciable effect on turnover or exchange of nups.

How do my results compare to other nup dynamics studies?

There has been only one study, which analyzed the exchange rates of the majority of nups. Rabut *et al*. tagged and exogenously expressed 19 nups with 3EGFP (triple enhanced GFP) and analyzed the dynamics with a fluorescence assay in mammalian cells (Rabut, Doye et al. 2004). In **Table 4-1** I have

presented all the vertebrate nup residence half-lives that have yeast homologs and were measured in the Rabut *et al*. study. There is a remarkable agreement between yeast and vertebrate data (Pearson correlation 0.58, P-value = 0.04), despite 1.5 billion years of divergence between fungi and animals (Taylor and Berbee 2006) and the use of completely different experimental approaches. Although I was not able to measure the exchange rates of Nup2, Nup1 and Nup60, my assay has placed those proteins in the seconds to minutes exchange regime, which are the values observed in the mammalian system. The only protein that appears to have significantly different exchange rate is Pom152, which is a slow exchanger in my experiments while its ortholog Nup210 exchanges in minutes in the mammalian study. It is possible that the high mobility of the protein in the mammalian study is a result of overexpression or tagging. However, it is also possible that Nup210 does not play a constitutive structural role in the mammalian NPC as it is expressed in a tissue-specific manner (Olsson, Schéele et al. 2004, D'Angelo, Gomez-Cavazos et al. 2012).

In addition to this one fluorescent study on the mammalian NPC, my results are in agreement with multiple orthogonal studies, discussed below.

The stability of scaffold proteins in my study is in agreement with a fluorescent study in *C. elegans* (D'Angelo, Raices et al. 2009) and a metabolic labeling study in rats (Toyama, Savas et al. 2013). While these studies could not directly measure or distinguish turnover from exchange, the latter study identified some members of the inner ring, outer ring and linker nups as exceptionally

stable proteins even after 9-12 months. Interestingly, in this study the members of the inner ring and linker nups were shown to be more stable than the outer ring. In my analysis, the members of the outer ring nups (first 7 protein in **Table 4-1**) appear as the most stable proteins, which is expected, since the affinity tagged protein, Nup84, is in the outer ring. Hence, if Nup84-GFP exchanges out, even marginally slowly, it would appear that the proteins around it, such as the inner ring and linker nups, are exchanging faster (**Fig. 4-4**).

One way to test if this is the case would be to use a member of the inner ring or a linker nup as an affinity handle. Indeed, my preliminary studies with GFP-Nic96 (linker) as an affinity handle are consistent with a more stable Nic96 and inner ring (not shown). However, since Nup84 exchange is so slow, it is an

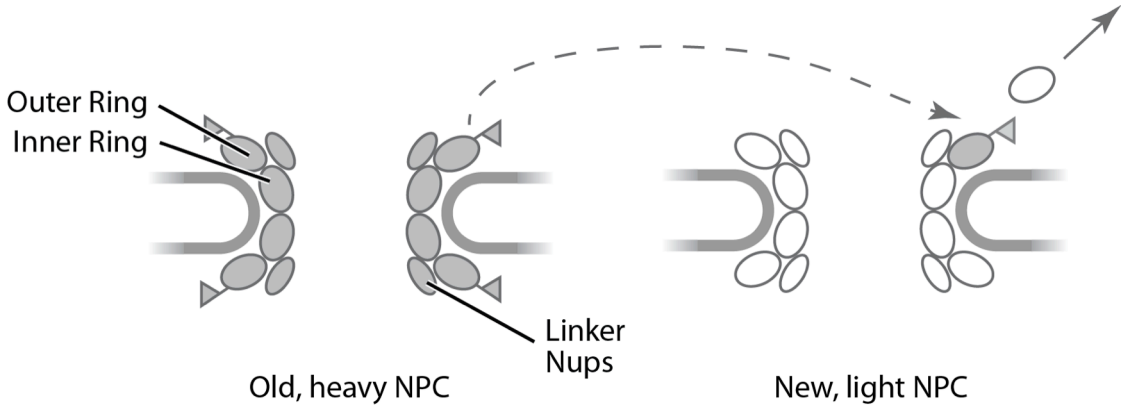

Figure 4-4: A hypothetical diagram of the Nup84 complex (outer ring) exchange between NPCs. For simplicity, only the scaffold is shown. On the left there is a heavy labeled, old NPC, which contains GFP-Nup84 in the outer ring (oval with the flag); on the right there is a new, light labeled NPC. If the Nup84 complex exchanges out, then in my assay it would appear that the entire scaffold has exchanged, since the new, light labeled NPC will be affinity purified.

acceptable trade off for the superior yield and quality of the affinity capture (only 8 nups were reliably measured in GFP-Nic96 affinity capture). However, I will complete the GFP-Nic96 studies, as these may help calibrate those from the GFP-Nup84 studies.

The majority of proteins identified as intermediate exchangers in my study (**Table 4-1**) are known or suspected dynamic members of the NPC or transport factors. The mammalian homolog of Nup100/Nup116/Nup145N, Nup98, displays transcription-dependent mobility at the NPC, potentially implicating this protein in guiding mRNAs to NPCs (Griffis, Altan et al. 2002). Gle2 is a shuttling RNA export factor / nup, which associates with Nup116 (Murphy, Watkins et al. 1996, Pritchard, Fornerod et al. 1999). Gle1 is also a shuttling mRNA export factor / nup, which binds to Nup42 on the cytoplasmic face of the NPC (Strahm, Fahrenkrog et al. 1999, Kendirgi, Rexer et al. 2005).

The majority of fast exchangers identified in my study (**Table 4-1**) are also known mobile members of the NPC or transport factors. For example Nup2, which was originally identified as an NPC component, but later, was also shown to be a cofactor for karyopherin α:β import and recycling (Dilworth, Suprapto et al. 2001, Lindsay, Plafker et al. 2002, Matsuura and Stewart 2005). Moreover, this protein was demonstrated to be mobile with a fluorescent heterokaryon assay (Dilworth, Suprapto et al. 2001). Among fast exchangers in my assay was Nup60, the anchor point for Nup2 (Denning, Mykytka et al. 2001, Dilworth, Suprapto et al. 2001), which has been recently shown to be a dynamic nup in a

ubiquitylation dependent manner (Niño, Guet et al. 2016). Nup153, the mammalian homologue of Nup60 and its paralog Nup1, has been shown to shuttle between the nuclear and cytoplasmic faces of the NPC (Nakielny, Shaikh et al. 1999) and its dynamics was dependent on ongoing transcription (Griffis, Craige et al. 2004). Nup1 and Nup60 also serve as two of the identified anchors for basket proteins Mlp1 and Mlp2 (the other anchor is Nup84), which might explain the mobility of the basket (Niepel, Molloy et al. 2013). The other fast exchanger, Dyn2, is potentially a transient interactor of the NPC. It acts as molecular glue to dimerize the Nup82 complex. Moreover, Dyn2 molecules can polymerize to aid in the assembly process (Stelter, Kunze et al. 2007, Stelter, Kunze et al. 2012, Gaik, Flemming et al. 2015). Hence the association of this protein with NPCs can be variable.

Finally, Ndc1, a transmembrane nup, was also identified as a fast exchanger in my study. Ndc1 is an essential protein, which is shared between the NPC and spindle pole body and is involved in the assembly and insertion of both complexes in the pore membrane ((Chial, Rout et al. 1998, Araki, Lau et al. 2006, Madrid, Mancuso et al. 2006, Onischenko, Stanton et al. 2009, Casey, Dawson et al. 2012) and references therein). It is possible that Ndc1 acts on the initial stages of NPC assembly and insertion, and once other NPC members have stabilized the pore membrane (reviewed in (Fernandez-Martinez and Rout 2009, Doucet, Talamas et al. 2010, Capelson, Doucet et al. 2011) it can leave the complex or exchange out.

In summary, my nup dynamics results are in good agreement with characterized physiological functions and dynamics of nups in the literature, though they now provide the first comprehensive analysis of the dynamics of components at the NPC.

How do nup exchange rates relate to the location of nups within the NPC?

To gain a better understanding about the relative location of stable and mobile nups within the NPC I mapped the average nup residence half-lives onto the NPC structure from the Alber *et al*. publication (Alber, Dokudovskaya et al. 2007) (**Fig. 4-5**). Nups can be classified as either belonging to a core scaffold structure, or to a set of more peripherally associated nups that are attached to the scaffold (Alber, Dokudovskaya et al. 2007) (see Chapter 1, **Fig. 1-3** for reference). Notably, we observe that the inner scaffold, composed of the outer ring, inner ring and linker nups is largely stable with residence times of 8-16h. The periphery, comprising FG Nups, the cytoplasmic filaments, transmembrane ring and nuclear basket, is where the major variation of nup mobilities is observed. Those FG-nups that are symmetrically distributed are largely stable, with the exception of Nup53, which faces the membrane and has a residence half-life of 6 h. Curiously, Nup53 has differential affinity for two of its interaction partners Nup170 and Nic96 (both scaffold proteins) during different stages of the cell cycle (Lusk, Makhnevych et al. 2002, Makhnevych, Lusk et al. 2003). This

molecular rearrangement might be responsible for its slightly increased mobility (see also Chapter 6 discussion).

The asymmetrically distributed FG-nups are highly dynamic, with the exception of Nup159 (cytoplasmic), which is as stable as the scaffold. The stability of central channel FG-nups (Nsp1, Nup49, Nup57) and Nup159 (cytoplasmic FG-nup) is consistent with the structure of modules containing those proteins. Nup49, Nup57 and Nsp1 form a well-characterized trimeric coiled-coil interaction and bind Nic96, a scaffold protein (Grandi, Schlaich et al. 1995, Schlaich, Häner et al. 1997, Bailer, Balduf et al. 2001). The Nup82 (scaffold)–Nsp1–Nup159 complex is also formed with a trimeric coiled-coil interaction (Belgareh, Snay-Hodge et al. 1998, Bailer, Balduf et al. 2001, Gaik, Flemming et al. 2015). Presumably, repeated breaking and making of those strong interactions would be energetically unfavorable. In contrast to stable, symmetric FG-nups, the dynamic FGs Nup100, Nup116 and Nup145N (3 paralogs) (Teixeira, Siniossoglou et al. 1997) associate with the scaffold via weaker interactions (Fischer, Teimer et al. 2015). Moreover, those proteins have multiple alternate binding sites (Nup82 complex and Nup84 complex) and compete with each other for binding (Robinson, Park et al. 2005, Ratner, Hodel et al. 2007, Yoshida, Seo et al. 2011).

The membrane ring composed of three transmembrane nups shows great variation of half-lives. Two of the three proteins are highly stable, similar to the scaffold, and Ndc1 is highly mobile. The structural reason for this difference is

unknown as the three transmembrane nups bind one another and scaffold proteins (Alber, Dokudovskaya et al. 2007, Alber, Dokudovskaya et al. 2007, Onischenko, Stanton et al. 2009).

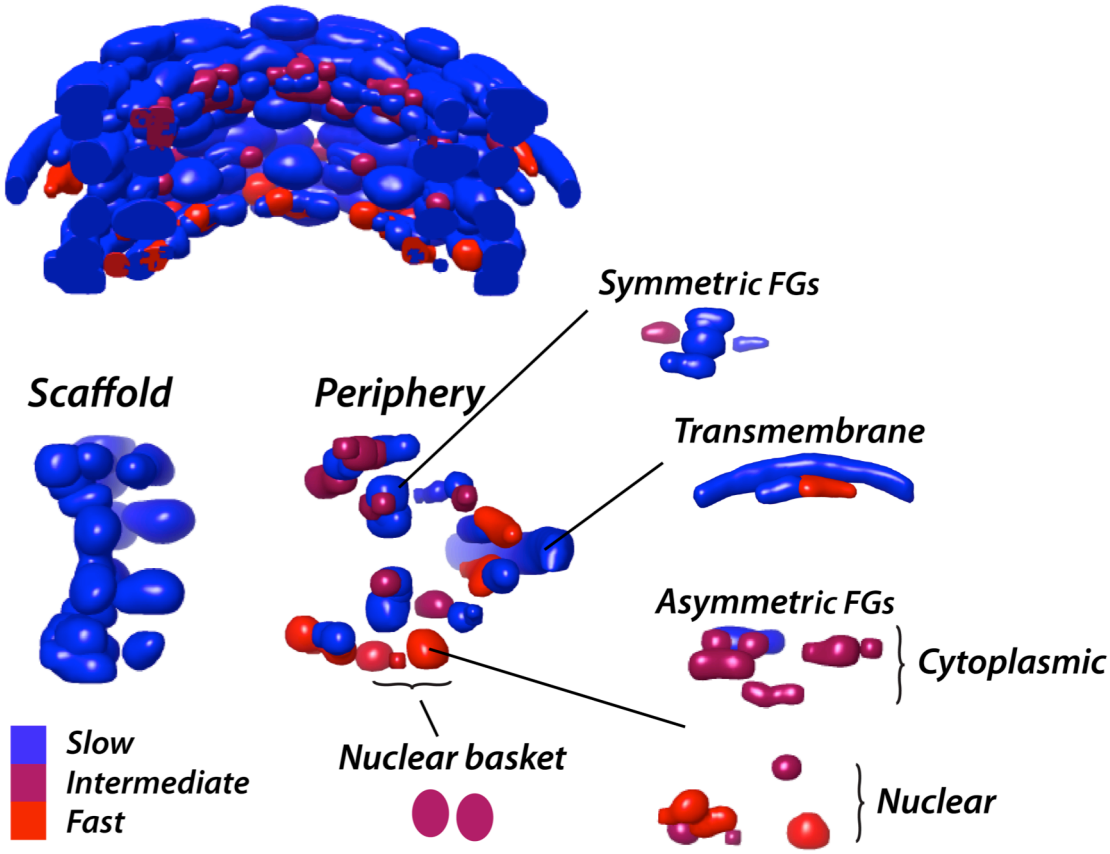

Figure 4-5: Heat map of the relative mobility of nups. Slow exchangers are in blue (8-16 h residence half-life); intermediate exchangers are purple (3-6 h residence half-life); the fast exchangers are in red (minutes to seconds). The whole structure is split in two parts: the scaffold and the periphery. The scaffold consists of inner ring, outer ring and linker nups and is entirely stable. The periphery is split into functional protein groups.

Although it has not been characterized in detail how the remaining asymmetric FG-Nups Nup42, Nup1 and Nup60 bind the scaffold, based on the domain prediction for those proteins their interactions likely occur through flexible loops or short folded surfaces and are not strong (Devos, Dokudovskaya et al. 2006, Schwartz 2016). Nup1 and Nup60 have also been implicated in membrane binding interactions (Mészáros, Cibulka et al. 2015).

The nuclear basket, which was not included in the original structure and is represented by two ovals, is highly dynamic. Protein truncation analyses have narrowed down the NPC binding site to only a ~300 amino acid stretch in the flexible region, where there is a discontinuity of coiled coil domain (Niepel, Molloy et al. 2013). This is also consistent with a weaker interaction.

Summary of nup dynamics comparison with the location and function

One of the patterns observed from my nup dynamics data is that peripheral components (including FG nups), which form strong interactions with the scaffold, are stable; whereas the peripheral components, which likely form weaker interactions with the scaffold are dynamic. ~2/3 of nups identified as intermediate or fast exchangers in my study are characterized either as FG-nups or transport factor like nups. Based on those observations, we wondered whether the scaffold interactions are a major determinant of nup dynamics, and if transport flux and its interaction with the FG repeat regions has a destabilizing effect on peripheral nups. I will address these questions in the next chapter.

CHAPTER 5: NPC DYNAMICS PERTURBATION

Chapter introduction

In the previous chapter I have mapped the relative stability of the nuclear pore proteins within the structure of the NPC. One of my key observations was that the strong interaction with the scaffold is a possible cause for the stability of nups, as proteins strongly associated with the scaffold exchange at the slowest rate. How can I test this observation? An immediate prediction from the scaffold interaction strength as a cause for stability is that increasing the strength of the interaction of a peripheral protein with the scaffold will slow down its mobility.

Another observation I made is that all asymmetrically distributed FG-nups with the exception of Nup159 are highly dynamic. Is it possible that the transport flux of 1000/sec (Ribbeck and Görlich 2001, Smith, Slepchenko et al. 2002, Yang, Gelles et al. 2004, Yang and Musser 2006) also influences this dynamics by "sweeping" FG-nups that are not bound by strong interactions out of the NPC? A prediction from this conjecture is that eliminating the binding between transport factors and a rapidly exchanging FG-nup will slow down the exchange of the latter. I have tested both propositions concerning the scaffold and transport influences and the results are presented in this chapter in two parts.

Part 1: Increasing the interaction strength of a mobile nup with the scaffold slows it down.

Design of the yeast strain for scaffold interaction test

To determine whether it is the slow or fast exchanging behavior that dominates, we could engineer a strong interaction between two nups, one of which shows slow exchange and the other fast. The simplest way to increase the interaction strength between two proteins is fusing them. For this I needed to identify appropriate fusion partners with the following characteristics:

1. One protein is mobile, the other is stable.
2. The proteins normally bind each other in the NPC.
3. The fusion does not significantly perturb the NPC function.

Point 2 is important to minimize the restructuring of the NPC architecture, e.g. by fusing two proteins that do not normally interact. Points 2 and 3 are important to minimize pleiotropic effects.

Fortuitously, such a pair exists in nature. Nup145 is an evolutionarily conserved, essential nucleoporin with an interesting maturation pathway: it is synthesized as a full-length precursor protein, which undergoes autocatalytic cleavage *in vivo* to generate two proteins with distinct functions. The N-terminal half of Nup145 is an FG-nup, which is biased towards the nuclear side and is mobile, and the C-terminal piece forms part of the outer ring (Nup84 complex) and is stable (Emtage, Bucci et al. 1997, Teixeira, Siniossoglou et al. 1997, Teixeira, Fabre et al. 1999, Rout, Aitchison et al. 2000). Nup145N and Nup145C

interact at the NPC after cleavage, although the evidence is largely *in vitro* ((Hodel, Hodel et al. 2002, Ratner, Hodel et al. 2007) and Fernandez-Martinez *et al.* submitted). The cleavage itself is not essential for growth or localization to the NPC in either baker's or fission yeast (Emtage, Bucci et al. 1997, Teixeira, Siniossoglou et al. 1997, Asakawa, Mori et al. 2015). In fact, in some organisms, such as Trypanasoma and Plasmodium, the conserved cleavage site is absent and the two pieces do not separate (Degrasse, DuBois et al. 2009, Iwamoto, Asakawa et al. 2010, Obado, Brillantes et al. 2016).

I have engineered a Nup145N-C fusion strain by replacing the cleavage site with a 6xHA tag (as a flexible linker), since Nup145N and Nup145C satisfy all the characteristics outlined above. I also introduced the conditional GFP-Nup84 expression construct into this strain. **Fig. 5-1a** displays GFP-Nup84 localization in wild type and fusion mutant strains. The NPCs appear evenly distributed, which strongly suggests that the function of Nup145C is unaffected by the fusion as outer ring loss of function mutants exhibit clustering phenotypes (Aitchison, Blobel et al. 1995, Belgareh and Doye 1997, Fernandez-Martinez, Phillips et al. 2012). I have not assessed the function of Nup145N directly in the fusion strain; however, since the growth fitness of the mutant is not appreciably different from the wild type and Nup145N is dispensable for growth (Teixeira, Siniossoglou et al. 1997) it is unlikely that the fusion protein has broad pleiotropic effects.

Results and discussion: How are nup dynamics affected in the fusion mutant?

To assess this I measured the turnover and exchange rates of nups in the fusion mutant strain. Two biological replicates were performed and the results are presented as the average of the two (see Appendix, ZH38 strain for the fit data). Firstly, I measured the turnover rates of nups and compared them to the wild type values (**Fig. 5-1b**). The scatter is largely distributed around the y=x line and there are no notable changes, except for the tagged protein, GFP-Nup84, which turns over a little faster in the mutant. Next, I plotted the exchange half-lives of nups in the fusion strain against the wild type values (**Fig. 5-1c**). I have also plotted the average ± 2 standard deviations from the reference distribution calculated for co-purifying proteins (gray lines **Fig. 5-1c**). Finally, I mapped the relative location of all the proteins that were affected in the fusion mutant (**Fig. 5-1d**).

From the NPC diagram we observe several changes in the mutant.

1. The mobility of the fusion protein Nup145N-C is comparable to the mobility of Nup145C in the wild type and not that of Nup145N. So the fusion of Nup145N to Nup145C has greatly stabilized it.

2. Members of the outer ring became more destabilized, their residence half-lives now being more similar to the residence half-lives of the inner ring.

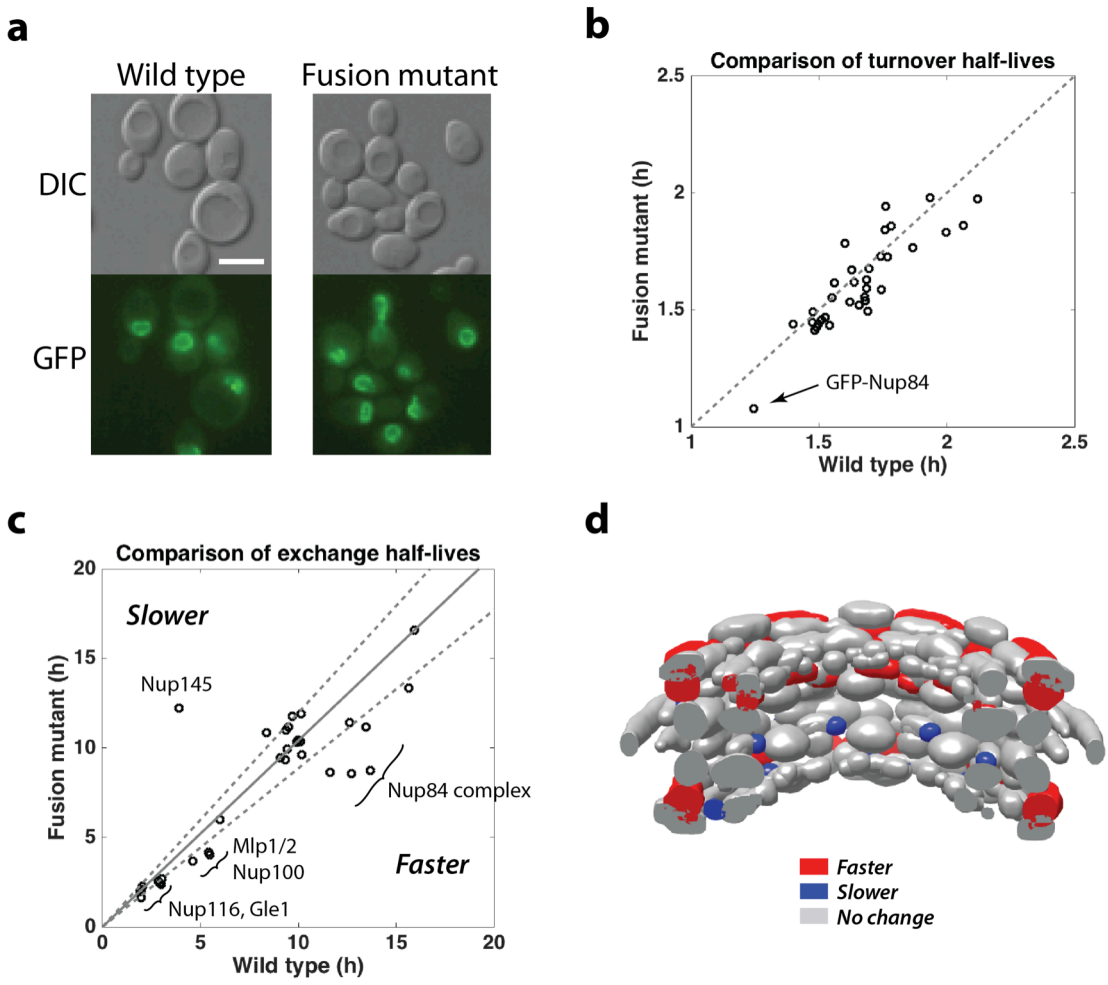

Figure 5-1: Analysis of the Nup145N-C fusion mutant. a. DIC and fluorescence images of the wild type and mutant cells. Scale bar 5 is μm. **b.** The comparison of nup turnover half-lives in the mutant and wild-type cells. The average of the two replicates is plotted. Standard deviation is ≤20% and is omitted for clarity. **c.** The comparison of nup exchange half-lives in the mutant and wild type cells. The diagonal and two dashed lines are the average ± standard deviations from the distribution calculated for co-purifying non-NPC proteins. The proteins discussed in the text are marked on the graph. **d.** The relative location of nups, with significantly altered half-lives in the mutant. The change was in ±15-40% range. Note the color scale does not indicate magnitude but relative change. Gray means no change. The map was produced in Chimera.

3. A number of dynamic proteins asymmetrically distributed on the cytoplasmic face of the NPC became more mobile. Most notably the two paralogs of Nup145N: Nup100 and Nup116 (Fabre, Boelens et al. 1994) and Gle1 (not shown on Chimera map).

4. The nuclear basket got destabilized (not shown on Chimera map).

A potential cause for the outer ring destabilization is forcing an extra protein mass (Nup145N) onto the structure due to fusion (Lutzmann, Kunze et al. 2002, Fernandez-Martinez, Phillips et al. 2012, Shi, Fernandez-Martinez et al. 2014). To investigate this I also mapped the dynamics changes on the Nup84 structure from (Fernandez-Martinez, Phillips et al. 2012) (**Fig. 5-2**).

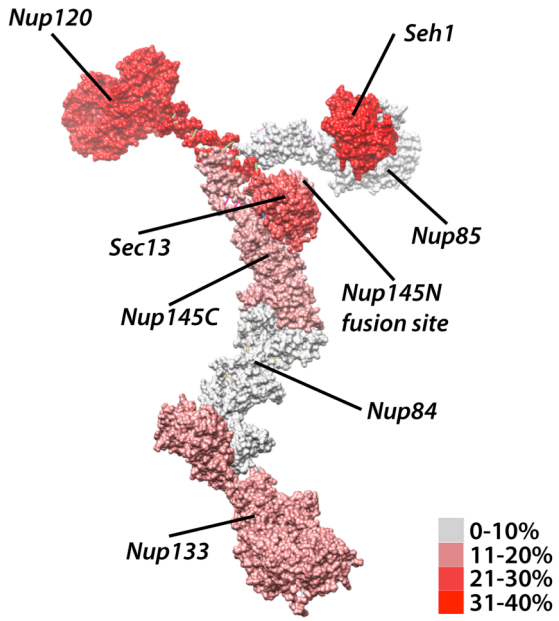

Figure 5-2: The dynamics of Nup84 complex constituents. Structure from (Fernandez-Martinez, Phillips et al. 2012). The degree of destabilization is shown with white to red gradient. The location of the fusion is indicated. This image was produced in Chimera.

Indeed, Nup145N is attached to Nup145C N-terminal domain, which is in the midst of multiple protein-protein interactions. Hence, an extra protein mass can sterically hinder the binding of the other members. Indeed Nup120, Seh1 and Sec13 were the most affected proteins in the outer ring. Nup133 was also affected, which could be because of its putative interaction with Nup120 (of an adjacent Nup84 complex) (Fernandez-Martinez, Phillips et al. 2012).

The destabilization of cytoplasmic proteins can also be explained either as a result of competition for binding to the outer ring or steric occlusion. E.g. Nup100 and Nup116 compete with Nup145N for binding to Nup145C and Nup82 in a mutually exclusive fashion ((Ratner, Hodel et al. 2007, Yoshida, Seo et al. 2011) and Javier Fernandez-Martinez *et al*, submitted)). Moreover, these proteins

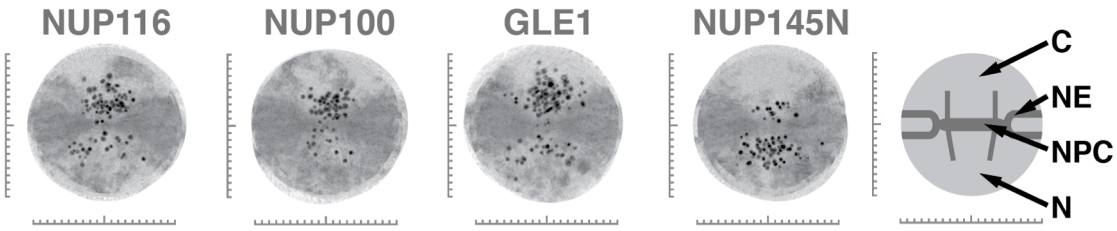

Figure 5-3: Immunoelectron localization of asymmetrically biased nups. Reprinted with permission from Rockefeller University Press from (Rout, Aitchison et al. 2000); permission conveyed through Copyright Clearance Center, Inc. Nup145N is biased towards the nuclear face in wild type cells, while in the fusion mutant it is forced on both sides of the NPC, where it can potentially displace cytoplasmically biased nups, e.g. Nup116, Nup100 and Gle1.

are biased towards the cytoplasmic side of the NPC, whereas wild type Nup145N is biased towards the nuclear side (Rout, Aitchison et al. 2000) (**Fig. 5-3**). Hence, forcing Nup145N to be on both sides can lead to steric occlusion.

Finally, the nuclear basket got destabilized, which can also result from steric occlusion. Although the exact anchoring location of the nuclear basket is not known, Nup84, Nup60 and Nup1 are the likely interaction partners (Niepel, Molloy et al. 2013). Thus stably attached Nup145N (in Nup84 complex) can sterically hinder the attachment of the basket, increasing its mobility.

Summary of Part 1

Stability of Nup145N-C fusion protein at the NPC is evidence that the scaffold interactions play a major role in dictating nup dynamics. Destabilization of nups in the cytoplasmic face, nuclear basket and outer ring implies that competition and steric hindrance can also play a role in determining nup dynamics. Importantly, this data presents evidence that modulating the stability of a single component can alter the dynamic organization of the NPC, which can be used for functional regulation (more on this in Chapter 6).

Part 2: Interactions with transport factors do not affect the dynamics of a mobile nup

Design of the yeast strain for test of transport influence on nup dynamics

To test the effect of transport flux on a dynamic nup stability we need to assess the nup dynamics in the absence of the interactions with transport factors. One way to eliminate the interaction between an FG-nup and transport factors is to delete the intrinsically disordered FG-domain. Similar to the previous strain design I needed to identify a target nup with the following characteristics:

1. An FG-nup with short residence time at the NPC.
2. The truncated protein localizes to the NPC.
3. The truncation of the FG-domain does not severely affect the cells.

I consulted a systematic FG-domain deletion study (Strawn, Shen et al. 2004) and identified Nup145N as an appropriate FG-nup candidate. It exhibits high dynamics in my study. The truncated structural region of Nup145N localizes to the NPC and the strain does not exhibit fitness defects (Strawn, Shen et al. 2004). More than half of the total FG-domain mass can be deleted from the NPC without loss of viability or the permeability barrier, presumably, due to redundancy in transport pathways and NPC structure (Strawn, Shen et al. 2004, Alber, Dokudovskaya et al. 2007, Alber, Dokudovskaya et al. 2007).

The function of Nup145N in all the many nucleocytoplasmic transport pathways has not yet been fully elucidated. However, much is known: for example it has been implicated as an important player in the transport of integral

nuclear membrane proteins in a triple Nup100, Nup57, Nup145N FG-deletion mutant strain. Curiously, none of the individual deletions exhibited an observable defect in integral nuclear membrane protein transport (Meinema, Laba et al. 2011). Again, this is probably due to redundancy in the FG-nup function (Strawn, Shen et al. 2004). Given that Nup145N satisfies all the requirements outlined above, I obtained the Nup145NΔFG strain from Prof. Wente and introduced the conditional GFP-Nup84 expression construct into the strain (**Fig. 5-5a**). Morphologically, the cells appear similar to the wild type strain.

Results and discussion: How is the nup dynamics affected in the truncation mutant?

I performed turnover and exchange experiments with two biological replicates and compared the average half-lives to the wild type values (**Fig. 5-4**, see Appendix, ZH42 strain for the fit data). The rates of turnover are largely similar and again distributed around y=x axis (**Fig. 5-4b**). It is notable that in the exchange experiment a large number of proteins became more stable in the mutant (**Fig. 5-4c**). I also mapped the relative location of the affected proteins onto the diagram of the NPC structure (**Fig. 5-4d**). Most notably, the exchange rate of the truncated Nup145NΔFG was not appreciably affected. Which is consistent with the scaffold interaction being more important for stability and the transport flux likely having a minor contribution. Another implication of this result is that it does not favor higher order FG meshwork formation model of transport

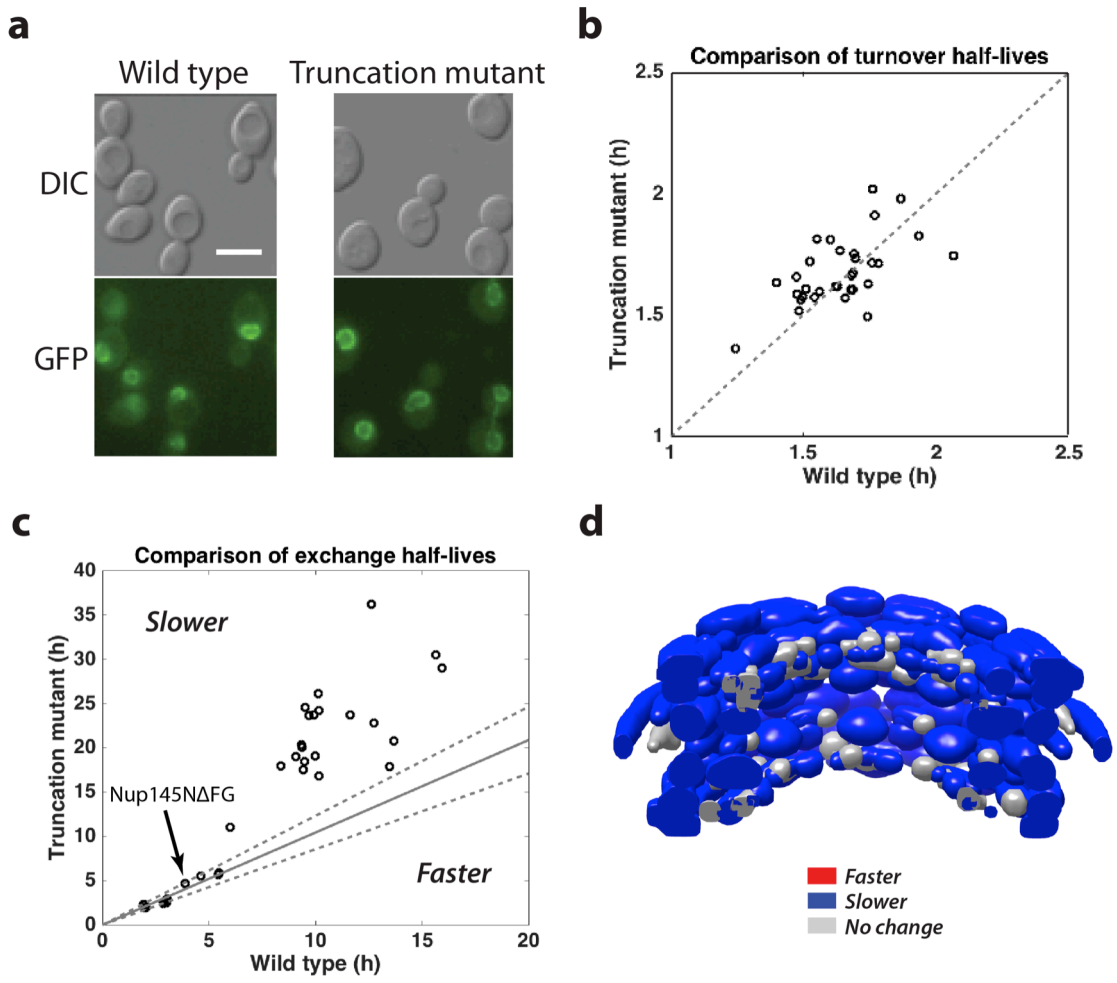

Figure 5-4: Analysis of the Nup145NΔFG truncation mutant. a. DIC and fluorescence images of the wild type and mutant cells. Scale bar is 5 μm. **b.** The comparison of nup turnover half-lives in the mutant and wild-type cells. The average of the two replicates is plotted. Standard deviation is ≤20% and is omitted for clarity. **c.** The comparison of nup exchange half-lives in the mutant and wild type cells. The diagonal and two dashed lines are the average ± standard deviations from the distribution calculated for co-purifying proteins. **d.** The relative location of nups, with significantly altered half-lives in the mutant (15-40% change). Note the color scale does not indicate magnitude but relative change. Gray means no change. The map was produced with Chimera.

(Ribbeck and Görlich 2001, Ribbeck and Görlich 2002) because the removal of the FG domain of Nup145N had no effect on other FG nups; dynamic nups in the wild type strain were not affected in this mutant. After the structural mapping the obvious pattern is that stable scaffold and peripheral proteins became more stable. This implies that the interaction between Nup145N FG region and transport factors or the FG region itself is a destabilizing force for the core scaffold. Although the reason for this stability change is unknown, I present two speculative explanations here.

One potential explanation is the transport model for integral inner nuclear membrane proteins, e.g. Heh2. The transport is facilitated by soluble transport factors, which bind the nuclear localization signal on the long unfolded soluble linker on the cargo, sticking out of the membrane. While the transport factor passes through the central channel of the pore, the integral membrane protein diffuses laterally through the pore membrane. Thus, the transmembrane protein passage can either destabilize the interaction between two Nup84 complex copies or between the outer ring and the membrane (Ohba, Schirmer et al. 2004, King, Lusk et al. 2006, Meinema, Laba et al. 2011, Meinema, Poolman et al. 2014). If this model is a good representation, then a reduced import of integral nuclear proteins due to lack of FG domains on Nup145N can lead to the outer ring stabilization, which in turn can lead to the whole scaffold stabilization (more on this in Chapter 6).

An alternative explanation is based on the structure of the NPC. Nupp145N homolog in the thermophilic fungus *Chaetomium thermophilum* has been shown to connect the inner ring and the Nup82 complex in an *in vitro* reconstitution study (Fischer, Teimer et al. 2015). In addition, yeast Nup145N has been reconstituted with inner ring member Nup157 and Nup84 complex (Lutzmann 2004). This suggests that Nup145N and its homologs may be involved in connecting different modules of the NPC and hence removing the FG region from Nup145N may release steric hindrance of scaffold protein binding and make the scaffold overall more stable.

Summary of Part 2

Since the stability of Nup145N at the NPC was not appreciably affected by the absence of the FG-domain it is unlikely that the interaction with transport factors is a major driving force for FG-nup dynamics. Also, since the dynamics of other FG proteins was not appreciably affected, the FG meshwork (hydrogel) model of transport is not supported by my study. The reason for overall stabilization of the scaffold in the absence of Nup145N FG domain is still a mystery. The effect can result from the reduction of transmembrane protein traffic or release of steric hindrance.

CHAPTER 6: DISCUSSION

What are the implications of my findings for interphase NPC assembly?

Although the coarse sequence of steps and many proteins participating in the different steps are known, the exact mechanisms governing NPC biogenesis during interphase are still an enigma. A current consensus model of NPC biogenesis is shown in **Fig. 6-1** (reviewed in (Fernandez-Martinez and Rout 2009, Capelson, Doucet et al. 2011, Imamoto and Funakoshi 2012, Rothballer and Kutay 2013)).

Nuclear pore complex assembly starts by membrane remodeling of the nuclear envelope, during which the inner and outer nuclear membranes (INM and ONM) are brought closer together, thus pinching the envelope, by a yet uncharacterized mechanism. Transmembrane nucleoporins, inner nuclear membrane proteins, ER membrane-shaping factors as well as membrane binding domains of the scaffold proteins are thought to participate in the membrane curving and fusion. Recently, membrane-binding domains of peripheral FG-nup Nup1 in both vertebrates and yeast have also been implicated in membrane shaping (Mészáros, Cibulka et al. 2015, Vollmer, Lorenz et al. 2015) suggesting that the initial step might be even more complex than depicted. Next, the curved membrane, transmembrane nups and scaffold proteins already present on the nascent pre-pore recruit other scaffold components to the assembly site, which can further stabilize the curved membranes.

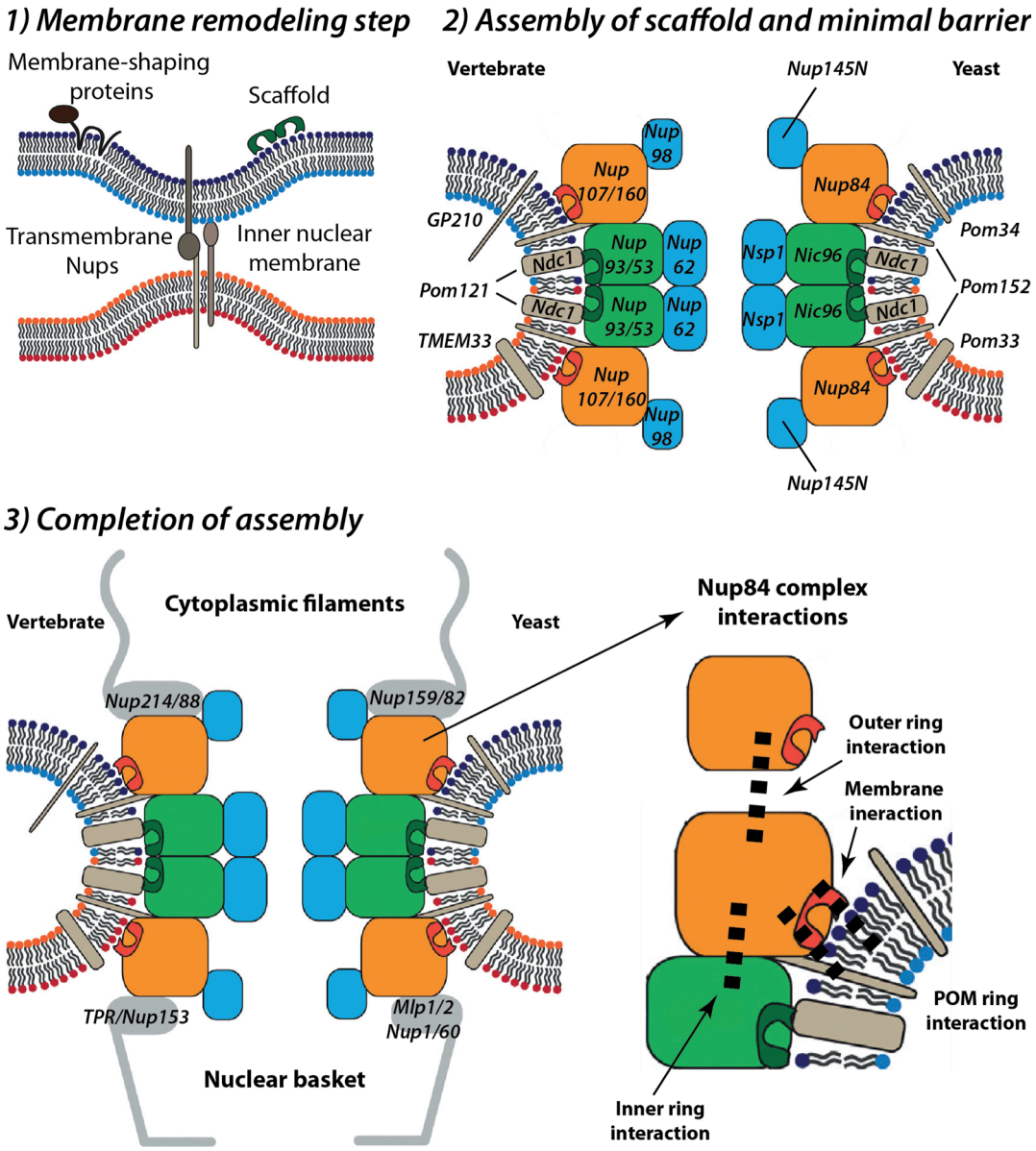

Figure 6-1: Schematic representation of NPC assembly. Adapted and reprinted with permission from Elsevier Science & Technology Journals from (Rothballer and Kutay 2013); permission conveyed through Copyright Clearance Center, Inc. 1) Membrane remodeling step: ER membrane shaping proteins, transmembrane nups, inner nuclear membrane proteins and scaffold proteins with amphipathic helices curve the membrane. 2) Assembly of scaffold and minimal barrier; recruitment of outer ring (orange), inner ring (green), central channel FG complex and Nup98 (Nup145N) forms a pre-pore with minimal transport barrier. 3) Completion of assembly: recruitment of cytoplasmic filaments and the nuclear basket completes the assembly. Nup84 complex interactions affecting its stability are shown on the right.

It is thought that pre-assembled building blocks are used in NPC assembly. Incorporation of the central channel FG complex and Nup98 homologs creates the minimal diffusion barrier (Strawn, Shen et al. 2004, Hülsmann, Labokha et al. 2012). Lastly, the asymmetric components of the cytoplasmic filaments and the nuclear basket are recruited and assembled on the NPC, completing the production of a mature NPC.

One of the major observations in my studies was that the outer ring scaffold is very stable and Nup84 complex members barely exchange out. Moreover, the members of the Nup84 complex had similar half-lives, which were longer than the rest of the NPC proteins. This suggests that the Nup84 complex largely exchanges out as a unit. It also implies that the protein-protein interactions within the Nup84 complex are stronger than the interactions the Nup84 complex forms with other members of the NPC and the membrane, consistent with published biochemical data (Lutzmann 2004, Alber, Dokudovskaya et al. 2007, Alber, Dokudovskaya et al. 2007, Fernandez-Martinez, Phillips et al. 2012). It has been suggested that eight copies of the Nup84 complex form a ring by interacting with one another in a head to tail fashion (Alber, Dokudovskaya et al. 2007, Alber, Dokudovskaya et al. 2007, Seo, Ma et al. 2009, Fernandez-Martinez, Phillips et al. 2012) (**Fig. 6-1**). What might those interaction strengths imply in terms of NPC assembly? The strong interactions within the Nup84 complex could ensure that the assembly of the Nup84 complex is fast and energetically favored. The weaker interactions

between the Nup84 complex units, other members of the NPC and the membrane may prevent off target assembly initiation or aggregation. For example, if the Nup84 complex units could form strong interactions with each other, they would polymerize in the cytoplasm after synthesis. Nonetheless, the outer ring is remarkably stable once assembled into the NPC. The increased avidity of multivalent interactions can be the reason for this (Kitov and Bundle 2003). After the Nup84 complex has formed in the cytoplasm, the local concentration of any one of its interaction partners is extremely low, because nups are unabundant proteins (Rout, Aitchison et al. 2000). However, once the Nup84 complex has been recruited to the site of NPC assembly (or a fully formed NPC), the local concentration of all of its interaction partners increases dramatically, enough for all the weak interactions described above to form. The combination of all the weak affinity interactions creates an overall high avidity interaction stabilizing the outer ring.

The inner ring complex also appears very stable within the NPC, but it is difficult to biochemically isolate it as a discrete subcomplex. One explanation for this behavior could be its assembly through multivalent low affinity interactions (as in the case of the outer ring) (Fischer, Teimer et al. 2015, Stuwe, Bley et al. 2015). Another key could be cooperativity (Williamson 2008), particularly for binding the pore membrane. Both vertebrate and yeast Nup53 play a crucial role in recruiting the inner ring complex to the pore membrane. Vertebrate Ndc1 binds Nup53, which improves the membrane binding capacity of the latter (cooperative

binding) (Eisenhardt, Redolfi et al. 2013). Nup53 dimerization and membrane binding have been implicated in *de novo* NPC assembly (Vollmer, Schooley et al. 2012). Another example of cooperativity is that only the fully assembled Nsp1 complex (and not individual proteins) can bind the inner ring with the aid of Nic96, as suggested by recent in vitro reconstitution and crystallography studies (Fischer, Teimer et al. 2015, Stuwe, Bley et al. 2015). Thus, because of low abundance of nups discussed earlier, those cooperative binding events may not happen outside the NPC and the nuclear membrane. However, in combination, those interactions can contribute to the inner ring stabilization within the NPC.

The exchange data for Nup145NΔFG mutant is consistent with multivalent weak interactions contributing to overall stability. Although, we cannot pinpoint yet which module or modules of the NPC were specifically stabilized by Nup145N truncation, the effect appears pleiotropic, as all stable proteins became more stable. It is conceivable that stabilizing just a few interactions could have caused the stabilization of the whole scaffold and stable peripheral proteins. On the other hand, it would be difficult to explain how Nup145N truncation could affect ~2/3 of the NPC at once without the additive effect.

The exchange data of Nup145N-C fusion mutant displays more local interaction destabilization effects. Nup145N and Nup145C fusion has likely weakened some protein-protein interactions because of steric occlusion of binding sites (Fernandez-Martinez, Phillips et al. 2012). However, Nup145N fusion is likely too far away from Nup133 to exert direct steric hindrance effects

(Chapter 5, **Fig. 5-2**). Nup133 and Nup120, two proteins on the opposite ends of the complex, are both de-stabilized. This could be explained by either overall destabilization of the outer ring, or reduced membrane interactions.

Another major observation of my study was that the intermediate and fast exchangers tended to be located peripherally in the NPC structure. It is not quite clear how those proteins contribute to NPC assembly. But most of them are thought to be assembled after the scaffold and after the minimal barrier (Nup145N and homologs and Nsp1 complex) is established (Strawn, Shen et al. 2004, Hulsmann, Labokha et al. 2012). It is possible that once the minimal barrier is established there is no “urgent” need to assemble the rest. Such that the dynamic nups could assemble on NPCs as they exchange in and out. Such an exchange-assembly mechanism would imply that it takes relatively longer for an NPC to mature. Indeed, in mammalian cells the interphase NPC assembly kinetics was found to be much longer than the reassembly after mitosis, ~30 min vs. ~10 min (Dultz and Ellenberg 2010). Slow assembly could explain the observation that the yeast daughter cell receives a large fraction of old maternal NPCs (for competent nucleocytoplasmic transport) (Khmelinskii, Keller et al. 2012, Colombi, Webster et al. 2013, Makio, Lapetina et al. 2013). But this is highly speculative.

Summary of NPC dynamics and assembly relationship

Affinity purification experiments on the NPC have revealed stable sub-complexes that can be readily purified biochemically (Alber, Dokudovskaya et al. 2007, Alber, Dokudovskaya et al. 2007). As revealed by my study and others (Rabut, Lénárt et al. 2004, Savas, Toyama et al. 2012, Toyama, Savas et al. 2013), these sub-complexes also appear to be present as stable modules in vivo, which combine to form a stable scaffold. The interactions between modules are likely weak outside the NPC to prevent off target assembly and aggregation; but once at the site of NPC assembly, those modules cooperatively form multiple low affinity protein-protein and protein-membrane interactions, which create an overall high avidity interaction network (a stable scaffold).

What are the implications of nup dynamics for NPC function?

The high enrichment of FG-nups in the intermediate to fast exchangers group implies that the weak interactions those proteins form with the scaffold are relevant for their transport function. As transient protein-protein interactions are often involved in biological function regulation (Nooren and Thornton 2003, Nooren and Thornton 2003), perhaps, transport can be modulated by altering the dynamics of FG nups. Here I present two examples where transport is altered concomitantly with alterations in NPC composition.

Transport is altered during cell division

Among the symmetric FG-nups, Nup53 appears the most labile with half residence time of 6h compared to the average ~9h for the rest. This could be because Nup53 undergoes a molecular rearrangement during cell division. The protein has differential affinity to its interaction partners Nup170 and Nic96 during mitosis, presumably due to regulation by phosphorylation (Marelli, Aitchison et al. 1998). Makhnevych *et al* have demonstrated that Nup53 binds to Nup170 during the interphase and S phase, and to Nic96 – during G2/M phase (Makhnevych, Lusk et al. 2003). Such a molecular rearrangement exposes a Kap121 binding domain on Nup53, which overlaps with Nup170 binding region (Lusk, Makhnevych et al. 2002). Nup53 biding to Kap121 is thought to inhibit Kap121-mediated nuclear import by releasing its cargo on the cytoplasmic side. A recent study has found structural evidence for Nup53 competing with Kap121 cargo for the same binding site (Kobayashi and Matsuura 2013). This transport inhibition appears necessary for the normal mitosis progression (Makhnevych, Lusk et al. 2003). Thus, the dynamic interaction of Nup53 with different interaction partners can modulate transport during the cell cycle.

Transport is altered in response to stress

Following heat shock the majority of mRNA export is shut down, while heat shock genes (mainly encoding chaperones) are induced and their transcripts effectively exported (Saavedra, Tung et al. 1996). The FG-nup Nup42,

which is dispensable for growth under normal conditions, is essential for heat shock mRNA export following stress (Saavedra, Hammell et al. 1997). Curiously, it is the carboxyl terminus and its interaction with the mRNA export mediator Gle1 that are important, while the amino terminal FG-region of Nup42 does not seem to have a major contribution (Stutz, Kantor et al. 1997). mRNP export factors have also been implicated in transport shutdown. Following stress induction one of the major mRNA binding proteins, Npl3, stops associating with mRNA particles thus inhibiting transport (Krebber, Taura et al. 1999). Because heat shock mRNA is successfully exported after stress, while the rest of the mRNA cannot leave the nucleus, it was suggested that the export is carried out by a specialized export factor or pathway (Saavedra, Tung et al. 1996, Saavedra, Hammell et al. 1997). However, it is unlikely that heat shock protein mRNA export is carried out by a specialized export factor or pathway as Mex67, a major mRNP exporter was demonstrated to export heat shock mRNA (Hurt, Strässer et al. 2000). If the changes in mRNA export factor behavior alone cannot explain all the changes in mRNA transport during heat shock, the other likely possibility is the modification of the NPC itself. Gle2, a dynamic RNA export factor, which binds Nup116 and exhibits nuclear rim localization under normal conditions, dissociates from NPCs and diffuses into the cytoplasm upon heat shock treatment. The release of Gle2 is correlated with bulk mRNA export block (Izawa, Takemura et al. 2004). Additionally, the nuclear basket protein Mlp1 dissociates from NPCs and accumulates in intranuclear foci, which also contain important mRNA export

factors such as Nab2 and Yra1. This sequestration of export factors is also thought to inhibit bulk mRNA export (Hurt, Strässer et al. 2000). Thus, the cell regulates transport upon stress both at the level of export factors and NPC composition. Notably, all of these regulated nups – Mlp1, Nup42, Gle2, Nup116, and Gle1 – are among the fastest exchanging nups in my assays.

Summary of the relationship between NPC dynamics and nuclear transport

Dynamic, fast exchanging nups seem to form weaker associations with the scaffold that can be modulated by posttranslational modifications such as phosphorylation and monoubiquitylation (Makhnevych, Lusk et al. 2003, Niño, Guet et al. 2016). Altering the association of a dynamic nup with the NPC may either specifically modify a transport pathway or have a general effect on multiple pathways. This plasticity of the NPC with respect to peripheral, transport factor-interacting nups thus may allow the cell to quickly tune nucleocytoplasmic transport in response to the physiological needs or the changing environment of the cell.

Future directions

Can the nuclear pore complex be repaired?

It is currently unknown whether there is a repair mechanism for the NPC scaffold, which is largely stable (Daigle 2001, Rabut, Doye et al. 2004, D'Angelo, Raices et al. 2009, Savas, Toyama et al. 2012, Toyama, Savas et al. 2013).

While in dividing cells old NPCs are diluted out by new NPC synthesis, such a mechanism is absent in post-mitotic cells. The very slow exchange rate of the scaffold, together with a possible partial loss of some scaffold nups from NPCs and “leakiness” of NPCs to cytoplasmic proteins in old rat and *C. elegans* neurons, has led to the proposal that there is no repair mechanism for NPCs in post-mitotic cells; instead, the scaffold exchanges at a very slow or negligible rate, and at some point the accumulated nup damage leads to deterioration of the transport barrier function, which contributes to aging (D'Angelo, Raices et al. 2009, Savas, Toyama et al. 2012, Toyama, Savas et al. 2013).

Although yeast is a short-lived organism, it has proven a good system for studying aging. It is presumed that due to the asymmetric cell divisions the mother cell retains aging factors such as ERCs (Extrachromosomal rDNA circle) and oxidatively damaged proteins (reviewed in (Bitterman, Medvedik et al. 2003, Longo, Shadel et al. 2012)). Until recently it was controversial whether mother cells also retain “old” NPCs. Shcheprova *et al.* utilized a FLIP (fluorescence loss in photobleaching) technique to conclude that there was little to no inheritance of maternal NPCs in the bud and instead most bud NPCs were synthesized *de novo* (Shcheprova, Baldi et al. 2008). However, this was in disagreement with previously reported data that the number of NPCs increases continuously throughout the cell cycle, with a small peak in the S phase (Winey, Yarar et al. 1997). A later study used the photoconvertible fluorescent protein Dendra fused to several nups to demonstrate conclusively that NPCs can migrate effectively

from the mother to the bud cell (Khmelinskii, Keller et al. 2010). In fact, a later study by the same group showed that, if anything, the bud contains a higher proportion of the maternal NPCs, implying that “old” NPCs are not necessarily synonymous with “bad” NPCs (Khmelinskii, Keller et al. 2012). However, the passage of maternal NPCs to the daughter is not passive. Compromised and damaged NPCs can be prevented from segregating to the daughter. Two groups have independently discovered an NPC distribution barrier, which requires Nsp1 and the proteins in its interaction network for allowing NPC passage to the bud (Colombi, Webster et al. 2013, Makio, Lapetina et al. 2013)

The rate of nup scaffold replacement I have measured for yeast is very slow, and is generally in agreement with the maintenance model proposed earlier. However, at any given time only a fraction of the cells in culture are replicatively aged and since I do not separate young and old cells I always measure the average exchange for both populations of cells. With the inclusion of a specific genetic perturbation my assay is uniquely positioned to test the existence of a potential scaffold repair mechanism (described below).

I can simulate the protein damage resulting from aging by specifically inducing degradation of an incorporated scaffold protein. For example, an auxin-inducible degron can be fused to one copy of Nup170 (inner ring member). Upon auxin addition the tagged Nup170 in both the soluble and NPC-bound pool will be polyubiquitylated and should be targeted for proteasomal degradation, thus acting like a damaged protein (Nishimura, Fukagawa et al. 2009, Nishimura and

Kanemaki 2014). Having a wild type copy of Nup170 will ensure that undamaged, fresh protein is available for repair. In the exchange experiment, I will induce the degradation of the Degron-Nup170 protein and monitor its replacement with mass spectrometry (**Fig. 6-2**). For simplicity, only the scaffold proteins are shown. The three potential scenarios are:

i) The stability of the "damaged" Nup170 does not change. If the proteasome cannot pull the scaffold protein out of the NPC, then it will not be degraded. The heavy label decay for Nup170 will be similar to wild type strain (some slow exchange). Degron heavy labeled fraction should not decay, because all newly synthesized Degron-Nup170 proteins will be rapidly degraded, and the fraction heavy for degron peptides will remain constant and equal to 1. This would be in favor of no repair mechanism and damaged protein propagation in aging.

ii) The damaged Nup170 is pulled out of the NPC and degraded, but cannot be replaced by a new copy of Nup170. The heavy label decay for Nup170 will be similar to that of the wild type strain (some slow exchange). However, the degron tag peptides in the NPC affinity capture will disappear. This would also be in favor of no repair mechanism and loss of damaged protein in aging.

iii) The damaged Nup170 is pulled out and replaced by a new copy of Nup170. I will observe this as increased exchange (faster loss of old Nup170 fraction). The degron tag peptides will disappear as in ii). This observation will be in favor of an existence of a repair mechanism in actively dividing cells.

Although neurons in a rat brain do not assemble new NPCs (the density of NPCs remains constant), ribosome-profiling experiments have demonstrated that the translation of NPC scaffold proteins is ongoing (Toyama, Savas et al. 2013). This indicates that functional protein would be available for repair. Thus, the detection of a NPC scaffold repair mechanism in yeast would be relevant for the mammalian system, as it would most likely constitute a conserved one.

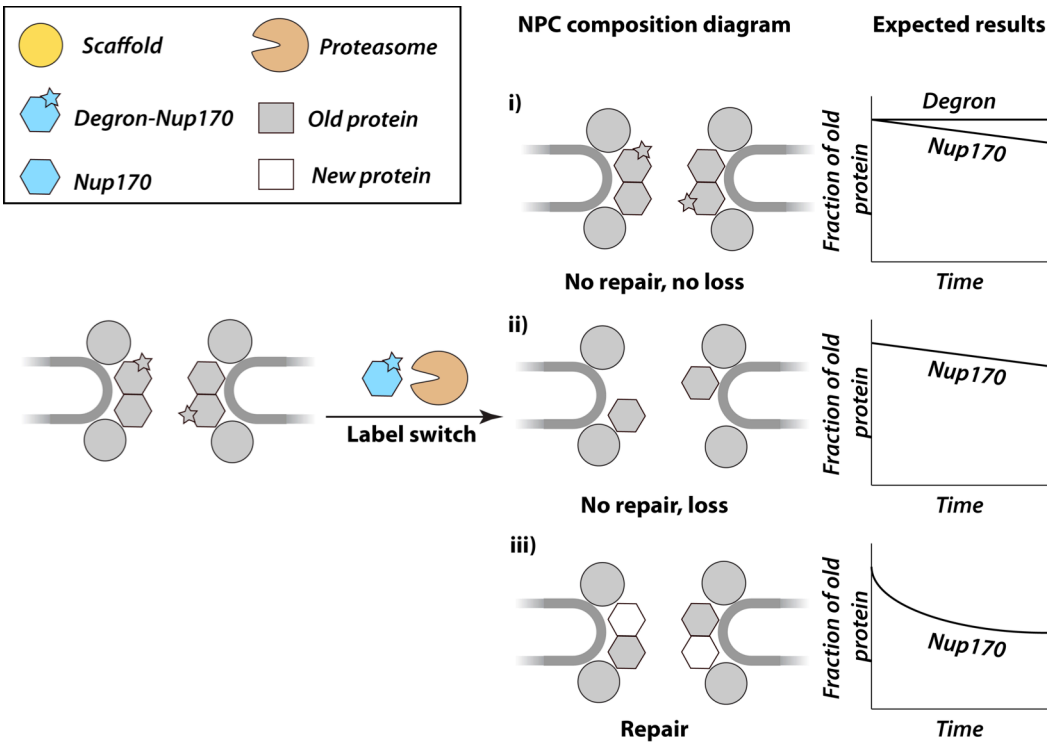

Figure 6-2: An experiment to test a potential NPC repair mechanism. Only the scaffold is shown. In the exchange experiment the rate of replacement of Degron-Nup170 is monitored after the degradation of the latter is induced. Three possible scenarios are presented and discussed in the main text.

Summary of NPC repair mechanism test

It has been suggested that the scaffold nups of post-mitotic cells are exceptionally stable and are rarely replaced (Savas, Toyama et al. 2012, Toyama, Savas et al. 2013). This is a controversial and astonishing suggestion in view of human longevity. There is some but limited regeneration of nervous tissue in adult brain (Martino, Pluchino et al. 2011). Could it really be that a substantial fraction of the scaffold nups in a 100 years' old *Homo sapiens* brain are also ~100 years old? I propose an assay in yeast, which will preemptively damage the scaffold nups instead of waiting for time to take its toll. The experimental methodology I have developed is sensitive enough to reveal if the damaged scaffold nups are replaced. An evidence for repair or absence thereof would be a valuable insight into the NPC biology and aging of all eukaryotes.

CHAPTER 7: MATERIALS AND METHODS

96-well affinity capture methods

The materials, methods and analysis for the 96-well affinity capture study presented in Chapter 2 have been published (Hakhverdyan, Domanski et al. 2015).

Yeast strains construction and culture

All *S. cerevisiae* strains used in this study are presented in **Table 7-1**, plasmids – **Table 7-2** and primers – **Table 7-3**. The standard procedures for culturing, maintenance, transformation, mating, sporulation and selection were carried out according to methods described in *Yeast Protocols* (Xiao 2006). Unless otherwise specified the cells were grown at 30˚C with 220 rpm shaking.

To replace the endogenous promoter of NUP84 with TDH3 promoter, insert 3 tetracycline binding aptamers encoding sequence in the 5'-UTR and tag Nup84 N-terminally with GFP a transformation cassette was amplified by PCR with ZH105 and ZH106 oligos and Ttc3GFP-His5 as a template. The cassette was transformed via Lithium Acetate method and integrated by homologous recombination. Positive clones were selected on SD-His medium. The correct insertion as well as the retention of one wild type copy of NUP84 gene in the diploid strain was verified by PCR (with ZH92, JFM39 and N84Prom-F, JFM39 oligo pairs respectively). Lastly, the proper nuclear rim and NPC localization of

the GFP tagged Nup84 were confirmed by fluorescence microscopy and biochemical purification of the whole NPC through the GFP tag. This cassette was integrated in all of the strains used in the turnover and exchange experiments.

To construct the Nup145N-C fusion a diploid DF5 strain was first transformed with a PCR cassette integrating two LoxP sites flanking kanMX4 gene followed by 6xHA tag sequence at the site where Nup145 precursor protein auto-cleaves: F605-S606 (Teixeira, Siniossoglou et al. 1997, Teixeira, Fabre et al. 1999), with ZH127 and ZH128 primers and pOM10 as template. Positive transformants were selected on YPD+G418 medium. Targeted insertion was verified via PCR with ZH131 and ZH132 oligos (priming in NUP145 and the transformation cassette respectively). Next, pSH47 plasmid was transformed and positive transformants selected on SD-Ura plate. A single colony was grown in SD-Ura medium, diluted to OD 0.2/mL and grown 6h with 1% Raffinose and 2% Galactose as carbon source to induce the Cre recombinase expression. After the successful recombination between the two LoxP sites the cells were expected to lose the kanMX4 gene and start expressing the full length Nup145N-C fusion protein with a 6xHA tag inserted at the cleavage site. To screen for recombinants the cells were plated on YPD and replica plated on YPD+G418 medium. Colonies that were viable on YPD but absent from YPD+G418 plates were analyzed by anti-HA western blot (WB) to verify the expression of Nup145N-C fusion protein. Next, the

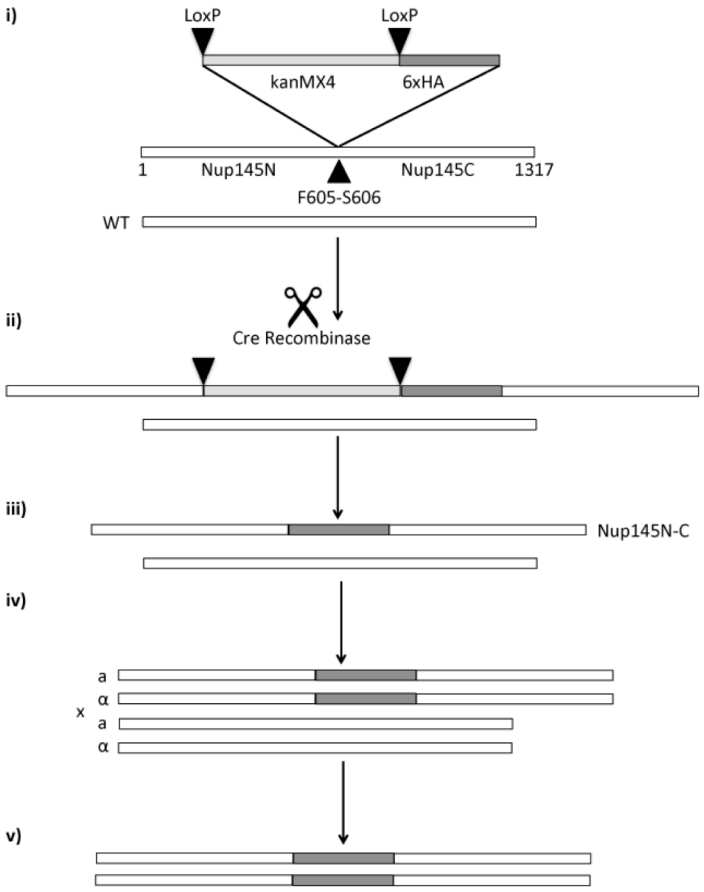

Figure 7-1: Schematic of diploid Nup145N-C fusion strain construction. **i)** Transformation of kanamycin resistance cassette and integration at the cleavage site. KanMX4 is flanked by LoxP sites and followed by 6xHA coding sequence. **ii)** After integration one copy of NUP145 is disrupted and the strain is resistant to G418. The construct expressing Cre recombinase is transformed into the strain. **iii)** Cre recombinase cuts out the DNA region between LoxP sites (leaving behind a single LoxP site), thereby restoring Nup145 expression. The full length Nup145 is unable to self-cleave and has a 6xHA tag instead of the cleavage site. **iv)** The diploid strain is sporulated and the tetrads dissected, generating 4 haploid strains, each containing either the wild type or Nup145N-C allele. Haploid Nup145N-C strains are viable. **v)** a and α strains each containing the Nup145N-C allele are mated to produce the diploid Nup145N-C strain.

strain was sporulated and 6 tetrads were dissected. Four haploid colonies resulting from each tetrad dissection were grown and subjected to WB to test for Nup145N-C fusion protein expression. The mating type of positive clones was determined with mating type locuc PCR (Huxley, Green et al. 1990). Finally, the haploid strains of opposite mating type containing the Nup145N-C allele were mated and the successful mating verified by PCR (Huxley, Green et al. 1990).

All the steps of strain construction are diagrammed in (**Fig. 7-1**).

SWY2870 was a generous gift from Prof. Susan Wente (Strawn, Shen et al. 2004). A single wild type LYS2 gene was knocked out with a disruption cassette generated with PCR amplification from pUG73 template with ZH150 and ZH151 oligos and SD-Leu selection.

Plasmid construction

To swap the S. pombe His5 gene from pUG27 into pTDH3-tc3-3xHA instead of the KanR marker both plasmids were digested with NcoI and SacI. DNA fragments were purified after agarose gel electrophoresis and the insert from pUG27 digest was ligated to the backbone from pTDH3-tc3-3xHA digest to obtain Ttc3HAHis5. To introduce the GFP sequence into the previous construct I PCR-amplified GFP from p404GALL-GFP with ZH90 and ZH94 oligos. The PCR product and Ttc3HAHis5 plasmid were subjected to a double digest with BamHI and HindIII. The backbone was treated with CIP. The backbone and insert were

ligated to obtain Ttc3GFP-His5. Finally, the correct sequence of the GFP integration site was verified by sequencing with tc3HA-F primer.

Table 7-1: List of strains.

Strain	Genotype	Background	Reference
DF5	*MAT**a**/α his3-Δ200/his3-Δ200 leu2-3,112/leu2-3,112 lys2-801/lys2-801 trp1-1(am)/trp1-1(am) ura3-52ura3-52*	DF5	Rout lab
SWY2870	*MAT**a**/α ade2-1::ADE2/ade2-1::ADE2 trp1-1/TRP1 LYS2/lys2 ura3-1/ura3-1 leu2-3,112/leu2-3,112 his3-11,15/his3-11,15 can1-100/can1-100 myc-LoxP-nup145ΔGLFG/myc-LoxP-nup145ΔGLFG*	W303	Wente lab
AIR02 (GFP-Nup84)	*DF5, pTDH3-tc3-GFP-Nup84::SpHIS5*	DF5	This study
ZH38 (Nup145N-C, GFP-Nup84	*DF5, pTDH3-tc3-GFP-Nup84::SpHIS5, Nup145N-LoxP-6xHA-Nup145C/Nup145N-LoxP-6xHA-Nup145C*	DF5	This study
ZH42	*SWY2870, pTDH3-tc3-GFP-Nup84::SpHIS5, KanR::lys2/lys2*	W303	This study

Table 7-2: List of plasmids.

Plasmid	Description	Reference
pTDH3-tc3-3xHA	TDH3 promoter replacement and N-terminal tagging with tetracycline binding aptamers and 3HA tag, Amp, KanR	Euroscarf
pUG27	Gene deletion, Amp, HIS5	Euroscarf
Ttc3HAHis5	Replaced KanR marker with HIS5 in pTDH3-tc3-3xHA, Amp	This study
Ttc3GFP-His5	Inserted GFP encoding sequence in Ttc3HAHis5, Amp	This study
pOM10	N-terminal or internal 6xHA tagging, Amp, KanR	Euroscarf
pSH47	Transient, conditional expression of Cre recombinase under GAL1 promoter, Amp, URA3	Euroscarf
pUG73	Gene deletion, Amp, KILEU2	Euroscarf
p404GALL-GFP	Integratable plasmid, Amp, TRP1	Rout lab

Table 7-3: List of primers.

Primer	Sequence	Reference
ZH105	CTAATTCAACCTGAAAACCAATTGAGTGCTA CTTCGAAGTAAAATACATAGCCATTTCAAAG TGGATCTGATATCACCTA	This study
ZH106	TTCCTTTAAAGTGTCTGAGAACTTTGTGAAG CGTTCTGTTTGATAAGTAGGGGATAATTCTTT GTACAATTCATCCATAC	This study
N84Prom-F	CTATGCTGGTCCAACTTT	Rout lab

JFM39	GTCGGAAAGTTTAGCTTC	Rout lab
ZH92	GTGATGGTCCAGTCTTGT	This study
ZH127	GAAATGAACTATATATCCTATAATCCCTTTGGCGGGACTTGGACTTTCAAAGTCAATCCTTGCAGGTCGACAACCCTTAAT	This study
ZH128	ACTCAAATCGTCTTCATCTATTTCCGCATCTTCTTCATTGACTAACCCCCAAATGCTAGAGCTAGAAGCGTAATCTGGAAC	This study
ZH131	CCGCATCAGACAAATCAG	This study
ZH132	AAACGAGCTCTCGAGAAC	This study
ZH144	ATGACTAACGAAAAGGTCTGGATAGAGAAGTTGGATAATCCAACTCTTTCAGTGTTACCATGCAGGTCGACAACCCTTAAT	This study
ZH145	TTAAGCTGCTGCGGAGCTTCCACGAGCACCAGCACCTGAAGCAACTAGACTTATTTGCGCGCAGCGTACGGATATCACCTA	This study
ZH150	ATGACTAACGAAAAGGTCTGGATAGAGAAGTTGGATAATCCAACTCTTTCAGTGTTACCAGATCCGCAGGCTAACCGGAAC	This study
ZH151	TTAAGCTGCTGCGGAGCTTCCACGAGCACCAGCACCTGAAGCAACTAGACTTATTTGCGCAGCTCGCTGTGAAGATCCCAG	This study
ZH90	TATGAAGGATCCGGCCTGGAAGTTCTGTTCCA	This study
ZH94	GCACCGAAGCTTTTTGTACAATTCATCCATAC	This study
tc3HA-F	CCTCGAGAACATATGTACCC	This study

Whole cell lysis

1mL cell sample was pelleted down at 14k rpm for 1min and the supernatant discarded. The resulting pellet was re-suspended in 250uL lysis solution (1.85N NaOH, 7.4% v/v 2-mercaptoethanol) and incubated on ice for 10min. To precipitate the proteins in the lysate 250uL of 50% v/v trichloroacetic acid was added and the mixture incubated on ice for an additional 10min. The precipitated proteins were pelleted down at 14k rpm for 10 min and the supernatant replaced with 500uL of 100% cold acetone, after which the tubes were kept at -20˚C from 20min to overnight. After the acetone was aspirated the protein pellet was re-suspended in 200uL of 1x gel loading buffer.

Western blotting

For GFP detection the primary (1˚) incubation was carried out with anti-GFP monoclonal antibody, diluted 1:2000 in 2.5% milk containing TBST (Tris Buffer Saline Triton) buffer. The secondary (2˚) incubation was carried out with HRP-conjugated rabbit anti-mouse antibody at a 1:5000 dilution in 2.5% milk containing TBST buffer. For HA: 1˚ - 1:2000 mouse monoclonal anti-HA; 2˚ - same as for GFP. For Pgk1: 1˚ - 1:20000 mouse monoclonal anti-Pgk1; 2˚ - same as for GFP.

Conditional gene expression

To repress the translation of GFP-Nup84 mRNA 0.2mg/mL of cltc (chlortetracycline) HCl was added to the medium following the recommendation in the reference (Kotter, Weigand et al. 2009). Cltc HCl was used instead of Tetracycline for its superior stability (Okerman, Van Hende et al. 2007). The reduction of GFP-Nup84 amount over time was verified by anti-GFP WB. The rapid repression of GFP-Nup84 expression after ClTc HCl addition was confirmed by concurrent labeling with ^{13}C6 K (lysine) and monitoring the intensity of ^{13}C6 K over isotopically light K in GFP-Nup84 peptides by ESI-MS/MS.

Metabolic labeling

In order to label cells with ^{13}C6 K a single colony was inoculated into a small pre-culture of SCD-H-K dropout medium supplemented with 50mg/L of ^{13}C6 K and grown overnight. The resulting culture was diluted at least 20-fold in the same medium and grown until OD 1. To change the metabolic label to light K, the cells were spun down at 5000 rpm for 5 min, the supernatant decanted and the pellet re-suspended in SCD-H-K medium to OD 0.25, supplemented with 50mg/L of ^{12}C6 K, with or without 0.2 mg/mL cltc. The cells were grown for additional 5 h and each hour a sample of cells was harvested and flash frozen in liquid nitrogen.

The heavy labeling efficiency was confirmed by analyzing a fraction of proteins in the following way: firstly, WCL was performed on a 1mL aliquot of the labeled

cells, next, the precipitated cellular proteins were re-suspended in HU-SDS (8M Urea, 5% SDS, 200mM Tris pH 6.8, 1mM EDTA, w/ 0.05% bromophenol blue, 1.5% dithiothreitol (DTT)) protein loading buffer, reduced, alkylated and resolved on SDS-PAGE, next, a few abundant bands from 37-50 kDa were excised and processed for MS analysis. MS spectra were analyzed by MaxQuant software (Cox and Mann 2008), which produced both the identity of peptides and the relative intensity of heavy and light K containing peptides. The heavy/light ratio measurement was used to obtain the heavy labeled fraction, which provided the labeling efficiency. See bioinformatics analysis for details.

Affinity capture

The NPC AC was carried out as before (Hakhverdyan, Domanski et al. 2015) with minor modifications. Harvested cell mass was flash frozen in liquid nitrogen and ground to fine powder at cryogenic temperature (4 times 2 min, 200 rpm in a PM 100 Retsch grinder). 0.5g of the resulting disrupted cell material was re-suspended in 2mL of the room temperature extraction buffer:

20 mM HEPES, pH 7.4, 150 mM NaCl, 250 mM sodium citrate, 1% v/v Triton X-100, 1x protease inhibitor cocktail (PIC) and 10 mM glutaraldehyde (GA).

A mild fixation with GA was implemented to minimize the protein exchange in the lysate (Subbotin and Chait 2014). The reconstituted lysate was incubated on ice for 5 min, after which the GA cross linker was quenched by the addition of 100 mM Tris, pH 8. The lysate was clarified by centrifugation at 15k g for 10min. The

supernatant was incubated with 25 µL of anti-GFP antibody conjugated magnetic slurry with agitation at 4˚C. Bound beads were washed 3 times with 1mL of cold extraction buffer without PIC and GA. After the removal of the final wash the beads were re-suspended in 30 µL of 1x LDS (lithium dodecyl sulfate loading buffer) and incubated for 10 min at 70˚C to elute the bound protein complexes.

In-gel digestion and peptide extraction

Before running on the gel the samples were reduced for 10 min at 70˚C with 20 mM DTT and alkylated with 100 mM iodoacetamide (IAM) for 30 min in the dark. The samples were run on a 4-16% Bis-Tris gel at 200 V either for 55 min to fully resolve proteins or 3 min to gel-purify the sample from contaminants interfering with downstream MS, resulting in a “gel plug”. The gel was fixed for 5 min in 16% methanol, 10% acetic acid, washed thrice for 5 min in ddH_2O, stained for 1 h with Imperial Coomassie stain and destained in water overnight. The image of the gel was recorded and either the protein bands or gel plugs (containing the entire affinity purified sample) were excised out of the gel, placed in Eppendorf tubes and chopped into 1mm^3 pieces. The gel pieces were destained with 500 µL 50mM ammonium bicarbonate (AmBic), 50% acetonitrile (ACN) at 30˚C, periodically replacing the destaining solution with a fresh aliquot until the coomassie was fully gone. Following destaining the gel pieces were dehydrated in 100% ACN and rehydrated in digestion solution (10 ng/µL of Trypsin in 50 mM AmBic) and incubated at 37˚C overnight. To extract the digested peptides from

the gel 50uL of POROS R2 (reverse phase) beads slurry was added to the sample and incubated overnight at 4˚C. The peptides bound to POROS beads were desalted on 10 µL C18 tips according to manufacturer's instructions (OMIX tips, Agilent Technologies). To avoid particulates in the final sample, the POROS bead mixture was loaded on top of C18 resin and spun through at 1000 rpm for 1 min instead of pipetting up and down. Next, the peptides were eluted 2x each with 40% ACN, 0.1% trifluoroacetic acid (TFA) and 80% ACN, 0.1% TFA. Finally, the peptides were vacuum dried in SpeedVac.

Mass spectrometry

Mass spectrometry was carried out by Kelly Molloy in Professor Chait's laboratory.

Bioinformatic analysis

The RAW mass spectrometric files were searched with the MaxQuant software (Cox and Mann 2008) both to identify peptides and measure the heavy/light ratio of lysine containing peptides. For MaxQuant analysis mostly default parameters were used with the following exceptions: the multiplicity was set to 2, for the light sample all amino acids were set to light, for the heavy sample "lys6" was selected; the yeast translated ORF sequences – http://www.yeastgenome.org/ – reversed sequences and contaminants database were searched; "Re-quantify" and "Match between runs" were enabled with the default parameters; "I=L" box

was checked. The data was extracted from the master table outputted by MaxQuant called “Evidence.txt”, containing all the peptide identification and intensity measurement information. The analysis consisted of the following steps performed by a custom Python script:

1. The peptides mapping to the contaminants, decoy reversed sequence or those containing no lysine were filtered out.
2. For the remaining peptides the heavy label fraction (HLF) was calculated by using heavy/light intensity ratio measurement produced by MaxQuant with following conversion:

$$HLF = \frac{h}{h+l} = \frac{\frac{h}{l}}{\frac{h+l}{l}} = \frac{\frac{h}{l}}{\frac{h}{l}+1}$$

3. To calculate the HLF of a protein the HLFs of its constituent peptides were averaged. For proteins with 4 or more peptides contributing to the HLF calculation, the outlier measurement was filtered out using the following criteria: if the HLF measurement of a peptide < Q1 (first quartile) - 1.5 x IQR (interquartile range) or > Q3 (third quartile) + (1.5 x IQR), that peptide measurement was excluded. No more than one peptide measurement was removed per protein.
4. For all proteins the HLF for each hour of the time course was collated and a Matlab script was used to fit a single exponential model: f(x) = a*exp(b*x), summed spectral counts for the protein in each time point were used as weights. A successful fit was produced if there were four or

five data points. For each model fit the 95% confidence intervals corresponding to **a** and **b** parameters, as well as the R^2 (goodness of fit) were extracted.

5. Finally, SGD annotations for all the protein hits that produced a successful model fit, were searched for key words corresponding nuclear pore complex components and nucleocytoplasmic transport factors to group the data into 3 categories: NPC, transport factors, other.
6. The remaining analysis was performed manually in Excel.

Chimera rendering of NPC dynamics maps

UCSF Chimera package was used to render and color the whole NPC and individual complexes (Pettersen, Goddard et al. 2004) using the map from reference publications (Alber, Dokudovskaya et al. 2007, Alber, Dokudovskaya et al. 2007, Fernandez-Martinez, Phillips et al. 2012).

APPENDIX

Legend

Y_0 – parameter estimate of the heavy label fraction at t_0

95% CI – 95% confidence interval of the parameter estimate

K – the fitted coefficient of the exponential heavy label decay

R^2 – R squared goodness of fit estimate

- total number of unique peptides observed in five samples

AIR02 (wild type) exchange data, 1st replicate

Protein	Y_0	95% CI	K	95% CI	R^2	#
NUP60	1.04	0.08	-0.39	0.04	1.00	131
NUP100	0.82	0.02	-0.14	0.01	1.00	61
NUP1	0.93	0.05	-0.38	0.03	1.00	120
MLP1	0.91	0.08	-0.14	0.03	0.98	198
NDC1	1.10	0.07	-0.39	0.03	1.00	5
NUP159	0.90	0.04	-0.07	0.01	0.98	177
NUP42	0.96	0.11	-0.25	0.05	0.99	17
GLE2	1.04	0.07	-0.24	0.03	1.00	24
NUP2	1.08	0.09	-0.37	0.04	1.00	197
GLE1	0.84	0.22	-0.22	0.11	0.91	26
NUP170	0.81	0.04	-0.07	0.02	0.98	132
NUP188	0.90	0.04	-0.07	0.02	0.98	135
NUP82	0.89	0.03	-0.07	0.01	0.99	63
NUP49	0.80	0.06	-0.07	0.02	0.96	37
SEC13	0.79	0.01	-0.06	0.01	1.00	82
NUP57	0.81	0.04	-0.07	0.02	0.98	56
SEH1	0.97	0.06	-0.06	0.02	0.95	40
MLP2	0.85	0.13	-0.16	0.05	0.96	129
DYN2	1.22	0.20	-0.39	0.08	0.99	19
NUP84	1.04	0.06	-0.05	0.02	0.94	101
POM34	0.86	0.03	-0.08	0.01	0.99	25
NUP85	0.83	0.06	-0.06	0.03	0.93	73
POM152	0.82	0.05	-0.07	0.02	0.96	183
NUP157	0.85	0.04	-0.07	0.01	0.99	133
ASM4	0.74	0.05	-0.07	0.02	0.96	58
NUP192	0.90	0.03	-0.07	0.01	0.99	138
NUP145C	0.79	0.06	-0.05	0.02	0.91	150
NUP145N	0.91	0.06	-0.18	0.02	0.99	54
NUP53	0.83	0.02	-0.11	0.01	1.00	66
NSP1	0.95	0.05	-0.07	0.02	0.98	187
NUP120	0.85	0.04	-0.06	0.02	0.96	87
NUP133	0.90	0.06	-0.05	0.02	0.93	202
NUP116	0.96	0.02	-0.25	0.01	1.00	75
NIC96	0.79	0.03	-0.07	0.01	0.99	131

AIR02 (wild type) turnover data, 1st replicate

Protein	Y_0	95% CI	K	95% CI	R^2	#
NUP60	1.04	0.09	-0.42	0.05	1.00	137
NUP100	1.03	0.07	-0.47	0.04	1.00	68
NUP1	0.96	0.10	-0.47	0.06	1.00	122
SEH1	1.26	0.14	-0.42	0.06	1.00	43
MLP1	1.19	0.16	-0.38	0.06	0.99	153
NDC1	1.04	0.12	-0.39	0.06	0.99	11
NUP159	1.26	0.13	-0.45	0.05	1.00	171
NUP42	1.01	0.25	-0.43	0.14	0.97	19
NUP2	1.07	0.10	-0.39	0.05	1.00	202
GLE2	1.17	0.10	-0.40	0.04	1.00	28
GLE1	1.02	0.20	-0.44	0.10	0.99	29
NUP170	1.06	0.09	-0.49	0.05	1.00	152
NUP188	1.22	0.07	-0.46	0.03	1.00	156
NUP82	1.26	0.08	-0.46	0.03	1.00	73
NUP49	1.11	0.12	-0.51	0.07	1.00	39
SEC13	1.02	0.10	-0.43	0.05	1.00	86
NUP57	1.11	0.07	-0.49	0.04	1.00	55
MLP2	1.06	0.18	-0.39	0.08	0.99	82
DYN2	1.19	0.08	-0.41	0.03	1.00	21
NUP84	0.86	0.24	-0.57	0.18	0.98	140
POM34	1.19	0.08	-0.50	0.03	1.00	25
NUP85	0.99	0.09	-0.44	0.05	1.00	83
POM152	1.15	0.09	-0.50	0.05	1.00	187
NUP157	1.19	0.09	-0.49	0.04	1.00	139
ASM4	1.03	0.12	-0.50	0.06	1.00	59
NUP192	1.23	0.11	-0.48	0.05	1.00	157
NUP145C	0.94	0.10	-0.43	0.06	1.00	168
NUP145N	1.06	0.14	-0.45	0.07	0.99	54
NUP53	1.03	0.04	-0.47	0.02	1.00	65
NSP1	1.33	0.16	-0.45	0.06	0.99	198
NUP120	1.03	0.10	-0.44	0.05	1.00	101
NUP133	0.90	0.13	-0.51	0.08	0.99	238
NUP116	1.09	0.07	-0.44	0.04	1.00	75
NIC96	1.09	0.08	-0.50	0.04	1.00	143

AIR02 (wild type) exchange data, 2nd experiment

Protein	Y_0	95% CI	K	95% CI	R^2	#
NUP60	1.10	0.22	-0.31	0.09	0.97	130
NUP100	0.85	0.13	-0.11	0.05	0.91	39
NUP1	1.10	0.22	-0.32	0.09	0.97	104
MLP1	0.95	0.01	-0.12	0.01	1.00	164
NUP159	0.98	0.05	-0.08	0.02	0.98	137
NDC1	1.18	0.23	-0.33	0.11	0.99	10
NUP42	0.99	0.16	-0.23	0.07	0.97	9
NUP2	1.13	0.22	-0.31	0.09	0.98	145
GLE2	1.08	0.15	-0.22	0.06	0.99	26
GLE1	1.02	0.13	-0.24	0.07	0.98	10
NUP82	0.92	0.03	-0.06	0.01	0.99	59
NUP170	0.89	0.03	-0.07	0.01	0.99	65
NUP188	0.96	0.07	-0.07	0.03	0.95	51
NUP49	0.89	0.03	-0.08	0.01	0.99	37
SEC13	0.86	0.04	-0.06	0.02	0.96	57
NUP57	0.90	0.05	-0.08	0.02	0.98	66
MLP2	0.90	0.04	-0.14	0.02	0.99	106
DYN2	1.12	0.30	-0.30	0.13	0.97	16
NUP84	1.03	0.08	-0.04	0.03	0.86	78
POM34	0.92	0.06	-0.08	0.02	0.97	20
NUP85	0.87	0.06	-0.05	0.03	0.91	35
NUP157	0.92	0.04	-0.07	0.02	0.98	82
SEH1	0.99	0.08	-0.05	0.03	0.89	45
ASM4	0.85	0.04	-0.09	0.02	0.98	39
NUP192	0.97	0.06	-0.07	0.02	0.97	28
NUP145C	0.85	0.05	-0.04	0.02	0.90	119
NUP145N	0.97	0.20	-0.18	0.08	0.93	41
POM152	0.91	0.05	-0.07	0.02	0.97	119
NUP53	0.93	0.04	-0.12	0.02	0.99	51
NSP1	1.01	0.04	-0.07	0.01	0.99	161
NUP120	0.89	0.07	-0.05	0.03	0.87	38
NUP133	0.97	0.06	-0.05	0.02	0.93	103
NUP116	1.00	0.08	-0.22	0.03	0.99	65
NIC96	0.86	0.07	-0.07	0.03	0.95	68

AIR02 (wild type) turnover data, 2nd replicate

Protein	Y_0	95% CI	K	95% CI	R^2	#
NUP60	1.13	0.22	-0.35	0.10	0.98	120
NUP100	1.10	0.45	-0.38	0.20	0.91	30
NUP1	1.15	0.20	-0.42	0.09	0.99	79
MLP1	1.18	0.26	-0.30	0.10	0.98	78
NUP159	1.30	0.27	-0.36	0.10	0.98	97
NUP2	1.11	0.21	-0.32	0.09	0.98	146
GLE2	0.97	0.91	-0.25	0.40	0.72	28
GLE1	1.17	0.23	-0.38	0.09	0.98	11
NUP170	1.19	0.19	-0.41	0.09	0.99	42
NUP188	1.27	0.32	-0.36	0.12	0.96	25
NUP82	1.32	0.28	-0.39	0.10	0.98	24
NUP49	1.17	0.28	-0.44	0.12	0.99	26
SEC13	1.07	0.19	-0.37	0.09	0.98	32
NUP57	1.19	0.17	-0.42	0.07	0.99	53
SEH1	1.29	0.30	-0.36	0.10	0.97	46
MLP2	1.14	0.33	-0.35	0.14	0.98	30
DYN2	0.83	0.43	-0.28	0.24	0.82	8
NUP84	0.99	0.16	-0.54	0.10	0.99	111
POM34	1.26	0.24	-0.42	0.10	0.98	33
NUP85	1.11	0.14	-0.39	0.06	0.99	30
POM152	1.25	0.15	-0.42	0.07	0.99	73
NUP157	1.30	0.16	-0.45	0.06	0.99	47
ASM4	1.15	0.17	-0.44	0.08	0.99	30
NUP192	1.36	0.55	-0.41	0.20	0.97	6
NUP145C	1.08	0.09	-0.39	0.04	1.00	121
NUP145N	1.08	0.26	-0.37	0.12	0.97	31
NUP53	1.12	0.14	-0.38	0.07	0.99	38
NSP1	1.32	0.32	-0.35	0.12	0.97	112
NUP120	1.13	0.16	-0.39	0.07	0.99	48
NUP133	1.09	0.04	-0.48	0.02	1.00	115
NUP116	1.10	0.20	-0.35	0.09	0.98	61
NIC96	1.17	0.31	-0.43	0.14	0.99	43

ZH38 (Nup145N-C fusion) exchange data, 1st replicate

Protein	Y_0	95% CI	K	95% CI	R^2	#
NUP60	1.07	0.08	-0.29	0.04	1.00	131
NUP100	0.81	0.04	-0.14	0.02	0.99	48
NUP1	1.05	0.07	-0.37	0.04	1.00	72
MLP1	0.98	0.13	-0.16	0.05	0.97	222
NUP159	0.93	0.09	-0.06	0.03	0.87	110
NUP42	0.99	0.10	-0.24	0.06	0.99	11
GLE2	1.08	0.05	-0.23	0.02	1.00	37
NUP2	1.00	0.12	-0.25	0.06	0.98	147
GLE1	0.92	0.19	-0.25	0.09	0.96	14
NUP188	0.94	0.09	-0.06	0.04	0.87	18
NUP170	0.84	0.08	-0.05	0.04	0.82	41
NUP82	0.88	0.19	-0.04	0.09	0.49	32
NUP49	0.87	0.10	-0.05	0.04	0.79	41
SEC13	0.77	0.13	-0.08	0.07	0.72	21
NUP57	0.87	0.11	-0.05	0.04	0.77	69
MLP2	0.92	0.14	-0.18	0.06	0.96	161
DYN2	1.21	0.19	-0.31	0.08	0.98	9
NUP84	0.96	0.07	-0.02	0.03	0.63	37
POM34	0.89	0.15	-0.06	0.07	0.66	21
NUP85	0.77	0.23	-0.03	0.11	0.21	15
POM152	0.89	0.11	-0.06	0.05	0.80	93
NUP157	0.86	0.09	-0.05	0.04	0.83	57
SEH1	0.98	0.06	-0.07	0.02	0.95	39
ASM4	0.78	0.12	-0.05	0.06	0.63	31
NUP192	0.88	0.13	-0.05	0.07	0.51	18
NUP145C	0.74	0.08	-0.04	0.04	0.78	66
NUP145N	0.74	0.12	-0.05	0.06	0.62	47
NUP53	0.88	0.06	-0.10	0.03	0.97	51
NSP1	0.96	0.09	-0.05	0.03	0.87	132
NUP116	1.03	0.04	-0.25	0.02	1.00	71
NUP120	0.85	0.13	-0.07	0.06	0.79	11
NUP133	0.91	0.06	-0.05	0.03	0.91	42
NIC96	0.84	0.12	-0.05	0.05	0.69	49

ZH38 (Nup145N-C fusion) turnover data, 1st replicate

Protein	Y_0	95% CI	K	95% CI	R^2	#
NUP60	1.10	0.08	-0.34	0.04	1.00	128
NUP100	1.06	0.08	-0.40	0.04	1.00	61
NUP1	1.04	0.06	-0.41	0.03	1.00	89
MLP1	1.19	0.08	-0.34	0.03	1.00	196
NUP159	1.31	0.17	-0.38	0.07	0.99	194
NDC1	1.10	0.09	-0.33	0.04	1.00	32
NUP42	1.05	0.10	-0.34	0.05	0.99	24
GLE2	1.18	0.06	-0.33	0.02	1.00	37
NUP2	1.09	0.10	-0.32	0.04	0.99	195
GLE1	1.13	0.14	-0.40	0.06	0.99	36
NUP170	1.21	0.09	-0.45	0.04	1.00	187
NUP188	1.28	0.14	-0.38	0.05	0.99	166
NUP82	1.28	0.13	-0.38	0.05	0.99	94
NUP49	1.22	0.09	-0.44	0.04	1.00	42
SEC13	1.04	0.09	-0.41	0.05	1.00	68
NUP57	1.23	0.08	-0.44	0.03	1.00	61
SEH1	1.31	0.12	-0.37	0.04	1.00	55
MLP2	1.08	0.07	-0.37	0.03	1.00	132
DYN2	1.21	0.11	-0.35	0.05	1.00	26
NUP84	1.14	0.36	-0.66	0.21	0.98	133
POM34	1.27	0.10	-0.44	0.04	1.00	33
NUP85	1.11	0.10	-0.44	0.05	1.00	78
POM152	1.25	0.06	-0.44	0.03	1.00	222
NUP157	1.22	0.09	-0.43	0.04	1.00	182
ASM4	1.14	0.12	-0.45	0.06	1.00	50
NUP192	1.28	0.11	-0.39	0.04	1.00	166
NUP145C	0.99	0.10	-0.43	0.06	1.00	142
NUP145N	0.98	0.11	-0.44	0.06	1.00	57
NUP53	1.17	0.11	-0.43	0.05	1.00	69
NSP1	1.33	0.21	-0.36	0.07	0.99	204
NUP120	1.15	0.10	-0.42	0.05	1.00	84
NUP133	1.13	0.17	-0.46	0.08	0.99	235
NUP116	1.10	0.05	-0.36	0.02	1.00	79
NIC96	1.22	0.08	-0.45	0.04	1.00	148

ZH38 (Nup145N-C fusion) exchange data, 2nd replicate

Protein	Y_0	95% CI	K	95% CI	R^2	#
NUP60	1.03	0.13	-0.37	0.06	0.99	125
NUP100	0.84	0.03	-0.21	0.01	1.00	69
NUP1	1.00	0.05	-0.47	0.03	1.00	81
SEH1	0.96	0.01	-0.10	0.00	1.00	50
MLP1	0.91	0.13	-0.17	0.05	0.96	304
NUP159	0.89	0.04	-0.08	0.02	0.99	175
NDC1	1.04	0.08	-0.35	0.04	1.00	13
NUP42	0.94	0.28	-0.30	0.14	0.97	10
NUP2	1.05	0.11	-0.36	0.05	0.99	161
GLE2	1.06	0.07	-0.29	0.03	1.00	42
GLE1	0.96	0.08	-0.34	0.04	1.00	28
NUP170	0.82	0.03	-0.08	0.01	0.99	158
NUP188	0.90	0.01	-0.08	0.00	1.00	150
NUP82	0.86	0.05	-0.08	0.02	0.98	85
NUP49	0.81	0.02	-0.07	0.01	0.99	38
SEC13	0.74	0.05	-0.08	0.03	0.97	63
NUP57	0.82	0.03	-0.07	0.01	0.99	47
MLP2	0.83	0.12	-0.19	0.06	0.97	239
DYN2	1.13	0.11	-0.37	0.05	1.00	22
NUP84	1.01	0.04	-0.06	0.01	0.99	87
POM34	0.85	0.04	-0.09	0.01	0.99	29
NUP85	0.80	0.03	-0.09	0.02	0.99	58
NUP157	0.86	0.04	-0.10	0.02	0.99	153
ASM4	0.76	0.02	-0.08	0.01	0.99	52
NUP192	0.90	0.02	-0.08	0.01	0.99	144
NUP145C	0.72	0.02	-0.06	0.01	0.99	120
NUP145N	0.71	0.02	-0.07	0.01	0.99	63
POM152	0.83	0.03	-0.08	0.01	0.99	172
NUP53	0.85	0.02	-0.14	0.01	1.00	59
NSP1	0.94	0.02	-0.08	0.01	1.00	193
NUP120	0.82	0.02	-0.09	0.01	1.00	96
NUP133	0.90	0.03	-0.07	0.01	0.99	173
NUP116	0.98	0.06	-0.31	0.03	1.00	79
NIC96	0.79	0.03	-0.07	0.01	0.99	127

ZH38 (Nup145N-C fusion) turnover data, 2nd replicate

Protein	Y_0	95% CI	K	95% CI	R^2	#
NUP60	1.08	0.13	-0.40	0.06	0.99	129
NUP100	1.07	0.08	-0.46	0.04	1.00	69
NUP1	1.04	0.12	-0.48	0.07	1.00	109
MLP1	1.21	0.12	-0.41	0.05	1.00	197
NUP159	1.27	0.17	-0.45	0.07	0.99	199
NDC1	1.07	0.16	-0.38	0.07	0.99	25
NUP42	1.18	0.22	-0.44	0.08	0.99	13
NUP2	1.09	0.14	-0.38	0.06	0.99	184
GLE2	1.15	0.10	-0.37	0.04	1.00	34
GLE1	1.10	0.08	-0.47	0.04	1.00	29
NUP170	1.18	0.13	-0.52	0.06	1.00	189
NUP188	1.29	0.18	-0.47	0.07	0.99	171
NUP82	1.22	0.12	-0.45	0.05	1.00	86
NUP49	1.19	0.08	-0.52	0.04	1.00	43
SEC13	1.01	0.09	-0.46	0.05	1.00	63
NUP57	1.21	0.09	-0.51	0.04	1.00	72
SEH1	1.29	0.16	-0.43	0.06	0.99	46
MLP2	1.05	0.06	-0.42	0.03	1.00	154
DYN2	1.20	0.18	-0.41	0.07	0.99	22
NUP84	0.89	0.15	-0.63	0.11	0.99	136
POM34	1.24	0.14	-0.52	0.06	1.00	34
NUP85	1.06	0.08	-0.47	0.04	1.00	78
POM152	1.20	0.09	-0.51	0.04	1.00	214
NUP157	1.19	0.12	-0.50	0.06	1.00	199
ASM4	1.10	0.12	-0.53	0.07	1.00	63
NUP192	1.29	0.14	-0.47	0.06	1.00	161
NUP145C	0.96	0.07	-0.48	0.04	1.00	154
NUP145N	0.95	0.11	-0.49	0.06	1.00	61
NUP53	1.11	0.08	-0.48	0.04	1.00	69
NSP1	1.34	0.32	-0.44	0.13	0.98	194
NUP120	1.09	0.06	-0.47	0.03	1.00	92
NUP133	1.03	0.07	-0.50	0.04	1.00	229
NUP116	1.05	0.07	-0.40	0.04	1.00	82
NIC96	1.18	0.10	-0.52	0.05	1.00	145

ZH42 (Nup145NΔFG) exchange data, 1st replicate

Protein	Y_0	95% CI	K	95% CI	R^2	#
NUP60	1.05	0.20	-0.33	0.09	0.98	158
NUP100	0.82	0.06	-0.11	0.02	0.98	64
NUP1	0.93	0.13	-0.28	0.06	0.98	129
MLP1	0.91	0.03	-0.11	0.01	1.00	131
NDC1	1.09	0.14	-0.29	0.07	0.99	20
NUP159	0.85	0.04	-0.04	0.01	0.94	173
NUP42	0.98	0.10	-0.27	0.05	0.99	13
GLE2	1.05	0.13	-0.22	0.05	0.98	54
NUP2	1.07	0.17	-0.32	0.07	0.98	181
GLE1	1.01	0.18	-0.26	0.07	0.97	13
NUP170	0.79	0.04	-0.03	0.02	0.87	80
NUP188	0.85	0.04	-0.03	0.02	0.91	49
NUP82	0.89	0.02	-0.04	0.01	0.99	58
NUP49	0.89	0.03	-0.04	0.01	0.97	39
SEC13	0.84	0.02	-0.03	0.01	0.97	40
NUP57	0.90	0.00	-0.04	0.00	1.00	92
SEH1	0.97	0.07	-0.03	0.02	0.74	52
MLP2	0.88	0.02	-0.12	0.01	1.00	94
DYN2	1.19	0.51	-0.34	0.19	0.91	12
NUP84	0.98	0.04	-0.02	0.01	0.80	75
POM34	0.84	0.02	-0.04	0.01	0.99	44
NUP85	0.82	0.03	-0.01	0.02	0.11	38
NUP157	0.81	0.02	-0.03	0.01	0.97	89
ASM4	0.80	0.02	-0.04	0.01	0.98	48
NUP192	0.85	0.02	-0.03	0.01	0.98	36
NUP145C	0.86	0.03	-0.02	0.01	0.83	132
NUP145N	0.88	0.08	-0.14	0.03	0.98	45
POM152	0.83	0.02	-0.03	0.01	0.98	134
NUP53	0.84	0.08	-0.06	0.03	0.88	62
NSP1	0.86	0.02	-0.04	0.01	0.98	148
NUP116	1.00	0.12	-0.23	0.05	0.98	106
NUP120	0.89	0.15	-0.03	0.06	0.36	46
NUP133	0.88	0.03	-0.04	0.01	0.97	85
NIC96	0.79	0.01	-0.03	0.00	1.00	90

ZH42 (Nup145NΔFG) turnover data, 1st replicate

Protein	Y_0	95% CI	K	95% CI	R^2	#
NUP60	1.06	0.18	-0.38	0.09	0.99	150
NUP100	0.99	0.12	-0.37	0.06	0.99	87
NUP1	0.94	0.12	-0.35	0.06	0.99	137
SEH1	1.26	0.19	-0.36	0.07	0.99	59
MLP1	1.12	0.27	-0.33	0.10	0.97	74
NUP159	1.18	0.20	-0.42	0.08	0.99	184
NDC1	0.99	0.09	-0.34	0.04	1.00	38
NUP42	1.03	0.13	-0.36	0.05	0.99	27
NUP2	1.08	0.16	-0.36	0.07	0.99	196
GLE2	1.17	0.16	-0.35	0.06	0.99	38
GLE1	1.05	0.11	-0.37	0.05	0.99	44
NUP170	1.01	0.10	-0.42	0.05	1.00	214
NUP188	1.13	0.13	-0.41	0.06	0.99	182
NUP82	1.22	0.22	-0.40	0.09	0.99	86
NUP49	1.17	0.13	-0.42	0.06	1.00	50
SEC13	1.00	0.08	-0.40	0.04	1.00	91
NUP57	1.20	0.17	-0.41	0.08	0.99	65
MLP2	1.05	0.18	-0.32	0.07	0.98	32
DYN2	1.19	0.39	-0.38	0.15	0.95	22
NUP84	1.02	0.26	-0.52	0.15	0.98	141
POM34	1.11	0.14	-0.41	0.07	0.99	29
POM152	1.08	0.10	-0.40	0.05	1.00	230
NUP85	1.03	0.08	-0.43	0.04	1.00	126
NUP157	1.04	0.10	-0.42	0.05	1.00	170
ASM4	1.08	0.12	-0.44	0.06	1.00	59
NUP192	1.12	0.11	-0.41	0.05	1.00	202
NUP145C	0.95	0.07	-0.41	0.03	1.00	203
NUP145N	0.99	0.10	-0.36	0.05	1.00	61
NUP53	1.03	0.10	-0.40	0.05	1.00	64
NSP1	1.16	0.19	-0.44	0.09	0.99	187
NUP120	1.03	0.07	-0.42	0.04	1.00	118
NUP133	1.03	0.08	-0.41	0.04	1.00	186
NUP116	1.08	0.15	-0.38	0.07	0.99	95
NIC96	1.04	0.09	-0.42	0.04	1.00	150

ZH42 (Nup145NΔFG) exchange data, 2nd replicate

Protein	Y_0	95% CI	K	95% CI	R^2	#
NUP60	1.00	0.10	-0.39	0.05	1.00	138
NUP100	0.78	0.07	-0.12	0.03	0.97	75
NUP1	0.87	0.09	-0.32	0.05	0.99	132
MLP1	0.89	0.09	-0.13	0.03	0.98	134
NDC1	0.97	0.05	-0.32	0.03	1.00	14
NUP159	0.79	0.05	-0.04	0.02	0.88	171
NUP42	0.96	0.06	-0.30	0.03	1.00	19
NUP2	1.01	0.10	-0.38	0.05	0.99	169
GLE2	1.02	0.09	-0.26	0.03	0.99	29
GLE1	0.94	0.04	-0.29	0.02	1.00	44
NUP170	0.77	0.04	-0.03	0.02	0.89	170
NUP188	0.80	0.04	-0.03	0.02	0.85	169
NUP82	0.85	0.04	-0.04	0.02	0.95	72
NUP49	0.84	0.05	-0.03	0.02	0.86	45
SEC13	0.83	0.01	-0.03	0.01	0.99	82
NUP57	0.86	0.04	-0.03	0.02	0.92	65
SEH1	0.99	0.03	-0.03	0.01	0.97	46
MLP2	0.83	0.12	-0.13	0.05	0.94	95
DYN2	1.13	0.11	-0.39	0.05	1.00	25
NUP84	1.00	0.04	-0.03	0.01	0.94	105
POM34	0.81	0.05	-0.04	0.02	0.91	33
NUP85	0.87	0.03	-0.03	0.01	0.96	92
POM152	0.80	0.05	-0.03	0.02	0.84	197
NUP157	0.77	0.05	-0.04	0.02	0.88	179
ASM4	0.75	0.05	-0.04	0.02	0.88	56
NUP192	0.80	0.04	-0.03	0.02	0.84	152
NUP145C	0.86	0.03	-0.03	0.01	0.93	155
NUP145N	0.84	0.07	-0.16	0.03	0.99	56
NUP53	0.83	0.04	-0.07	0.01	0.98	61
NSP1	0.81	0.04	-0.03	0.02	0.92	176
NUP116	0.94	0.05	-0.28	0.02	1.00	82
NUP120	0.89	0.03	-0.03	0.01	0.96	87
NUP133	0.83	0.02	-0.04	0.01	0.98	162
NIC96	0.75	0.04	-0.03	0.02	0.83	145

ZH42 (Nup145NΔFG) turnover data, 2nd replicate

Protein	Y_0	95% CI	K	95% CI	R^2	#
NUP60	1.02	0.12	-0.43	0.06	0.99	121
NUP100	0.95	0.07	-0.41	0.04	1.00	72
NUP1	0.91	0.10	-0.41	0.06	0.99	136
MLP1	1.09	0.28	-0.37	0.11	0.97	71
NUP159	1.06	0.11	-0.46	0.05	1.00	171
NDC1	0.99	0.08	-0.38	0.03	1.00	17
NUP42	0.83	0.28	-0.34	0.12	0.95	17
NUP2	1.03	0.09	-0.41	0.04	1.00	175
GLE2	1.13	0.11	-0.40	0.05	1.00	26
GLE1	1.02	0.15	-0.42	0.07	0.99	39
NUP170	0.95	0.11	-0.46	0.06	0.99	175
NUP188	1.06	0.09	-0.46	0.05	1.00	161
NUP82	1.15	0.11	-0.45	0.05	1.00	81
NUP49	1.12	0.10	-0.46	0.05	1.00	43
SEC13	0.88	0.10	-0.42	0.06	0.99	84
NUP57	1.14	0.12	-0.45	0.06	1.00	65
SEH1	1.21	0.15	-0.39	0.06	0.99	49
MLP2	1.10	0.15	-0.38	0.05	0.99	36
DYN2	1.20	0.14	-0.45	0.06	0.99	22
NUP84	0.77	0.16	-0.49	0.12	0.98	133
POM34	1.04	0.15	-0.47	0.08	0.99	30
NUP85	0.91	0.12	-0.46	0.07	0.99	110
POM152	1.02	0.10	-0.45	0.05	1.00	201
NUP157	0.98	0.09	-0.46	0.05	1.00	151
ASM4	1.00	0.14	-0.48	0.08	0.99	56
NUP192	1.04	0.11	-0.46	0.06	1.00	166
NUP145C	0.83	0.10	-0.43	0.06	0.99	185
NUP145N	0.95	0.08	-0.43	0.04	1.00	54
NUP53	0.99	0.11	-0.45	0.06	1.00	62
NSP1	1.12	0.14	-0.49	0.07	0.99	174
NUP120	0.92	0.10	-0.44	0.06	1.00	109
NUP133	0.87	0.09	-0.43	0.05	1.00	167
NUP116	1.04	0.08	-0.43	0.04	1.00	75
NIC96	0.97	0.12	-0.46	0.06	0.99	133

BIBLIOGRAPHY

Aitchison, J. D., G. Blobel and M. P. Rout (1995). "Nup120p: a yeast nucleoporin required for NPC distribution and mRNA transport." The Journal of Cell Biology **131**(6 Pt 2): 1659-1675.

Aitchison, J. D. and M. P. Rout (2012). "The Yeast Nuclear Pore Complex and Transport Through It." Genetics **190**(3): 855-883.

Alber, F., S. Dokudovskaya, L. M. Veenhoff, W. Zhang, J. Kipper, D. Devos, A. Suprapto, O. Karni-Schmidt, R. Williams, B. T. Chait, M. P. Rout and A. Sali (2007). "Determining the architectures of macromolecular assemblies." Nature **450**(7170): 683-694.

Alber, F., S. Dokudovskaya, L. M. Veenhoff, W. Zhang, J. Kipper, D. Devos, A. Suprapto, O. Karni-Schmidt, R. Williams, B. T. Chait, A. Sali and M. P. Rout (2007). "The molecular architecture of the nuclear pore complex." Nature **450**(7170): 695-701.

Alberts, B. (1998). The cell as a collection of protein machines: preparing the next generation of molecular biologists. Cell.

Araki, Y., C. K. Lau and H. Maekawa (2006). The Saccharomyces cerevisiae spindle pole body (SPB) component Nbp1p is required for SPB membrane insertion and interacts with the integral membrane …. Molecular biology of ….

Asakawa, H., C. Mori, C. Ohtsuki, M. Iwamoto, Y. Hiraoka and T. Haraguchi (2015). Uncleavable Nup98-Nup96 is functional in the fission yeast Schizosaccharomyces pombe. FEBS Open Bio. **5:** 508-514.

Babu, M., J. Vlasblom, S. Pu, X. Guo, C. Graham, B. D. M. Bean, H. E. Burston, F. J. Vizeacoumar, J. Snider, S. Phanse, V. Fong, Y. Y. C. Tam, M. Davey, O. Hnatshak, N. Bajaj, S. Chandran, T. Punna, C. Christopolous, V. Wong, A. Yu, G. Zhong, J. Li, I. Stagljar, E. Conibear, S. J. Wodak, A. Emili and J. F. Greenblatt (2012). "Interaction landscape of membrane-protein complexes in Saccharomyces cerevisiae." Nature **489**(7417): 585-589.

Bailer, S. M., C. Balduf and E. Hurt (2001). "The Nsp1p carboxy-terminal domain is organized into functionally distinct coiled-coil regions required for assembly of nucleoporin subcomplexes and nucleocytoplasmic transport." Mol Cell Biol **21**(23): 7944-7955.

Belgareh, N. and V. Doye (1997). "Dynamics of nuclear pore distribution in nucleoporin mutant yeast cells." The Journal of Cell Biology **136**(4): 747-759.

Belgareh, N., C. Snay-Hodge, F. Pasteau, S. Dagher, C. N. Cole and V. Doye (1998). "Functional characterization of a Nup159p-containing nuclear pore subcomplex." Mol Biol Cell **9**(12): 3475-3492.

Berens, C., A. Thain and R. Schroeder (2001). A tetracycline-binding RNA aptamer. Bioorg. Med. Chem. **9:** 2549-2556.

Beynon, R. J. (2005). The dynamics of the proteome: Strategies for measuring protein turnover on a proteome-wide scale. Briefings in Functional Genomics and Proteomics, Oxford University Press. **3:** 382-390.

Beynon, R. J. (2005). Metabolic Labeling of Proteins for Proteomics. Molecular & Cellular Proteomics. **4:** 857-872.

Bitterman, K. J., O. Medvedik and D. A. Sinclair (2003). Longevity regulation in Saccharomyces cerevisiae: linking metabolism, genome stability, and heterochromatin. Microbiol Mol Biol Rev, American Society for Microbiology. **67:** 376-399- table of contents.

Boehlke, K. W. and J. D. Friesen (1975). Cellular content of ribonucleic acid and protein in Saccharomyces cerevisiae as a function of exponential growth rate: calculation of the apparent peptide chain elongation rate. J. Bacteriol. **121:** 429-433.

Boisvert, F.-M., Y. Ahmad, M. Gierliński, F. Charrière, D. Lamont, M. Scott, G. Barton and A. I. Lamond (2012). A quantitative spatial proteomics analysis of proteome turnover in human cells. Molecular & Cellular Proteomics, American Society for Biochemistry and Molecular Biology. **11:** M111.011429-M011111.011429.

Boström, M., F. W. Tavares, S. Finet, F. Skouri-Panet, A. Tardieu and B. W. Ninham (2005). Why forces between proteins follow different Hofmeister series for pH above and below pI. Biophysical Chemistry. **117:** 217-224.

Breitkreutz, B. J., C. Stark, T. Reguly, L. Boucher, A. Breitkreutz, M. Livstone, R. Oughtred, D. H. Lackner, J. Bahler, V. Wood, K. Dolinski and M. Tyers (2007). The BioGRID Interaction Database: 2008 update. Nucleic Acids Res. **36:** D637-D640.

Cambridge, S. B., F. Gnad, C. Nguyen, J. L. Bermejo, M. Krüger and M. Mann (2011). "Systems-wide Proteomic Analysis in Mammalian Cells Reveals Conserved, Functional Protein Turnover." Journal of proteome research **10**(12): 5275-5284.

Capelson, M., C. Doucet and M. W. Hetzer (2011). "Nuclear Pore Complexes: Guardians of the Nuclear Genome." Cold Spring Harbor Symposia on Quantitative Biology: 1-14.

Casey, A. K., T. R. Dawson, J. Chen, J. M. Friederichs, S. L. Jaspersen and S. R. Wente (2012). Integrity and Function of the Saccharomyces cerevisiae Spindle Pole Body Depends on Connections Between the Membrane Proteins Ndc1, Rtn1, and Yop1. Genetics. **192:** 441-455.

Chen, S. S., E. Sperling, J. M. Silverman, J. H. Davis and J. R. Williamson (2012). Measuring the dynamics of E. coli ribosome biogenesis using pulse-labeling and quantitative mass spectrometry. Mol. BioSyst., The Royal Society of Chemistry. **8:** 3325-3310.

Chial, H. J., M. P. Rout, T. H. Giddings and M. Winey (1998). "Saccharomyces cerevisiae Ndc1p is a shared component of nuclear pore complexes and spindle pole bodies." The Journal of Cell Biology **143**(7): 1789-1800.

Christiano, R., N. Nagaraj, F. Fröhlich and T. C. Walther (2014). Global Proteome Turnover Analyses of the Yeasts S. cerevisiae and S. pombe. CellReports, The Authors. **9:** 1959-1965.

Ciechanover, A. (2005). Intracellular protein degradation: from a vague idea thru the lysosome and the ubiquitin–proteasome system and onto human diseases and drug targeting*. Cell Death Differ. **12:** 1178-1190.

Colombi, P., B. M. Webster, F. Frohlich and C. P. Lusk (2013). The transmission of nuclear pore complexes to daughter cells requires a cytoplasmic pool of Nsp1. The Journal of Cell Biology. **203:** 215-232.

Cox, J. and M. Mann (2008). "MaxQuant enables high peptide identification rates, individualized p.p.b.-range mass accuracies and proteome-wide protein quantification." Nature biotechnology **26**(12): 1367-1372.

Cristea, I. M., R. Williams, B. T. Chait and M. P. Rout (2005). Fluorescent proteins as proteomic probes. Mol Cell Proteomics. **4:** 1933-1941.

D'Angelo, M. A., J. S. Gomez-Cavazos, A. Mei, D. H. Lackner and M. W. Hetzer (2012). A Change in Nuclear Pore Complex Composition Regulates Cell Differentiation. Developmental Cell. **22:** 446-458.

D'Angelo, M. A., M. Raices, S. H. Panowski and M. W. Hetzer (2009). "Age-dependent deterioration of nuclear pore complexes causes a loss of nuclear integrity in postmitotic cells." Cell **136**(2): 284-295.

Daigle, N. (2001). Nuclear pore complexes form immobile networks and have a very low turnover in live mammalian cells. The Journal of Cell Biology. **154:** 71-84.

Davis, L. I. and G. Blobel (1986). Identification and characterization of a nuclear pore complex protein. Cell. **45:** 699-709.

Dawson, T. R., M. D. Lazarus, M. W. Hetzer and S. R. Wente (2009). "ER membrane-bending proteins are necessary for de novo nuclear pore formation." The Journal of Cell Biology **184**(5): 659-675.

De Craene, J.-O., J. Coleman, P. Estrada de Martin, M. Pypaert, S. Anderson, J. R. Yates, S. Ferro-Novick and P. Novick (2006). "Rtn1p is involved in structuring the cortical endoplasmic reticulum." Molecular biology of the cell **17**(7): 3009-3020.

De Souza, C. P. C., A. H. Osmani, S. B. Hashmi and S. A. Osmani (2004). "Partial nuclear pore complex disassembly during closed mitosis in Aspergillus nidulans." Curr Biol **14**(22): 1973-1984.

De Souza, C. P. C. and S. A. Osmani (2007). Mitosis, Not Just Open or Closed. Eukaryotic Cell. **6:** 1521-1527.

Degrasse, J. A., K. N. DuBois, D. Devos, T. N. Siegel, A. Sali, M. C. Field, M. P. Rout and B. T. Chait (2009). "Evidence for a shared nuclear pore complex architecture that is conserved from the last common eukaryotic ancestor." Mol Cell Proteomics **8**(9): 2119-2130.

Denning, D., B. Mykytka, N. P. Allen, L. Huang, A. Burlingame and M. Rexach (2001). The nucleoporin Nup60p functions as a Gsp1p-GTP-sensitive tether for Nup2p at the nuclear pore complex. The Journal of Cell Biology, Rockefeller Univ Press. **154:** 937-950.

Devos, D., S. Dokudovskaya, R. Williams, F. Alber, N. Eswar, B. T. Chait, M. P. Rout and A. Sali (2006). "Simple fold composition and modular architecture of the nuclear pore complex." Proc Natl Acad Sci USA **103**(7): 2172-2177.

Dilworth, D. J., A. Suprapto, J. C. Padovan, B. T. Chait, R. W. Wozniak, M. P. Rout and J. D. Aitchison (2001). Nup2p dynamically associates with the distal regions of the yeast nuclear pore complex. The Journal of Cell Biology. **153:** 1465-1478.

Doherty, M. K., D. E. Hammond, M. J. Clague, S. J. Gaskell and R. J. Beynon (2009). Turnover of the Human Proteome: Determination of Protein Intracellular Stability by Dynamic SILAC. J Proteome Res. **8:** 104-112.

Doucet, C. M., J. A. Talamas and M. W. Hetzer (2010). "Cell cycle-dependent differences in nuclear pore complex assembly in metazoa." Cell **141**(6): 1030-1041.

Dultz, E. and J. Ellenberg (2010). "Live imaging of single nuclear pores reveals unique assembly kinetics and mechanism in interphase." The Journal of Cell Biology **191**(1): 15-22.

Dundr, M., M. D. Hebert, T. S. Karpova, D. Stanek, H. Xu, K. B. Shpargel, U. T. Meier, K. M. Neugebauer, A. G. Matera and T. Misteli (2004). In vivo kinetics of Cajal body components. The Journal of Cell Biology, Rockefeller Univ Press. **164:** 831-842.

Eisenhardt, N., J. Redolfi and W. Antonin (2013). Nup53 interaction with Ndc1 and Nup155 are required for nuclear pore complex assembly. J Cell Sci.

Emtage, J. L., M. Bucci, J. L. Watkins and S. R. Wente (1997). Defining the essential functional regions of the nucleoporin Nup145p. J Cell Sci, The Company of Biologists Ltd. **110 (Pt 7):** 911-925.

Fabre, E., W. C. Boelens, C. Wimmer, I. W. Mattaj and E. C. Hurt (1994). Nup145p is required for nuclear export of mRNA and binds homopolymeric RNA in vitro via a novel conserved motif. Cell. **78:** 275-289.

Fernandez-Martinez, J., J. Phillips, M. D. Sekedat, R. Diaz-Avalos, J. Velazquez-Muriel, J. D. Franke, R. Williams, D. L. Stokes, B. T. Chait, A. Sali and M. P. Rout (2012). Structure-function mapping of a heptameric module in the nuclear pore complex. The Journal of Cell Biology. **196:** 419-434.

Fernandez-Martinez, J., J. Phillips, M. D. Sekedat, R. Diaz-Avalos, J. Velázquez-Muriel, J. D. Franke, R. Williams, D. L. Stokes, B. T. Chait, A. Sali and M. P. Rout (2012). Structure-function mapping of a heptameric module in the nuclear pore complex. The Journal of Cell Biology, Rockefeller Univ Press. **196:** 419-434.

Fernandez-Martinez, J. and M. P. Rout (2009). "Nuclear pore complex biogenesis." Curr Opin Cell Biol **21**(4): 603-612.

Fernandez-Martinez, J. and M. P. Rout (2009). Nuclear pore complex biogenesis. Curr Opin Cell Biol. **21:** 603-612.

Fischer, J., R. Teimer, S. Amlacher, R. Kunze and E. Hurt (2015). Linker Nups connect the nuclear pore complex inner ring with the outer ring and transport channel. Nat Struct Mol Biol, Nature Publishing Group**:** 1-10.

Fröhlich, F., R. Christiano and T. C. Walther (2013). Native SILAC: metabolic labeling of proteins in prototroph microorganisms based on lysine synthesis

regulation. Molecular & Cellular Proteomics, American Society for Biochemistry and Molecular Biology. **12:** 1995-2005.

Gaik, M., D. Flemming, A. von Appen, P. Kastritis, N. Mücke, J. Fischer, P. Stelter, A. Ori, K. H. Bui, J. Baßler, E. Barbar, M. Beck and E. Hurt (2015). Structural basis for assembly and function of the Nup82 complex in the nuclear pore scaffold. The Journal of Cell Biology. **208:** 283-297.

Garlick, P. J. and D. J. Millward (1972). An appraisal of techniques for the determination of protein turnover in vivo. Proceedings of the Nutrition Society, Cambridge University Press. **31:** 249-255.

Gavin, A.-C., P. Aloy, P. Grandi, R. Krause, M. Boesche, M. Marzioch, C. Rau, L. J. Jensen, S. Bastuck, B. Dümpelfeld, A. Edelmann, M.-A. Heurtier, V. Hoffman, C. Hoefert, K. Klein, M. Hudak, A.-M. Michon, M. Schelder, M. Schirle, M. Remor, T. Rudi, S. Hooper, A. Bauer, T. Bouwmeester, G. Casari, G. Drewes, G. Neubauer, J. M. Rick, B. Kuster, P. Bork, R. B. Russell and G. Superti-Furga (2006). "Proteome survey reveals modularity of the yeast cell machinery." Nature **440**(7084): 631-636.

Grandi, P., N. Schlaich, H. Tekotte and E. C. Hurt (1995). "Functional interaction of Nic96p with a core nucleoporin complex consisting of Nsp1p, Nup49p and a novel protein Nup57p." EMBO J **14**(1): 76-87.

Griffis, E. R., N. Altan and J. Lippincott-Schwartz (2002). Nup98 is a mobile nucleoporin with transcription-dependent dynamics. Molecular biology of ….

Griffis, E. R., B. Craige, C. Dimaano, K. S. Ullman and M. A. Powers (2004). Distinct functional domains within nucleoporins Nup153 and Nup98 mediate transcription-dependent mobility. Mol Biol Cell, American Society for Cell Biology. **15:** 1991-2002.

Gruhler, A., J. V. Olsen, S. Mohammed, P. Mortensen, N. J. Faergeman, M. Mann and O. N. Jensen (2005). Quantitative phosphoproteomics applied to the yeast pheromone signaling pathway. Mol Cell Proteomics, American Society for Biochemistry and Molecular Biology. **4:** 310-327.

Hakhverdyan, Z., M. Domanski, L. E. Hough, A. A. Oroskar, A. R. Oroskar, S. Keegan, D. J. Dilworth, K. R. Molloy, V. Sherman, J. D. Aitchison, D. Fenyö, B. T. Chait, T. H. Jensen, M. P. Rout and J. LaCava (2015). Rapid, optimized interactomic screening. Nat Meth. **12:** 553-560.

Hanson, S., K. Berthelot, B. Fink, J. E. G. McCarthy and B. Suess (2003). "Tetracycline-aptamer-mediated translational regulation in yeast." Mol Microbiol **49**(6): 1627-1637.

Heider, M. R., M. Gu, C. M. Duffy, A. M. Mirza, L. L. Marcotte, A. C. Walls, N. Farrall, Z. Hakhverdyan, M. C. Field, M. P. Rout, A. Frost and M. Munson (2015). Subunit connectivity, assembly determinants and architecture of the yeast exocyst complex. Nat Struct Mol Biol. **23:** 59-66.

Helbig, A. O., A. J. R. Heck and M. Slijper (2010). "Exploring the membrane proteome—Challenges and analytical strategies." Journal of Proteomics **73**(5): 868-878.

Hodel, A. E., M. R. Hodel, E. R. Griffis, K. A. Hennig and G. A. Ratner (2002). The three-dimensional structure of the autoproteolytic, nuclear pore-targeting domain of the human nucleoporin Nup98. Mol Cell. **10:** 347-358.

Hoedt, E., G. Zhang and T. A. Neubert (2014). Stable Isotope Labeling by Amino Acids in Cell Culture (SILAC) for Quantitative Proteomics. Cancer Biology and the Nuclear Envelope, Springer International Publishing. **806:** 93-106.

Hulsmann, B. B., A. A. Labokha and D. Gorlich (2012). "The permeability of reconstituted nuclear pores provides direct evidence for the selective phase model." Cell **150**(4): 738-751.

Hülsmann, B. B., A. A. Labokha and D. Görlich (2012). The Permeability of Reconstituted Nuclear Pores Provides Direct Evidence for the Selective Phase Model. Cell, Elsevier. **150:** 738-751.

Hurt, E., K. Strässer, A. Segref, S. Bailer, N. Schlaich, C. Presutti, D. Tollervey and R. Jansen (2000). Mex67p mediates nuclear export of a variety of RNA polymerase II transcripts. J Biol Chem, American Society for Biochemistry and Molecular Biology. **275:** 8361-8368.

Hurt, E. C. (1988). "A novel nucleoskeletal-like protein located at the nuclear periphery is required for the life cycle of Saccharomyces cerevisiae." EMBO J **7**(13): 4323-4334.

Huxley, C., E. D. Green and I. Dunham (1990). Rapid assessment of S. cerevisiae mating type by PCR. Trends Genet. **6:** 236.

Imamoto, N. and T. Funakoshi (2012). Nuclear pore dynamics during the cell cycle. Curr Opin Cell Biol, Elsevier Ltd. **24:** 453-459.

Iwamoto, M., H. Asakawa, Y. Hiraoka and T. Haraguchi (2010). Nucleoporin Nup98: a gatekeeper in the eukaryotic kingdoms. Genes to Cells, Blackwell Publishing Ltd. **15:** 661-669.

Izawa, S., R. Takemura and Y. Inoue (2004). Gle2p is essential to induce adaptation of the export of bulk poly(A)+ mRNA to heat shock in Saccharomyces

cerevisiae. J Biol Chem, American Society for Biochemistry and Molecular Biology. **279:** 35469-35478.

Jiang, H. and A. M. English (2002). Quantitative Analysis of the Yeast Proteome by Incorporation of Isotopically Labeled Leucine. J Proteome Res. **1:** 345-350.

Kendirgi, F., D. J. Rexer, A. R. Alcázar-Román, H. M. Onishko and S. R. Wente (2005). Interaction between the shuttling mRNA export factor Gle1 and the nucleoporin hCG1: a conserved mechanism in the export of Hsp70 mRNA. Mol Biol Cell, American Society for Cell Biology. **16:** 4304-4315.

Khmelinskii, A., P. J. Keller, A. Bartosik, M. Meurer, J. D. Barry, B. R. Mardin, A. Kaufmann, S. Trautmann, M. Wachsmuth, G. Pereira, W. Huber, E. Schiebel and M. Knop (2012). Tandem fluorescent protein timers for in vivo analysis of protein dynamics. Nat Biotechnol, Nature Publishing Group**:** 1-9.

Khmelinskii, A., P. J. Keller, H. Lorenz, E. Schiebel and M. Knop (2010). "Segregation of yeast nuclear pores." Nature **466**(7305): E1.

King, M. C., C. P. Lusk and G. Blobel (2006). Karyopherin-mediated import of integral inner nuclear membrane proteins. Nature. **442:** 1003-1007.

Kirchhausen, T., D. Owen and S. C. Harrison (2014). Molecular structure, function, and dynamics of clathrin-mediated membrane traffic. Cold Spring Harbor Perspectives in Biology, Cold Spring Harbor Lab. **6:** a016725-a016725.

Kitov, P. I. and D. R. Bundle (2003). On the Nature of the Multivalency Effect: A Thermodynamic Model. J Am Chem Soc. **125:** 16271-16284.

Kobayashi, J. and Y. Matsuura (2013). Structural Basis for Cell-Cycle-Dependent Nuclear Import Mediated by the Karyopherin Kap121p. J Mol Biol, Elsevier Ltd. **425:** 1852-1868.

Kotter, P., J. E. Weigand, B. Meyer, K.-D. Entian and B. Suess (2009). "A fast and efficient translational control system for conditional expression of yeast genes." Nucleic Acids Research **37**(18): e120-e120.

Krebber, H., T. Taura, M. S. Lee and P. A. Silver (1999). Uncoupling of the hnRNP Npl3p from mRNAs during the stress-induced block in mRNA export. Genes & Development. **13:** 1994-2004.

Kutay, U. and M. W. Hetzer (2008). Reorganization of the nuclear envelope during open mitosis. Curr Opin Cell Biol. **20:** 669-677.

Lindsay, M. E., K. Plafker, A. E. Smith and B. E. Clurman (2002). Npap60/Nup50 is a tri-stable switch that stimulates importin-α: β-mediated nuclear protein import. Cell. **110:** 349-360.

Lippincott-Schwartz, J., E. Snapp and A. Kenworthy (2001). "Studying protein dynamics in living cells." Nat Rev Mol Cell Biol **2**(6): 444-456.

Liu, H.-L., C. P. C. De Souza, A. H. Osmani and S. A. Osmani (2009). "The three fungal transmembrane nuclear pore complex proteins of Aspergillus nidulans are dispensable in the presence of an intact An-Nup84-120 complex." Mol Biol Cell **20**(2): 616-630.

Longo, V. D., G. S. Shadel, M. Kaeberlein and B. Kennedy (2012). Replicative and Chronological Aging in Saccharomyces cerevisiae. Cell Metabolism, Elsevier Inc. **16:** 18-31.

Lusk, C. P., T. Makhnevych, M. Marelli, J. D. Aitchison and R. W. Wozniak (2002). "Karyopherins in nuclear pore biogenesis: a role for Kap121p in the assembly of Nup53p into nuclear pore complexes." The Journal of Cell Biology **159**(2): 267-278.

Lutzmann, M. (2004). "Reconstitution of Nup157 and Nup145N into the Nup84 Complex." Journal of Biological Chemistry **280**(18): 18442-18451.

Lutzmann, M., R. Kunze and A. Buerer (2002). Modular self-assembly of a Y-shaped multiprotein complex from seven nucleoporins. EMBO J.

Madrid, A. S., J. Mancuso, W. Z. Cande and K. Weis (2006). "The role of the integral membrane nucleoporins Ndc1p and Pom152p in nuclear pore complex assembly and function." The Journal of Cell Biology **173**(3): 361-371.

Makhnevych, T., C. P. Lusk, A. M. Anderson, J. D. Aitchison and R. W. Wozniak (2003). "Cell cycle regulated transport controlled by alterations in the nuclear pore complex." Cell **115**(7): 813-823.

Makio, T., D. L. Lapetina and R. W. Wozniak (2013). Inheritance of yeast nuclear pore complexes requires the Nsp1p subcomplex. The Journal of Cell Biology. **203:** 187-196.

Marelli, M., J. D. Aitchison and R. W. Wozniak (1998). Specific binding of the karyopherin Kap121p to a subunit of the nuclear pore complex containing Nup53p, Nup59p, and Nup170p. The Journal of Cell Biology. **143:** 1813-1830.

Martino, G., S. Pluchino, L. Bonfanti and M. Schwartz (2011). Brain Regeneration in Physiology and Pathology: The Immune Signature Driving Therapeutic Plasticity of Neural Stem Cells. Physiological Reviews. **91:** 1281-1304.

Matsuura, Y. and M. Stewart (2005). Nup50/Npap60 function in nuclear protein import complex disassembly and importin recycling. EMBO J, EMBO Press. **24:** 3681-3689.

Meinema, A. C., J. K. Laba, R. A. Hapsari and R. Otten (2011). Long unfolded linkers facilitate membrane protein import through the nuclear pore complex. Science.

Meinema, A. C., B. Poolman and L. M. Veenhoff (2014). The transport of integral membrane proteins across the nuclear pore complex. nucleus. **3:** 322-329.

Mellacheruvu, D., Z. Wright, A. L. Couzens, J.-P. Lambert, N. A. St-Denis, T. Li, Y. V. Miteva, S. Hauri, M. E. Sardiu, T. Y. Low, V. A. Halim, R. D. Bagshaw, N. C. Hubner, A. al-Hakim, A. Bouchard, D. Faubert, D. Fermin, W. H. Dunham, M. Goudreault, Z.-Y. Lin, B. G. Badillo, T. Pawson, D. Durocher, B. Coulombe, R. Aebersold, G. Superti-Furga, J. Colinge, A. J. R. Heck, H. Choi, M. Gstaiger, S. Mohammed, I. M. Cristea, K. L. Bennett, M. P. Washburn, B. Raught, R. M. Ewing, A.-C. Gingras and A. I. Nesvizhskii (2013). "The CRAPome: a contaminant repository for affinity purification–mass spectrometry data." Nature Methods: 1-11.

Mészáros, N., J. Cibulka, M. J. Mendiburo, A. Romanauska, M. Schneider and A. Köhler (2015). Nuclear Pore Basket Proteins Are Tethered to the Nuclear Envelope and Can Regulate Membrane Curvature. Developmental Cell, The Authors. **33:** 285-298.

Migneault, I., C. Dartiguenave, M. J. Bertrand and K. C. Waldron (2004). Glutaraldehyde: behavior in aqueous solution, reaction with proteins, and application to enzyme crosslinking. Biotech. **37:** 790-796- 798-802.

Muller, M. (2006). Thermodynamic characterization of an engineered tetracycline-binding riboswitch. Nucleic Acids Res. **34:** 2607-2617.

Murphy, R., J. L. Watkins and S. R. Wente (1996). GLE2, a Saccharomyces cerevisiae homologue of the Schizosaccharomyces pombe export factor RAE1, is required for nuclear pore complex structure and function. Mol Biol Cell, American Society for Cell Biology. **7:** 1921-1937.

Nakielny, S., S. Shaikh, B. Burke and G. Dreyfuss (1999). Nup153 is an M9-containing mobile nucleoporin with a novel Ran-binding domain. EMBO J. **18:** 1982-1995.

Niepel, M., K. R. Molloy, R. Williams, J. C. Farr, A. C. Meinema, N. Vecchietti, I. M. Cristea, B. T. Chait, M. P. Rout and C. Strambio-de-Castillia (2013). The nuclear basket proteins Mlp1p and Mlp2p are part of a dynamic interactome

including Esc1p and the proteasome. Mol Biol Cell, American Society for Cell Biology. **24:** 3920-3938.

Niño, C. A., D. Guet, A. Gay, S. Brutus, F. Jourquin, S. Mendiratta, J. Salamero, V. Géli and C. Dargemont (2016). Posttranslational marks control architectural and functional plasticity of the nuclear pore complex basket. The Journal of Cell Biology. **212:** 167-180.

Nishimura, K., T. Fukagawa, H. Takisawa, T. Kakimoto and M. Kanemaki (2009). An auxin-based degron system for the rapid depletion of proteins in nonplant cells. Nat Meth, Nature Publishing Group. **6:** 917-922.

Nishimura, K. and M. T. Kanemaki (2014). Rapid Depletion of Budding Yeast Proteins via the Fusion of an Auxin-Inducible Degron (AID). Curr Protoc Cell Biol. **64:** 20.29.21-16.

Nooren, I. M. A. and J. M. Thornton (2003). Diversity of protein-protein interactions. EMBO J. **22:** 3486-3492.

Nooren, I. M. A. and J. M. Thornton (2003). Structural Characterisation and Functional Significance of Transient Protein–Protein Interactions. J Mol Biol. **325:** 991-1018.

Obado, S. O., M. Brillantes, K. Uryu, W. Zhang, N. E. Ketaren, B. T. Chait, M. C. Field and M. P. Rout (2016). Interactome Mapping Reveals the Evolutionary History of the Nuclear Pore Complex. Plos Biol. **14:** e1002365-1002330.

Oeffinger, M. (2012). Two steps forward-one step back: Advances in affinity purification mass spectrometry of macromolecular complexes. Proteomics. **12:** 1591-1608.

Oeffinger, M., K. E. Wei, R. Rogers, J. A. Degrasse, B. T. Chait, J. D. Aitchison and M. P. Rout (2007). Comprehensive analysis of diverse ribonucleoprotein complexes. Nat Meth. **4:** 951-956.

Ohba, T., E. C. Schirmer, T. Nishimoto and L. Gerace (2004). Energy- and temperature-dependent transport of integral proteins to the inner nuclear membrane via the nuclear pore. The Journal of Cell Biology. **167:** 1051-1062.

Okerman, L., J. Van Hende and L. De Zutter (2007). Stability of frozen stock solutions of beta-lactam antibiotics, cephalosporins, tetracyclines and quinolones used in antibiotic residue screening and antibiotic susceptibility testing. Analytica Chimica Acta. **586:** 284-288.

Olsson, M., S. Schéele and P. Ekblom (2004). Limited expression of nuclear pore membrane glycoprotein 210 in cell lines and tissues suggests cell-type specific nuclear pores in metazoans. Experimental Cell Research. **292:** 359-370.

Onischenko, E., L. H. Stanton, A. S. Madrid, T. Kieselbach and K. Weis (2009). "Role of the Ndc1 interaction network in yeast nuclear pore complex assembly and maintenance." The Journal of Cell Biology **185**(3): 475-491.

Patel, S. S., B. J. Belmont, J. M. Sante and M. F. Rexach (2007). Natively Unfolded Nucleoporins Gate Protein Diffusion across the Nuclear Pore Complex. Cell. **129:** 83-96.

Pettersen, E. F., T. D. Goddard, C. C. Huang, G. S. Couch, D. M. Greenblatt, E. C. Meng and T. E. Ferrin (2004). "UCSF Chimera - A visualization system for exploratory research and analysis." Journal of Computational Chemistry **25**(13): 1605-1612.

Pratt, J., J. Petty, I. Riba-Garcia, D. Robertson, S. Gaskell, S. Oliver and R. Beynon (2002). "Dynamics of protein turnover, a missing dimension in proteomics." Molecular & cellular proteomics : MCP **1**(8): 579-591.

Pritchard, C. E., M. Fornerod, L. H. Kasper and J. M. van Deursen (1999). RAE1 is a shuttling mRNA export factor that binds to a GLEBS-like NUP98 motif at the nuclear pore complex through multiple domains. The Journal of Cell Biology. **145:** 237-254.

Rabut, G., V. Doye and J. Ellenberg (2004). "Mapping the dynamic organization of the nuclear pore complex inside single living cells." Nat Cell Biol **6**(11): 1114-1121.

Rabut, G., P. Lénárt and J. Ellenberg (2004). "Dynamics of nuclear pore complex organization through the cell cycle." Curr Opin Cell Biol **16**(3): 314-321.

Ratner, G. A., A. E. Hodel and M. A. Powers (2007). "Molecular determinants of binding between Gly-Leu-Phe-Gly nucleoporins and the nuclear pore complex." J Biol Chem **282**(47): 33968-33976.

Ribbeck, K. and D. Görlich (2001). Kinetic analysis of translocation through nuclear pore complexes. EMBO J, EMBO Press. **20:** 1320-1330.

Ribbeck, K. and D. Görlich (2002). The permeability barrier of nuclear pore complexes appears to operate via hydrophobic exclusion. EMBO J, EMBO Press. **21:** 2664-2671.

Rigaut, G., A. Shevchenko, B. Rutz, M. Wilm, M. Mann and B. Séraphin (1999). "A generic protein purification method for protein complex characterization and proteome exploration." Nat Biotechnol **17**(10): 1030-1032.

Robinson, M. A., S. Park, Z.-Y. J. Sun, P. A. Silver, G. Wagner and J. M. Hogle (2005). "Multiple conformations in the ligand-binding site of the yeast nuclear pore-targeting domain of Nup116p." J Biol Chem **280**(42): 35723-35732.

Rothballer, A. and U. Kutay (2013). Poring over pores: nuclear pore complex insertion into the nuclear envelope. Trends in Biochemical Sciences, Elsevier Ltd**:** 1-10.

Rout, M. P., J. D. Aitchison, A. Suprapto, K. Hjertaas, Y. Zhao and B. T. Chait (2000). "The yeast nuclear pore complex: composition, architecture, and transport mechanism." The Journal of Cell Biology **148**(4): 635-651.

Rout, M. P., J. D. Aitchison, A. Suprapto, K. Hjertaas, Y. Zhao and B. T. Chait (2000). The yeast nuclear pore complex: composition, architecture, and transport mechanism. The Journal of Cell Biology. **148:** 635-651.

Rout, M. P. and G. Blobel (1993). Isolation of the yeast nuclear pore complex. The Journal of Cell Biology, The Rockefeller University Press. **123:** 771-783.

Saavedra, C., K. S. Tung, D. C. Amberg, A. K. Hopper and C. N. Cole (1996). Regulation of mRNA export in response to stress in Saccharomyces cerevisiae. Genes & Development. **10:** 1608-1620.

Saavedra, C. A., C. M. Hammell, C. V. Heath and C. N. Cole (1997). Yeast heat shock mRNAs are exported through a distinct pathway defined by Rip1p. Genes & Development, Cold Spring Harbor Lab. **11:** 2845-2856.

Sahin, E., A. O. Grillo, M. D. Perkins and C. J. Roberts (2010). "Comparative effects of pH and ionic strength on protein-protein interactions, unfolding, and aggregation for IgG1 antibodies." Journal of pharmaceutical sciences **99**(12): 4830-4848.

Savas, J. N., B. H. Toyama, T. Xu, J. R. Yates and M. W. Hetzer (2012). "Extremely Long-Lived Nuclear Pore Proteins in the Rat Brain." Science (New York, NY) **335**(6071): 942-942.

Schlaich, N. L., M. Häner, A. Lustig, U. Aebi and E. C. Hurt (1997). "In vitro reconstitution of a heterotrimeric nucleoporin complex consisting of recombinant Nsp1p, Nup49p, and Nup57p." Molecular biology of the cell **8**(1): 33.

Schwartz, T. U. (2016). The Structure Inventory of the Nuclear Pore Complex. J Mol Biol, Elsevier B.V.**:** 1-32.

Seddon, A. M., P. Curnow and P. J. Booth (2004). "Membrane proteins, lipids and detergents: not just a soap opera." Biochimica et Biophysica Acta (BBA) - Biomembranes **1666**(1-2): 105-117.

Seo, H.-S., Y. Ma, E. W. Debler, D. Wacker, S. Kutik, G. Blobel and A. Hoelz (2009). Structural and functional analysis of Nup120 suggests ring formation of the Nup84 complex. Proceedings of the National Academy of Sciences, National Acad Sciences. **106:** 14281-14286.

Shcheprova, Z., S. Baldi, S. B. Frei, G. Gonnet and Y. Barral (2008). "A mechanism for asymmetric segregation of age during yeast budding." Nature: 1-8.

Shi, Y., J. Fernandez-Martinez, E. Tjioe, R. Pellarin, S. J. Kim, R. Williams, D. Schneidman, A. Sali, M. P. Rout and B. T. Chait (2014). Structural characterization by cross-linking reveals the detailed architecture of a coatomer-related heptameric module from the nuclear pore complex. Mol Cell Proteomics, American Society for Biochemistry and Molecular Biology**:** mcp.M114.041673.

Shumaker, D. (2003). The nucleoskeleton: lamins and actin are major players in essential nuclear functions. Curr Opin Cell Biol. **15:** 358-366.

Smith, A. E., B. M. Slepchenko, J. C. Schaff, L. M. Loew and I. G. Macara (2002). Systems analysis of Ran transport. Science. **295:** 488-491.

Sorokin, A. V., E. R. Kim and L. P. Ovchinnikov (2010). Proteasome system of protein degradation and processing. Biochemistry Moscow. **74:** 1411-1442.

Steinberg, G., M. Schuster, U. Theisen, S. Kilaru, A. Forge and M. Martin-Urdiroz (2012). Motor-driven motility of fungal nuclear pores organizes chromosomes and fosters nucleocytoplasmic transport. The Journal of Cell Biology, Rockefeller Univ Press. **198:** 343-355.

Stelter, P., R. Kunze, D. Flemming, D. Höpfner, M. Diepholz, P. Philippsen, B. Böttcher and E. Hurt (2007). Molecular basis for the functional interaction of dynein light chain with the nuclear-pore complex. Nat Cell Biol. **9:** 788-796.

Stelter, P., R. Kunze, M. Radwan, E. Thomson, K. Thierbach, M. Thoms and E. Hurt (2012). Monitoring Spatiotemporal Biogenesis of Macromolecular Assemblies by Pulse-Chase Epitope Labeling. Mol Cell, Elsevier Inc. **47:** 788-796.

Stevens, R. C. (2000). High-throughput protein crystallization. Curr Opin Struct Biol. **10:** 558-563.

Strahm, Y., B. Fahrenkrog and D. Zenklusen (1999). The RNA export factor Gle1p is located on the cytoplasmic fibrils of the NPC and physically interacts with the FG ‐ nucleoporin Rip1p, the DEAD ‐ box protein ⋯. The EMBO ⋯.

Strambio-de-Castillia, C., G. Blobel and M. P. Rout (1995). "Isolation and characterization of nuclear envelopes from the yeast Saccharomyces." The Journal of Cell Biology **131**(1): 19-31.

Strawn, L. A., T. Shen, N. Shulga, D. S. Goldfarb and S. R. Wente (2004). "Minimal nuclear pore complexes define FG repeat domains essential for transport." Nat Cell Biol **6**(3): 197-206.

Strawn, L. A., T. Shen, N. Shulga, D. S. Goldfarb and S. R. Wente (2004). Minimal nuclear pore complexes define FG repeat domains essential for transport. Nat Cell Biol. **6:** 197-206.

Stutz, F., J. Kantor, D. Zhang, T. McCarthy, M. Neville and M. Rosbash (1997). The yeast nucleoporin rip1p contributes to multiple export pathways with no essential role for its FG-repeat region. Genes & Development. **11:** 2857-2868.

Stuwe, T., C. J. Bley, K. Thierbach, S. Petrovic, S. Schilbach, D. J. Mayo, T. Perriches, E. J. Rundlet, Y. E. Jeon, L. N. Collins, F. M. Huber, D. H. Lin, M. Paduch, A. Koide, V. Lu, J. Fischer, E. Hurt, S. Koide, A. A. Kossiakoff and A. Hoelz (2015). Architecture of the fungal nuclear pore inner ring complex. Science, American Association for the Advancement of Science. **350:** 56-64.

Subbotin, R. I. and B. T. Chait (2014). A Pipeline for Determining Protein-Protein Interactions and Proximities in the Cellular Milieu. Molecular & Cellular Proteomics, American Society for Biochemistry and Molecular Biology**:** mcp.M114.041095.

Tackett, A. J., J. A. DeGrasse, M. D. Sekedat, M. Oeffinger, M. P. Rout and B. T. Chait (2005). "I-DIRT, a general method for distinguishing between specific and nonspecific protein interactions." J Proteome Res **4**(5): 1752-1756.

Taylor, J. W. and M. L. Berbee (2006). Dating divergences in the Fungal Tree of Life: review and new analyses. Mycologia. **98:** 838-849.

Teixeira, M. T., E. Fabre and B. Dujon (1999). Self-catalyzed cleavage of the yeast nucleoporin Nup145p precursor. J Biol Chem. **274:** 32439-32444.

Teixeira, M. T., S. Siniossoglou, S. Podtelejnikov, J. C. Bénichou, M. Mann, B. Dujon, E. Hurt and E. Fabre (1997). Two functionally distinct domains generated by in vivo cleavage of Nup145p: a novel biogenesis pathway for nucleoporins. EMBO J. **16:** 5086-5097.

Terry, L. J. and S. R. Wente (2009). Flexible Gates: Dynamic Topologies and Functions for FG Nucleoporins in Nucleocytoplasmic Transport. Eukaryotic Cell. **8:** 1814-1827.

Toyama, B. H., J. N. Savas, S. K. Park, M. S. Harris, N. T. Ingolia, I. Yates, John R and M. W. Hetzer (2013). "Identification of Long-Lived Proteins Reveals Exceptional Stability of Essential Cellular Structures." Cell **154**(5): 971-982.

Ugwu, S. O. and S. P. Apte (2004). "The effect of buffers on protein conformational stability." Pharmaceutical Technology **28**(3): 86-109.

Vollmer, B., M. Lorenz, D. Moreno-Andrés, M. Bodenhöfer, P. De Magistris, S. A. Astrinidis, A. Schooley, M. Flötenmeyer, S. Leptihn and W. Antonin (2015). Nup153 Recruits the Nup107-160 Complex to the Inner Nuclear Membrane for Interphasic Nuclear Pore Complex Assembly. Developmental Cell, Elsevier Inc.**:** 1-13.

Vollmer, B., A. Schooley, R. Sachdev, N. Eisenhardt, A. M. Schneider, C. Sieverding, J. Madlung, U. Gerken, B. Macek and W. Antonin (2012). Dimerization and direct membrane interaction of Nup53 contribute to nuclear pore complex assembly. EMBO J, Nature Publishing Group**:** 1-13.

Waldron, C. and F. Lacroute (1975). Effect of growth rate on the amounts of ribosomal and transfer ribonucleic acids in yeast. J. Bacteriol., American Society for Microbiology. **122:** 855-865.

Walther, T. C., A. Alves, H. Pickersgill, I. Loïodice, M. Hetzer, V. Galy, B. B. Hülsmann, T. Köcher, M. Wilm, T. Allen, I. W. Mattaj and V. Doye (2003). "The conserved Nup107-160 complex is critical for nuclear pore complex assembly." Cell **113**(2): 195-206.

Wente, S. R. and M. P. Rout (2010). "The Nuclear Pore Complex and Nuclear Transport." Cold Spring Harbor Perspectives in Biology **2**(10): a000562-a000562.

Wente, S. R. and M. P. Rout (2010). The Nuclear Pore Complex and Nuclear Transport. Cold Spring Harbor Perspectives in Biology. **2:** a000562-a000562.

Williamson, J. R. (2008). Cooperativity in macromolecular assembly. Nat Chem Biol. **4:** 458-465.

Winey, M., D. Yarar, T. H. Giddings and D. N. Mastronarde (1997). Nuclear pore complex number and distribution throughout the Saccharomyces cerevisiae cell cycle by three-dimensional reconstruction from electron micrographs of nuclear envelopes. Mol Biol Cell. **8:** 2119-2132.

Winey, M., D. Yarar, T. H. Giddings and D. N. Mastronarde (1997). "Nuclear pore complex number and distribution throughout the Saccharomyces cerevisiae cell cycle by three-dimensional reconstruction from electron micrographs of nuclear envelopes." Mol Biol Cell **8**(11): 2119-2132.

Wooh, J. W., R. D. Kidd, J. L. Martin and B. Kobe (2003). Comparison of three commercial sparse-matrix crystallization screens. Acta Cryst (2003). D59, 769-772 [doi:10.1107/S0907444903002919], International Union of Crystallography**:** 1-4.

Xiao, H., T. E. Edwards and A. R. Ferré-D'amaré (2008). Structural Basis for Specific, High-Affinity Tetracycline Binding by an In Vitro Evolved Aptamer and Artificial Riboswitch. Chemistry & Biology. **15:** 1125-1137.

Xiao, W. (2006). Yeast Protocols. Totowa, New Jersey, Humana Press Inc.

Yang, Q., M. P. Rout and C. W. Akey (1998). "Three-dimensional architecture of the isolated yeast nuclear pore complex: functional and evolutionary implications." Mol Cell **1**(2): 223-234.

Yang, W., J. Gelles and S. M. Musser (2004). Imaging of single-molecule translocation through nuclear pore complexes. Proc Natl Acad Sci USA, National Acad Sciences. **101:** 12887-12892.

Yang, W. and S. M. Musser (2006). Nuclear import time and transport efficiency depend on importin β concentration. The Journal of Cell Biology. **174:** 951-961.

Yoshida, K., H.-S. Seo, E. W. Debler, G. Blobel and A. Hoelz (2011). Structural and functional analysis of an essential nucleoporin heterotrimer on the cytoplasmic face of the nuclear pore complex. Proceedings of the National Academy of Sciences.

Zhang, Y. and P. Cremer (2006). "Interactions between macromolecules and ions: the Hofmeister series." Current Opinion in Chemical Biology **10**(6): 658-663.

Zhu, H., S. Pan, S. Gu, E. M. Bradbury and X. Chen (2002). Amino acid residue specific stable isotope labeling for quantitative proteomics. Rapid Commun. Mass Spectrom. **16:** 2115-2123.